Synthesis, Spectroscopy and Characterization of Titanium Dioxide Based Photocatalysts for the Degradative Oxidation of Organic Pollutants

Cláudia Sofia Castro Gomes da Silva

Thesis submitted in partial fulfillment of the requirements for the degree of Doctor of Philosophy in Chemical and Biological Engineering, at the Faculty of Engineering, University of Porto

Supervisor:
Prof. Joaquim Luís Bernardes Martins de Faria

Laboratório de Catálise e Materiais
Laboratório Associado LSRE/LCM
Departamento de Engenharia Química
Faculdade de Engenharia
Universidade do Porto

2008

Aos meus pais, Esperança e Manuel

Ao meu marido, Nuno

Agradecimentos

Cito aqui alguns daqueles que, de alguma forma, contribuíram para a realização deste trabalho. A todos o meu agradecimento e que me perdoem aqueles a quem o coração não esquece mas a memória atraiçoa.

Ao Prof. Doutor Joaquim Faria um agradecimento especial pela oportunidade concedida para a realização deste trabalho, pelo acompanhamento científico e por toda a dedicação e confiança em mim depositadas.

Agradeço ao Professor Doutor José Luís Figueiredo, director do Laboratório de Catálise e Materiais, por ter disponibilizado os recursos técnicos necessários à realização deste trabalho.

Aos colegas do Laboratório de Catálise e Materiais – Patrícia, Salomé, Vera, Filomena, Helder, Wang, Adrián, Bruno, Filipe e todos os outros que foram passando pelo laboratório – pelo seu apoio e amizade.

Aos Doutores Rui Boaventura (DEQ-FEUP), Carlos Sá (CEMUP) e Pedro Tavares (UTAD), gostaria de agradecer pela disponibilização e apoio na utilização de algumas das técnicas analíticas utilizadas no âmbito deste trabalho.

À Fundação para a Ciência e a Tecnologia o meu agradecimento pelo financiamento através da concessão da bolsa de doutoramento SFRH/BD/16966/2004.

Agradeço a toda a minha família, em particular aos meus pais, Esperança e Manuel, pelos seus ensinamentos, pelo seu constante incentivo e pela compreensão em todos os momentos. Aos meus avós, Celestina e Perfeito, agradeço o enorme carinho e orgulho que sempre demonstraram. À minha irmã Cátia, por me fazer ver que a vida também é feita de sonhos.

Ao Nuno agradeço a amizade, o amor, a sua infinita paciência, a cumplicidade nos momentos mais felizes e o apoio nos momentos mais difíceis.

Abstract

Heterogeneous photocatalysis is one of the most promising techniques for water treatment. Titanium dioxide (TiO_2) is the most used catalyst in photo-induced reactions, mainly due to its high photocatalytic activity, chemical stability and inexpensiveness. In this thesis is described the synthesis, spectroscopy and characterization of TiO_2 based photocatalysts, and their application to the detoxification of contaminated water containing organic pollutants.

The first part of this work is focused on the preparation and characterization of nanocrystalline TiO_2, and its use in the photocatalytic degradation of a model compound – phenol – by ultraviolet (UV) irradiation. Materials were synthesized by means of an acid catalyzed sol-gel technique using an alkoxide precursor (titanium isopropoxide). By controlling the temperature of the calcination step, materials with different crystalline, spectroscopic and morphologic properties are obtained. TiO_2 obtained at 673K, almost pure anatase is the most active catalyst, while pure rutile, obtained at 973K, showed poor photocatalytic efficiency. The catalytic materials are extensively characterized by several microscopic, spectroscopic and calorimetric techniques. The photocatalytic degradation process is characterized in terms of several operational parameters, namely pH of the medium, catalyst loading, phenol initial concentration, presence of oxidant species, oxygen partial pressure and photon flow. A modified Langmuir-Hinshelwood model with a pseudo-steady state approach is used for kinetic analysis. The dependence of both, kinetic and adsorption equilibrium constants, on light intensity is demonstrated.

In order to increase the TiO_2 photo-efficiency, in particular in the visible spectrum, composite photocatalysts using different supports are synthesized by means of a modified sol-gel technique. Materials such as zeolites, mesoporous molecular sieves, activated carbon, activated carbon fibers and multi-walled carbon nanotubes are used as supports. The prepared catalysts are tested in the photocatalytic degradation of phenol by visible irradiation.

The introduction of carbon based materials results in a positive effect in the photodegradation of phenol. This effect, quantified by means of a synergy factor, is more pronounced when carbon nanotube (CNT)-TiO_2 composite catalysts are used. The beneficial effect is explained by the action of carbon nanotubes as photosensitizers, injecting electrons into the conduction band of TiO_2.

Due to the improved performance of CNT-TiO_2 composite, a more detailed study on its properties is described. Catalysts with different CNT content are tested in the photocatalytic degradation of phenol under UV, UV-Visible and Visible irradiation wavelengths. The effect of the introduction of carbon nanotubes into the titania matrix is more obvious when irradiating in the Visible range, confirming the photosensitizing nature of their action. An optimal CNT to TiO_2 mass ratio of 1:5 is observed. Also, carbon nanotubes surface chemistry was found to be important in the photo-efficiency of the obtained composite catalyst. CNT with a moderate amount of surface oxygenated groups results in more efficient catalytic activity. Carboxylic and phenol groups are believed to be anchoring points for titania particles. An excess of surface groups leaded to the agglomeration of TiO_2 particles and, therefore, to a decrease in the photo-efficiency of the resulting composite catalyst. Besides phenol, the photocatalytic oxidation of other monosubstituted benzene derivatives such as aniline, nitrobenzene and benzoic acid, is investigated using visible irradiation with both TiO_2 and CNT-TiO_2 catalysts. The efficiency of CNT-TiO_2 catalysts in the photocatalytic oxidation of mono-substituted aromatic compounds appears to depend on aromatic ring activating/deactivating properties of the substituents.

The photo-efficiency of the CNT-TiO_2 catalyst is studied using 4-chlorophenol as model compound. The effect of several operation parameters, such as catalyst load, pH of the medium, concentration of hydrogen peroxide and concentration of substrate is described. CNT-TiO_2 catalyst is also tested in the photodegradation of other *para*-substituted phenols, such as 4-aminophenol, 4-hydroxybenzoic acid and 4-nitrophenol. A relationship between the Hammet constant of each compound and its degradability by TiO_2 and CNT-TiO_2 photocatalysts is demonstrated. These results appeared to be in line with the electron donor/withdrawing properties of the substituent groups in the phenol molecule.

Finally, an exploratory study on the photocatalytic oxidation of clofibric acid, a lipid regulator drug, under visible irradiation using nanocrystalline TiO_2 is described as a possible initiator for future work.

Resumo

A fotocatálise heterogénea é considerada uma das mais promissoras técnicas para aplicação ao nível do tratamento de águas. O dióxido de titânio (TiO_2) é o catalisador mais utilizado em reacções foto-induzidas, devido principalmente à sua elevada actividade fotocatalítica, estabilidade química e baixo custo. Nesta tese descreve-se a síntese, espectroscopia e caracterização de fotocatalisadores à base de TiO_2 e a sua aplicação no tratamento de águas contaminadas com poluentes orgânicos.

A primeira parte deste trabalho foca a preparação e caracterização de catalisadores nanocristalinos de TiO_2 e a sua utilização na degradação fotocatalítica de um composto modelo – o fenol – via irradiação no ultravioleta (UV). Os materiais foram sintetizados por um método sol-gel catalisado em meio ácido, usando um precursor do tipo alcóxido (isopropóxido de titânio). Através do controlo da temperatura da etapa de calcinação, obtiveram-se materiais com diferentes propriedades cristalinas, espectroscópicas e morfológicas. O TiO_2 obtido a 673K, constituído por anatase pura, revelou ser o catalisador mais activo, enquanto que o rutilo puro, obtido a 973K, apresentou uma baixa eficiência fotocatalítica. Os materiais catalíticos foram extensivamente caracterizados por técnicas microscópicas, espectroscópicas e calorimétricas. O processo de degradação fotocatalítica foi caracterizado em termos de vários parâmetros operacionais nomeadamente o pH do meio, a concentração de catalisador, a concentração inicial de fenol, a presença de espécies oxidantes, a pressão parcial de oxigénio e o fluxo fotónico. No que respeita à cinética, foi usado um modelo de Langmuir-Hinshelwood modificado, considerando uma aproximação a um estado pseudo-estacionário. Foi demonstrada a dependência das constantes cinética e de equilíbrio de adsorção em relação à intensidade da radiação utilizada.

No sentido de aumentar a foto-eficiência do TiO_2, em particular na região espectral do visível, sintetizaram-se fotocatalisadores compósitos com diferentes suportes, através de um método sol-gel modificado. Como suportes utilizaram-se zeólitos, peneiros moleculares mesoporosos, carvão activado, fibras de carbono activadas e nanotubos de carbono de parede múltipla. Os catalisadores foram testados na degradação fotocatalítica de fenol sob irradiação visível. A introdução de materiais à base de carbono produziu um efeito positivo na fotodegradação do fenol. Este efeito, quantificado em termos de um factor sinérgico, foi mais acentuado aquando da utilização do catalisador de nanotubos de carbono (NTC)-TiO_2.

O efeito benéfico é explicado pela acção dos nanotubos de carbono como agentes foto-sensibilizadores, injectando electrões na banda de condução do TiO_2.

Tendo em conta os resultados promissores obtidos com o compósito NTC-TiO_2, procedeu-se a um estudo mais detalhado sobre as propriedades deste material. Catalisadores com diferentes percentagens de nanotubos de carbono foram testados na degradação fotocatalítica de fenol sob irradiação no UV, UV-Visível e Visível. O efeito da introdução dos nanotubos de carbono na matriz de TiO_2 revelou ser mais evidente quando irradiados com luz visível, o que confirma a sua acção como agente foto-sensibilizador. Observou-se uma razão mássica óptima de NTC para TiO_2 de 1:5. Adicionalmente, a química superficial dos nanotubos de carbono revelou ser uma característica importante no desempenho dos materiais compósitos. NTC com quantidades moderadas de grupos superficiais oxigenados originam materiais com uma maior actividade catalítica. Os grupos ácido carboxílico e fenol constituem pontos de ancoragem das partículas de dióxido de titânio. Uma quantidade excessiva de grupos superficiais resultou na aglomeração das partículas de TiO_2 e, consequentemente, na diminuição da eficiência fotocatalítica do material resultante. Para além do fenol, foi também estudada a degradação fotocatalítica de outros derivados mono-substituidos do benzeno, tais como a anilina, o nitrobenzeno e o ácido benzóico, utilizando TiO_2 e NTC-TiO_2 como catalisadores. A eficiência do catalisador compósito na oxidação dos compostos aromáticos mostrou-se dependente das propriedades activantes/desactivantes de cada um dos substituintes no anel aromático.

A foto-eficiência do catalisador NTC-TiO_2 foi estudada usando o 4-clorofenol como composto modelo. É apresentado um estudo sobre a influência de vários parâmetros operacionais no desempenho do catalisador, nomeadamente a sua concentração, o pH do meio reaccional, a concentração de peróxido de hidrogénio e a concentração de substrato. O catalisador NTC-TiO_2 foi usado na degradação fotocatalítica de outros compostos fenólicos *para*-substituídos, designadamente o 4-aminofenol, o ácido 4-hidroxibenzóico e o 4-nitrofenol. Foi encontrada uma relação entre as constantes de Hammet de cada composto e a sua degradabilidade quer utilizando TiO_2 como NTC-TiO_2 como catalisadores. Estes resultados mostram-se de concordantes com as propriedades dadoras/receptoras de electrões dos grupos substituintes presentes na molécula derivada do fenol.

Por fim, e no sentido de explorar um possível objecto de trabalho futuro, é apresentado um trabalho sobre a degradação do ácido clofíbrico, um fármaco utilizado para a regulação lipídica, utilizando TiO_2 sob irradiação no Visível.

Résumé

La photocatalyse hétérogène est une des techniques prometteuses pour le traitement de l'eau. Le dioxyde de titane (TiO_2) est le catalyseur le plus utilizé dans les réactions photo-induites, principalement à cause de sa forte activité photocatalytique, stabilité chimique et sont bas prix. Dans cette thèse est décrit la synthèse, la spectroscopie et la caractérisation de photocatalyseurs de TiO_2, et ses applications dans la désintoxication de l'eau contenant des polluants organiques.

La première partie de ce travail est fixé sur la préparation et la caractérisation des TiO_2 nanocristalline, et son utilisation dans la dégradation photocatalytique d'un composé modèle – phénol – par irradiation dans l'ultraviolet (UV). Les matériaux ont été synthétisés par une méthode sol-gel catalysé dans acide moyen, en utilisant isopropoxide de titane comme précurseur. En contrôlant la température durant l'étape de calcination, on été obtenu des materiaux avec différentes propriétés cristallines, spectroscopiques et morphologiques. Le TiO_2 obtenu à 673K, constitué d'anatase pur, est le catalyseur le plus actif, tandis que le rutile pur, obtenue à 973K, a montré une faible efficacité photocatalytique. Les matériaux catalytiques sont caractérisée par differentes techniques microscopiques, spectroscopiques et calorimétriques. Le processus de dégradation photocatalytique est caractérisé pour plusieurs paramètres opérationnels, à savoir le pH du milieu, la charge de catalyseur, la concentration initiale de phénol, la présence d'espèces oxydants, la pression partielle d'oxygène et le flux de photons. L'analyse cinétique a été basé sur une modèle de Langmuir-Hinshelwood modifié, en considerant un état pseudo-stationnaire. La dépendance de la constante d'adsorption et de la constante cinétique sur l'intensité de la lumière a été démontrée.

Afin d'augmenter la photo-efficacité du TiO_2, en particulier dans le spectre visible, on été synthétisé des photocatalyseurs composites en utilisant différents supports par une méthode sol-gel modifié. Des matériaux tels que les zéolites, tamis moléculaires mésoporeux, charbon actif, fibres de carbone activé et nanotubes de carbone multi-parois on été utilisés comme supports. Les catalyseurs on été testés dans la dégradation photocatalytique du phénol par irradiation dans le visible. L'introduction de matériaux à base de carbone entraîne un effet positif dans la photodégradation du phénol. Cet effet, quantifiée à l'aide d'un facteur de synergie, est plus favorable quand les catalyseurs de nanotubes de carbone (NTC)-TiO_2 son utilisés. L'effet bénéfique s'explique par l'action de nanotubes de carbone comme

photo-sensibilisateurs, par l'injection des électrons dans la bande de conduction de TiO_2.

En raison de l'amélioration des performances du composite NTC-TiO_2, une étude plus détaillée sur ses propriétés a été décrite. Des catalyseurs avec différents CNT contenus ont été testés dans la dégradation photocatalytique du phénol sous irradiation dans des longueurs d'onde UV, UV-Visible et visible. L'effet de l'introduction de nanotubes de carbone dans la matrice de TiO_2 est plus évident lorsque l'irradiation dans le visible, ce qui confirme la nature photo-sensibilisant de son action. Une proportion massique optimale de CNT:TiO_2 de 1:5 a été determiné. La chimie de surface des nanotubes de carbone joue un rôle important dans la photo-efficacité du catalyseur composite obtenu. CNT avec une petite quantité de groupes superficiels a donné une activité catalytique plus grande. Les groupes superficiels carboxyliques et phénoliques sont des points d'ancrage pour les particules de TiO_2. Un excès de groupes oxygenés dans la surface des NTC provoque l'agglomération des particules de TiO_2 et, par conséquent, la diminution de la photo-efficacité du catalyseur composite. À côté du phénol, il y a aussi étudié l'oxydation photocatalytique d'autres dérivés du benzène tels que l'aniline, le nitrobenzène et l'acide benzoïque. L'efficacité de le catalyseur NTC-TiO_2 dans l'oxydation photocatalytique de composés substitués mono-aromatiques est influencé par les propriétés activants/désactivants des substituants dans le cycle aromatique.

La photo-efficacité du catalyseur NTC-TiO_2 a éte étudié en utilisant comme composé modèle le 4-chlorophénol. L'effet de plusieurs paramètres d'operation, comme la charge de catalyseur, le pH du milieu, la concentration de peroxyde d'hydrogène et la concentration de substrat a été décrit. Le catalyseur NTC-TiO_2 a été également testé dans la photodégradation d'autres phénols *para*-substitués, comme le 4-aminophénol, l'acide 4-hydroxybenzoïque et le 4-nitrophénol. Une relation entre la constante d'Hammet de chaque composé et sa dégradabilité avec les photocatalyseurs TiO_2 et NTC-TiO_2 a été démontrée. Ces résultats semblent être en ligne avec les propriétés donneur/de retrait d'électrons des groupes dans la molécule de phénol.

Finalememt, une étude exploratoire sur l'oxydation photocatalytique de l'acide clofibrique, une drogue régulateur de lipides, sous irradiation visible en utilisant le TiO_2 nanocristalline, a été décrit comme un possible initiateur pour les travaux futurs.

Part of this work was already published or is in the process of publication.

C.G. Silva, W. Wang, P. Selvam, S. Dapurkar, J.L. Faria, *Structured TiO_2 based catalysts for clean water technologies*, Stud. Surf. Sci. Catal. 162 (2006) 151-158.

C.G. Silva, W. Wang, J.L. Faria, *Nanocrystalline CNT-TiO_2 composites produced by an acid catalyzed sol-gel method*, Mater. Sci. Forum. 587-588 (2008) 849-853.

W. Wang, P. Serp, P. Kalck, C.G. Silva, J.L. Faria, *Preparation and characterization of nanostructured MWCNT-TiO_2 composite materials for photocatalytic water treatment applications*, Mater. Res. Bull. 43 (2008) 958-967.

C.G. Silva, J.L. Faria, *Effect of key operational parameters on the photocatalytic oxidation of phenol by nanocrystalline sol-gel TiO_2 under UV irradiation*, J. Mol. Catal. A: Chem. (2008), *submitted*.

C.G. Silva, J.L. Faria, *Synthesis, characterization and testing of nanocrystalline sol-gel TiO_2 catalysts: Anatase vs. rutile efficiency on the photocatalytic oxidation of clofibric acid under visible irradiation,* Photochem. Photobiol. Sci. ,*in preparation*.

C.G. Silva, J.L. Faria, *Carbon nanotube-TiO_2 Catalysts for the photocatalytic oxidation of benzene derivatives in aqueous suspensions*, *in preparation*.

C.G. Silva, J.L. Faria, *Photocatalytic oxidation of phenolic compounds using carbon nanotube-TiO_2 composite catalyst*, *in preparation*.

Table of Contents

Part IV. Carbon nanotube-TiO_2 catalysts

List of Figures

Chapter 1. Introduction

Chapter 2. Synthesis and characterization of nanocrystalline TiO_2 produced by an acid catalyzed sol-gel method

Chapter 3. Photocatalytic degradation of phenol under UV irradiation using nanocrystalline TiO_2 catalysts

Chapter 4. Nanostructured TiO_2 based materials for visible-light-driven photocatalysis

Chapter 5. Carbon Nanotube-TiO_2 catalysts for the photocatalytic oxidation of benzene derivatives in aqueous suspensions

Chapter 6. Photocatalytic oxidation of phenolic compounds using carbon nanotube-TiO_2 composite catalyst

Chapter 7. Photocatalytic oxidation of clofibric acid under visible irradiation using nanocrystalline sol-gel TiO_2 catalysts

List of Schemes

Chapter 6. Photocatalytic oxidation of phenolic compounds using carbon nanotube-TiO_2 composite catalyst

Chapter 7. Photocatalytic oxidation of clofibric acid under visible irradiation using nanocrystalline sol-gel TiO_2 catalysts

List of Tables

Chapter 1. Introduction

Chapter 2. Synthesis and characterization of nanocrystalline TiO_2 produced by an acid catalyzed sol-gel method

Chapter 3. Photocatalytic degradation of phenol under UV irradiation using nanocrystalline TiO_2 catalysts

Chapter 4. Nanostructured TiO_2 based materials for visible-light-driven photocatalysis

Chapter 5. Carbon Nanotube-TiO_2 catalysts for the photocatalytic oxidation of benzene derivatives in aqueous suspensions

Chapter 6. Photocatalytic oxidation of phenolic compounds using carbon nanotube-TiO_2 composite catalyst

Chapter 7. Photocatalytic oxidation of clofibric acid under visible irradiation using nanocrystalline sol-gel TiO_2 catalysts

Part I

General Introduction

Chapter 1

Introduction

An introduction to the photocatalytic oxidation process is presented in this first chapter. The main processes involved in the photoinduced reaction are here described. Catalysts used in photocatalytic oxidation reactions are presented, with special attention given to titanium dioxide. Operational parameters involved in photocatalytic degradation processes are discussed, namely catalyst loading, pollutant concentration, pH of the reaction media, presence of oxygen, temperature and photon flow. Additionally, intrinsic properties of the semiconductor catalysts (crystalline nature, surface area and particle dimensions), and their effect in the photo-efficiency of the photocatalytic degradation process are briefly discussed. Photoreactors and light sources are presented in a section of this chapter dedicated to photochemical technology. Current methods to improve TiO_2 photocatalytic efficiency are discussed. The aim of the present work and the outline of this thesis are given at the end of this chapter.

1.1 Water: the environmental problem

Environmental protection and the correction of environmental problems are major questions for an effective improvement of life quality and for a sustainable development.

Water is present in multiple human activities being used for very diverse purposes like in domestic use, agriculture, industry and energy production. Until a recent past, water demand increased with the slow population growth. The industrial revolution brought an improvement on people's quality of life and consequently a large increase in life expectancy. The exponential growth of human population and the intensification of agricultural and industrial activities leaded to a continuous increase in the demand for earth's limited supply of freshwater. Protection of natural water resources and development of new technologies for water and wastewater treatment became key environmental issues of the 21st century.

Globally, domestic use only represents 15% of the total water consumption, while 25% is used in industrial activities and 60% in agriculture (Fig. 1.1). Associated to each of these activities are distinct types of pollution and pollutant compounds. In the Iberian region, main wastewater producing industrial processes include petrochemical, chemical synthesis, textile, pharmaceutical, agrochemical, paper and food.

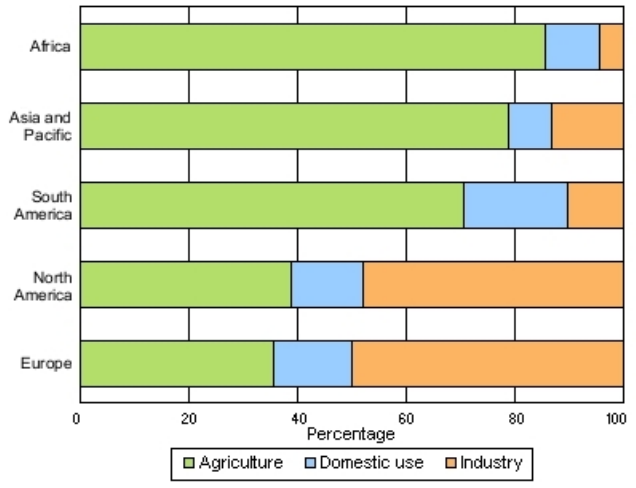

Figure 1.1 Water withdrawal by sector in the regions of the world (2000) [1].

Recently, the European Union Commission Services proposed a new Directive, amending Directive 2000/60/EC, where new Environmental Quality Standards (EQS) for hazardous priority substances have been defined within Europe [2]. In particular pesticides and phenols are referred, with admissible thresholds lower than 0.5 microgram per liter in water. Thus, adequate treatment of contaminated waters is of primary concern in order to preserve the natural ecosystem.

The biological processes are more natural and easy to implement but they have a major drawback, which is the production of sludge proportionally to the volume of treated water. When the volume to treat is huge, recycling is essential. Nevertheless, used water always requires some treatment prior to reuse, with or without addition of freshwater. The extent of the treatment depends either on the degree of contamination, or on the requirements of the next use. Chemical treatments provide adequate response to a number of specific cases, because with them the pollutant is not being transferred, rather converted, or in the ideal case mineralized.

1.2 Advanced oxidation processes

It has been frequently observed that pollutants not amenable to biological treatments may also be characterized by high chemical stability and/or by strong difficulty to be completely mineralized. In these cases, it is necessary to use reactive systems much more effective than those adopted in conventional purification processes. A lot of research work has been done in this direction in the last decades, pointing out the prominent role of a special class of oxidation techniques defined as Advanced Oxidation Processes (AOPs).

New developments in AOPs are attractive in providing a promising and competitive solution for the abatement of numerous hazardous compounds in wastewater including chemical oxidation processes (O_3, O_3/H_2O_2, Fenton), photochemical oxidation processes (UV/O_3, UV/H_2O_2) and photocatalytic processes (UV/TiO_2, photo-Fenton). AOPs feature the capability of utilizing the high reactivity of hydroxyl radicals ($HO^{\bullet}$) to drive oxidation processes, which are suitable for achieving the complete elimination and full mineralization of various pollutants. Hydroxyl radicals are characterized by being highly reactive

species (E^0= +2.8V), showing little selectivity of attack, which is a useful attribute for an oxidant to be used in wastewater treatment for solving pollution problems.

The possibilities offered by AOPs can be exploited in an integrated approach with biological treatment systems for the oxidative degradation of toxic or refractory substances. AOP application depends on the polluting load of wastes, normally expressed in chemical oxygen demand (COD). Only wastes with relatively small COD contents (≤5.0 g l^{-1}) can be suitably treated by means of advanced oxidation techniques. Higher COD contents would require the consumption of too large amounts of expensive reactants. Water streams with higher organic contents can be more conveniently treated by means of wet oxidation and incineration processes (Fig. 1.2).

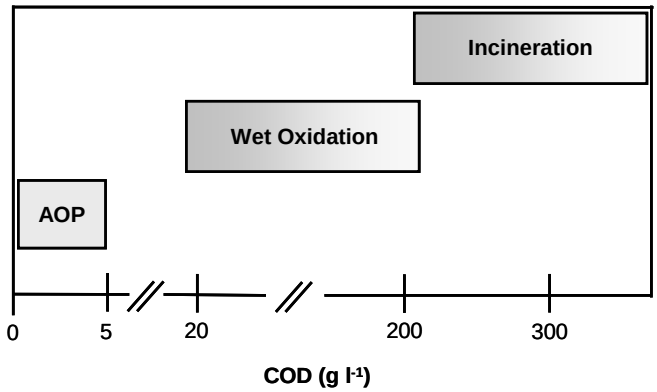

Figure 1.2 Suitability of water treatment technologies according to COD content (adapted from Ref. [3]).

In this sense, due to fast development of light related technologies, the photochemical processes are positioning themselves on a privileged situation to compete with other available technologies. Photocatalytic degradation processes, assisted by a semiconductor metal oxide (normally as photocatalyst) and oxygen (as primary oxidizing agent), earn increasing importance in the area of wastewater treatment as the most emerging destructive technology [3-9]. Contributing to this are the facts that these processes require mild operation conditions of temperature and pressure, offer the possibility of use of natural resources such as sunlight, which should result in considerable economic savings; use low cost and chemical stable TiO_2 (the most used photocatalyst) and in many cases result in total mineralization of the pollutants without any waste disposal problem.

The first contribution for understanding the heterogeneous photocatalytic process happened in 1972 with the pioneering research of Fujishima and Honda [10]. These authors revealed the possibility of water splitting by a photoelectrochemical cell a rutile TiO_2 photoanode and a Pt counter electrode. This finding opened the frontiers of titania photocatalysis for other type of applications. Four years later, Carey et al. first reported the photocatalytic degradation of organic molecules, biphenyl and chlorobiphenyl derivatives, in the presence of TiO_2 [11]. Since then, an enormous number of works have been published demonstrating the efficiency of the use of TiO_2 in photocatalytic processes as a mean of wastewater detoxification.

1.3 The photocatalytic reaction

In a photochemical process, light is always a reactant, never a catalyst. A photodegradation process is usually a photo-oxidation reaction due to the presence of oxygen. The photocatalyst is the agent capable to combine efficiently both reactants (light and oxygen) to promote the degradation of a third agent: the pollutant. By definition, photocatalysis has been described as a change in the rate of a chemical reaction or its initiation under the action of ultraviolet, visible, or infrared radiation in the presence of a substance - the photocatalyst - that absorbs light and is involved in the chemical transformation of the reaction partners [12]. However, there is no agreement on this definition and photocatalysis is probably better described as a catalytic reaction involving light absorption by a catalyst or by a substrate.

As for classical heterogeneous catalysis, the overall process can be decomposed into five independent steps [7]:

i. Diffusion of the reactants from the bulk phase to the surface of the catalyst;
ii. Adsorption of at least one of the reactants;
iii. Reaction in the adsorbed phase;
iv. Desorption of the products;
v. Removal of the products from the interface region.

The particularity of photocatalytic reactions, when compared to conventional catalysis, consists in the way the catalyst is activated, with thermal activation being replaced by photonic activation. Although photo-adsorption and

photo-desorption of some reactants can occur, the photonic activation is mainly concerned to step iii. The reaction in the adsorbed phase includes several photoelectronic processes such as: absorption of photons by the solid catalyst; creation of electron/hole pairs which dissociate into photoelectrons and positive photo-holes; electron transfer reactions. In heterogeneous photocatalysis either the catalyst (a semiconductor, *SC*), or the adsorbed molecule, or both, are in the excited state during the catalytic step iii.

Depending on where the initial excitation occurs, photocatalysis can be generally divided into two classes of processes [13]. When the initial photoexcitation occurs in the adsorbate molecule, which then interacts with the ground state catalyst substrate, the process is referred to as a catalyzed photoreaction. When the initial photoexcitation takes place in the catalyst substrate and the photoexcited catalyst then transfers an electron or energy into a ground state molecule, the process is referred to as a sensitized photoreaction. The initial excitation of the system is followed by subsequent electron and/or energy transfer. It is the subsequent de-excitation process that leads to chemical reactions in the heterogeneous photocatalytic process.

1.4 The sensitized photoreaction

Sensitized photoreactions are activated by absorption of a photon with sufficient energy, *i.e.*, equal or higher than the bandgap energy (E_g) of the catalyst. The absorption leads to a charge separation due to the promotion of an electron (e^-) from the valence band (VB) of the semiconductor catalyst to the conduction band (CB) thus generating a hole (h^+) in the valence band. For a semiconductor photocatalyst to be efficient, the different interfacial electronic processes involving e^- and h^+ must compete effectively with the major deactivation processes involving electron/hole recombination, which may occur in the bulk or at the surface of the photocatalyst (Fig. 1.3). Once at the surface, on the absence of any suitable acceptor (for e^-) and donor (for h^+) recombination can occur and then, no photocatalytic reaction occurs. Moreover, charge carriers can be single trapped in lattice defects, and recombination can occur through these defects. All these processes account for catalysts deactivation.

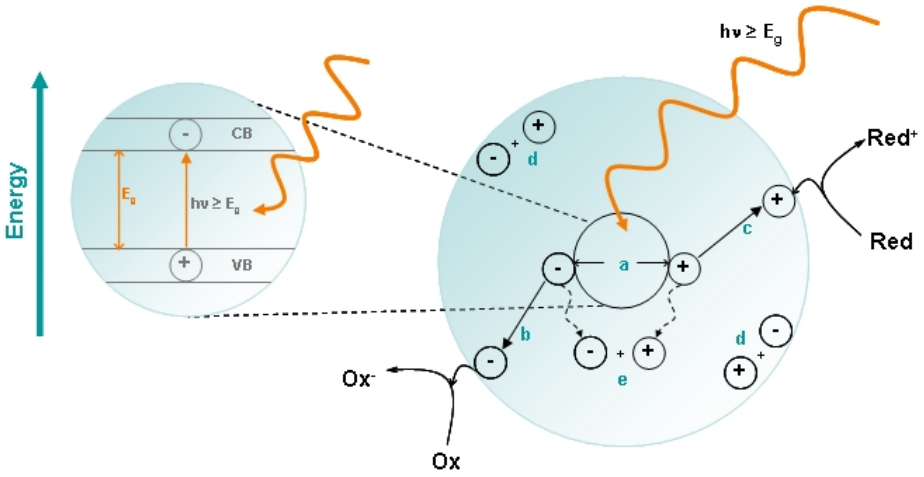

Figure 1.3 Main processes occurring on a semiconductor particle: (a) photogeneration of electron/hole pair; (b) diffusion of the electron acceptor and reduction at the surface of the semiconductor; (c) oxidation of the electron donor n the surface of the semiconductor particle; (d) and (e) electron/hole recombination at the surface and in the bulk, respectively.

The desired process consists in the reaction of the activated electron with an oxidant (*Ox*), yielding a reduced product (Ox^-), and the reaction of the photogenerated hole with a reductant (*Red*) to produce an oxidized product (Red^+), as indicated in the following equation:

$$(Ox)_{ads} + (Red)_{ads} \xrightarrow{SC,\ h\nu \geq E_g} Ox^- + Red^+ \qquad (1.1)$$

In aerated conditions, molecular oxygen adsorbed on the surface of the semiconductor acts as electron acceptor, while adsorbed water molecules and hydroxyl anions act as electron donors, leading to the formation of very powerful oxidizing $HO^\bullet$ radical. In the presence of an organic molecule (*M*) adsorbed in the catalyst surface, hydroxyl radical is the primary oxidizing entity, reacting by adduct formation, followed by structural breakdown into several intermediates till, eventually, total mineralization. The overall process can be described by the following reactions:

$$SC \xrightarrow{h\nu} SC(e^-_{CB} + h^+_{VB}) \qquad (1.2)$$

$$SC(e^-_{CB}) + (O_2)_{ads} \longrightarrow SC + (O_2^{\bullet -})_{ads} \qquad (1.3)$$

$$SC(h^+_{VB}) + (H_2O)_{ads} \longrightarrow SC + (HO^\bullet)_{ads} + (H^+)_{ads} \qquad (1.4)$$

$$SC(h_{VB}^{+}) + \left(HO^{-}\right)_{ads} \longrightarrow SC + \left(HO^{\bullet}\right)_{ads} \quad (1.5)$$

$$SC(h_{VB}^{+}) + M_{ads} \longrightarrow SC + \left(M^{\bullet+}\right)_{ads} \quad (1.6)$$

$$\left(HO^{\bullet}\right)_{ads} + M_{ads} \longrightarrow Intermediate \longrightarrow Mineralization \quad (1.7)$$

Analyzing Eq. 1.5 it is clear that the pH of the reaction medium affects the formation of hydroxyl radicals. Besides hydroxyl and superoxide radicals, other oxidizing species can be generated from the reduction of molecular oxygen and take part on the oxidation of the organic reactant:

$$O_2^{\bullet-} + H^{+} \longrightarrow HO_2^{\bullet} \quad (1.8)$$

$$O_2^{\bullet-} + HO_2^{\bullet} + H^{+} \longrightarrow H_2O_2 + O_2 \quad (1.9)$$

Hydrogen peroxide can undergo thermal desorption from the catalyst surface and, under UV irradiation conditions, can lead to the formation of hydroxyl radicals:

$$H_2O_2 \xrightarrow{h\nu} 2HO^{\bullet} \quad (1.10)$$

Nevertheless, the contribution of this process is not expected to be the most important concerning the generation of hydroxyl radicals, Eqs. 1.4 and 1.5 being the predominant reactions. In the presence of highly oxidizing radicals, oxidative degradation should occur through formation of oxygenated intermediates, which will break down to lower molecular weight species and possibly achieve mineralization.

1.5 Catalysts for photocatalytic reactions

Heterogeneous photocatalysts are solids that can promote reactions in the presence of light not being consumed in the overall reaction. Catalysts used in photocatalytic reactions are invariably semiconductor materials. The chalcogenide semiconductors used as photocatalysts include several metal oxides such as TiO_2, ZnO, ZrO_2, Fe_2O_3, CeO_2, WO_3, etc. or even sulfides like CdS, ZnS, MoS_2 and CdS [7].

An ideal photocatalyst should possess the following characteristics: i. photoactive; ii. have the ability to be excited with visible and/or near UV light; iii. biologically and chemically inert; iv. photostable (*i.e.*, not prone to photocorrosion); v. inexpensive and vi. non-toxic [14]. Furthermore, in order to a

catalyst to be photochemically active as a sensitizer, the redox potential of hydroxyl radical should lie in the bandgap of the semiconductor. Bandgap energies and redox potentials of the most common semiconductors used as catalysts are shown in Fig. 1.4.

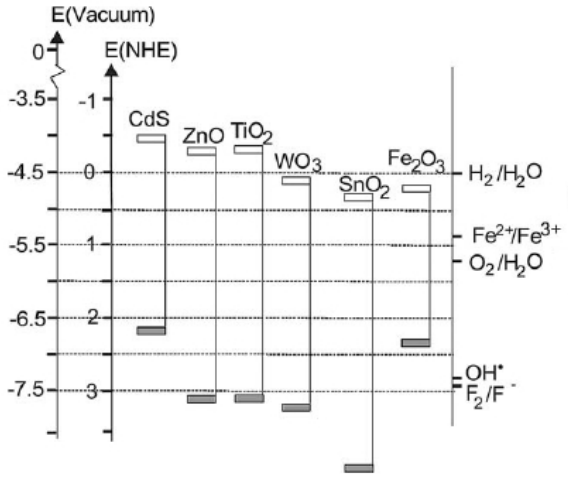

Figure 1.4 Bandgaps of some semiconductor materials together with some selected redox potentials (adapted from Ref. [15]).

Nonetheless, some of the semiconductor catalysts do not show long-term stability in aqueous media. Metal chalcogenides semiconductors such as CdS, CdSe and PbS are regarded as insufficiently stable for catalysis in aqueous media, since they readily undergo photoanodic corrosion, which can only be partly suppressed by the addition of sulfide and sulfite to the contacting solution [16]. These materials are also known to show some toxicity. Hematite (α-Fe_2O_3), for example, is absorptive in the visible region, but shows much lower photocatalytic activity than TiO_2 or ZnO, probably because of corrosion or the formation of short-lived metal-to-ligand or ligand-to-metal charge transfer states [4]. Although ZnO and TiO_2 have similar bandgap energies (3.2 eV), zinc oxide shows some instability in illuminated aqueous solutions, with $Zn(OH)_2$ being formed on the particle surface leading to the deactivation of the catalyst [17]. WO_3 has also been investigated as photocatalyst. However, it is generally less photocatalytic active than TiO_2 [17].

Because of its high photocatalytic activity, titanium dioxide has become the most used catalyst in photo-induced reactions. In the next section, a detailed description about this remarkable photocatalyst is presented.

1.6 Titanium dioxide

TiO_2 was firstly discovered, in form of black sand, on the beaches of Cornwall, England in the 1790s. William Gregor, a parish priest, found that a magnet could attract the black grains away from the ordinary silica sand. He treated this black sand with hydrochloric acid and dissolved out iron oxide, leaving a white residue which he dissolved in some sulphuric acid. By treating this solution with soda he obtained, after calcination, a white powder: TiO_2 [18]. In fact, William Gregor discovered the reactions by which almost all commercial TiO_2 was produced up to 1960.

In our days, TiO_2 is manufactured by either the sulfate or the chlorine processes [18]. In the former, ilmenite, a mineral found in metamorphic rocks, is transformed into iron and titanium sulfates by reaction with sulfuric acid. Titanium hydroxide is precipitated by hydrolysis, filtered and calcinated at high temperature. Alternatively, the seed crystals generated by alkaline hydrolysis are reacted with chlorine to produce titanium tetrachloride, which is purified and reoxidized, yielding very pure TiO_2.

Titanium dioxide has received a great deal of attention mainly due to its chemical stability, non-toxicity and low cost. Its main fields of application are as white pigment in paints (51% of the total production), plastic (19%) and paper (17%).

Four polymorphs of TiO_2 can be found in nature: anatase (tetragonal), rutile (tetragonal), brookite (orthorhombic) and TiO_2 (B) (monoclinic). Besides these crystalline forms, two high-pressure TiO_2 materials have been synthesized starting from rutile: TiO_2(II), which has the PbO_2 structure, and TiO_2(H) with the hollandite structure. Anatase, rutile and brookite structures can be resolved in terms of TiO_2^{6-} octahedrals. The three natural TiO_2 polymorphs differ on their crystal structure by the distortion of each TiO_2 octahedral and by the assemblage patterns of the octahedral chains. Anatase is constituted by octahedrals connected by their vertices (Fig. 1.5a), while in rutile, the edges are connected (Fig. 1.5b). In brookite, both vertices and edges are connected (Fig. 1.5c).

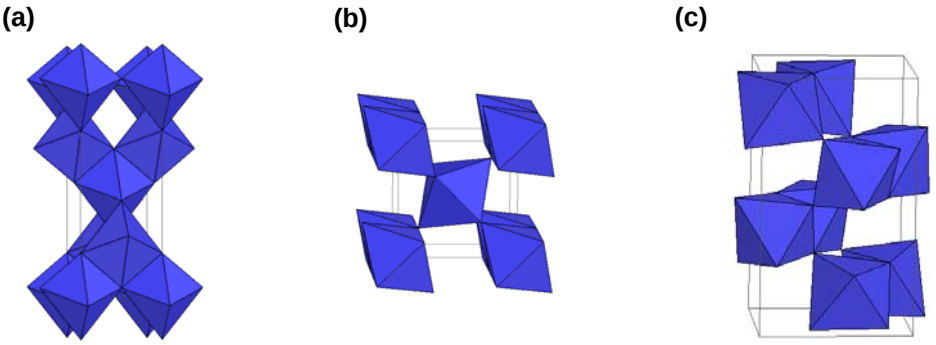

Figure 1.5 Crystal structures of anatase (a), rutile (b) and brookite (c) [15].

TiO_2 can be prepared in the form of powders, crystals or thin films, by either liquid or gas phase methods. Gas phase methods are generally used for the preparation of thin TiO_2 films. The main techniques are: chemical vapor deposition (CVD) [19], physical vapor deposition (PVD) [20] and spray pyrolysis deposition (SPD) [21]. Recently, other sophisticated thin-film techniques based on vapor-phase deposition have been used, including ion implantation [22], sputtering [23], molecular beam epitaxy [24] and dynamic ion beam mixing [25]. Although these new techniques provide an efficient control in the film growth and lead to the production of very pure materials, the very high energy consumption is considered a great disadvantage from the economical point of view. The solution routes are mostly used for the synthesis of thin films and powders. Main advantages of this type of preparation methods are the possibility to control stoichiometry, production of homogeneous materials, possibility of formation of complex shapes, and preparation of composite materials. However, some disadvantages are associated to liquid phase production techniques, including long processing times, use of expensive precursors and, in some cases, the presence of carbon as impurity.

TiO_2 liquid phase preparation procedures include precipitation and co-precipitation [26, 27], solvothermal and hydrothermal methods [28, 29], microemulsion [30], combustion and electrochemical synthesis [31, 32] and sol-gel method [33]. The later is one of the most popular techniques to synthesize titania, generally used for production of thin films, powders and membranes.

The sol-gel method has many advantages over the other production techniques including the formation of very pure and homogeneous materials. This technique also allows the introduction of other solid phases into the TiO_2 matrix to form composites [34], as well as dopant species to form TiO_2-doped materials [35],

with stoichiometric control and in an easy process. Depending on the type of titania precursor used, TiO_2 can be produced by means of alkoxide and non-alkoxide sol-gel routes. In the non-alkoxide route, inorganic salts such as nitrates, chlorides, acetates, carbonates, acetylacetonates, etc., are used and an additional step of removal of the inorganic anion is required [36]. In the alkoxide route (the more common), metal alkoxides like titanium ethoxide, titanium isopropoxide and titanium *n*-butoxide are used as precursors. This method involves the formation of a TiO_2 sol or gel, or precipitation by hydrolysis and condensation (with polymer formation) of titanium alkoxides. In order to have better control over the evolution of the microstructure, it is desirable to separate the hydrolysis and condensation steps. One way to achieve this is by means of acid-base catalysis. Acid catalysis increases hydrolysis rates leading to the formation of crystalline powders from fully hydrolyzed precursors. Base catalysis is thought to promote condensation to obtain amorphous powders, containing unhydrolyzed alkoxide ligands. These reactions are followed by a thermal treatment to remove the organic part and to promote crystallization either in anatase or rutile phase. TiO_2 can also be synthesized in special nanostructured morphologies like nanorods [37], nanowires [38], nanotubes [39], nanoribbons [37] and whiskers [40].

One of the most used commercial TiO_2 materials for photocatalytic oxidation applications is TiO_2 Degussa P25 (now commercially called AEROXIDE® TiO_2 P25 since September 2007, after Evonik Industries taking over Degussa to be its Chemicals Business Area). It consists in a highly dispersed powder manufactured according to the patented AEROSIL® process. This commercial catalyst is composed by a mixture of 80% of anatase and 20% of rutile, with a surface area of 50 $m^2\ g^{-1}$ and an average particle size of 21 nm (manufacturer data).

When TiO_2 is irradiated with light with higher energy than its bandgap, photoinduced phenomena occur (Fig. 1.6), with the promotion of an electron to the conduction band leaving a hole in the valence band. This excited electron can be used directly to create electricity in photovoltaic solar cells or drive photocatalytic reactions. Recently, a special feature of light-activated TiO_2 was discovered, related to the trapping of holes at the surface of the semiconductor causing a high wettability. This phenomenon was called photoinduced superhydrophilicity [41].

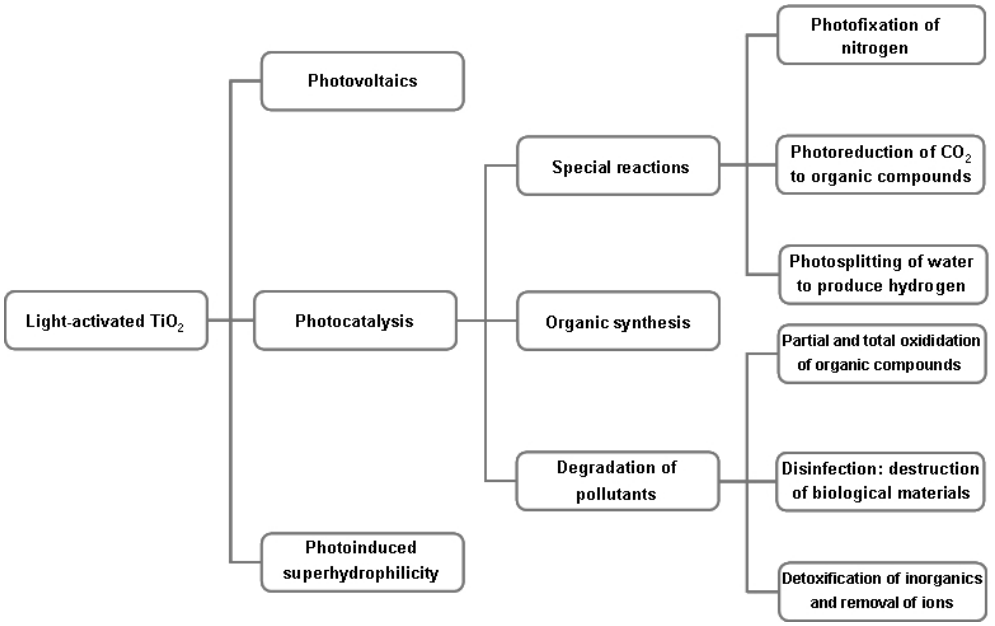

Figure 1.6 Photoinduced processes on TiO_2 (adapted from Ref. [15]).

TiO_2 meditated photocatalytic reactions are gaining nowadays increasingly attention, with the most active field of its application centered on the photodegradation of organic compounds in environmental decontamination of water and air.

For reactions in aqueous media, many elementary mechanistic processes have been described in the photocatalytic degradation of organic compounds over TiO_2 surface. The characteristics time for each elementary reaction has been reported in previous literature, based on studies of laser flash photolysis [42] (Table 1.1).

The $\{>Ti^{IV}OH^{\bullet+}\}$ and $\{>Ti^{III}OH\}$ represent the surface-trapped valence band hole and surface-trapped conduction band electron, respectively. The surface-bound hydroxyl radical represented by $\{>Ti^{IV}OH^{\bullet+}\}$ is chemically equivalent to the surface-trapped hole. Recombination is mediated primarily by $\{>Ti^{III}OH\}$ in the first 10 ns. Valence band holes are sequestered as long-lived $\{>Ti^{IV}OH^{\bullet+}\}$ after 10 ns. $>Ti^{IV}OH$ is reformed by recombination with conduction band electrons or oxidation of the substrate on the time scale of 100 ns.

Table 1.1 Primary processes and time domains in titania-catalyzed mineralization of organic pollutants.

Primary process	***Characteristic time***
Charge carrier generation	
$TiO_2 \xrightarrow{h\nu} e^-_{CB} + h^+_{VB}$	fs (very fast)
Charge carrier trapping	
$h^+_{VB} + > Ti^{IV}OH \longrightarrow \{> Ti^{IV}OH^{\bullet +}\}$	10 ns (fast)
$e^-_{CB} + > Ti^{IV}OH \longleftrightarrow \{> Ti^{III}OH\}$	100 ps (shallow trap; dynamic equilibrium
$e^-_{CB} + > Ti^{IV} \longrightarrow Ti^{III}$	10 ns (deep trap)
Charge carrier recombination	
$e^-_{CB} + \{> TiOH^{\bullet +}\} \longrightarrow > Ti^{IV}OH$	100 ns (slow)
$h^+_{VB} + \{> Ti^{III}OH\} \longrightarrow Ti^{IV}OH$	10 ns (fast)
Interfacial charge transfer	
$\{> Ti^{IV}OH^{\bullet +}\} + org \quad molec \longrightarrow > Ti^{IV}OH + oxid \quad molec$	100 ns (slow)
$\{> Ti^{III}OH\} + O_2 \longrightarrow > Ti^{IV}OH + O_2^{\bullet -}$	ms (very slow)

The dynamic equilibrium shown in Table 1.1 represents a reversible trapping of a conduction band electron in a shallow trap below the conduction band edge such that there is a finite probability that the trapped electron can be transferred back into the conduction band at room temperature.

1.7 Factors affecting the photocatalytic process

As showed earlier, photocatalytic reactions are extremely complex processes involving many participants namely water, organic substrate, catalyst, light and oxygen. Therefore, it is obvious that operational parameters related to each of these agents may affect the efficiency of the photocatalytic process. Photocatalytic reaction rates are known to be affected by several operation conditions including pH of the medium, catalyst loading, substrate concentration, light intensity (photonic flux), temperature and oxygen pressure. Also, physical and chemical intrinsic properties of the photocatalyst may affect its photoefficiency.

TiO_2 crystal composition, surface area, crystallite dimensions and presence of surface hydroxyl groups are known to be important parameters that influence the efficiency of the catalyst in photocatalytic reactions. Since these themes will be the subject of some of the studies presented in this research work, they will be discussed in detail in the chapters dedicated to results. However, a brief description of the effect caused by each operational parameter in the efficiency of the photocatalytic process is described in the following.

1.7.1 Operational parameters

1.7.1.1 Catalyst loading

In photocatalytic processes, the initial rates of reaction are found to be proportional to the mass of catalyst. However, above a certain amount, the reaction rate becomes independent of the mass of catalyst. This limit corresponds to the maximum amount of TiO_2 at which all particles are totally illuminated. Generally, in any given photocatalytic application, the optimum catalysts loading must be determined, in order to avoid excess catalyst and ensure total absorption of efficient photons [7].

1.7.1.2 Substrate concentration

In photocatalytic degradation reactions, the observed rate constant decreases with the increase of initial organic pollutant concentration. The main steps of the photocatalytic reaction occur on the surface of the catalyst, and therefore, a high adsorption capacity is associated with reaction favoring. It is assumed that most of the reactions follow a Langmuir-Hinshelwood kinetic rate model, meaning that for high initial concentration all catalytic sites are occupied. A further increase of the concentration does not affect the actual catalyst surface concentration, and therefore, this may result in a decrease of the observed rate constant.

Intermediates generated during the photocatalytic process also affect the rate constant of their parent compounds. A high initial concentration of the initial

pollutant means higher concentrations of adsorbed reaction intermediates, which will negatively affect the overall rate.

1.7.1.3 pH of the medium

The acid-basic properties of the reaction medium play an important role in the photocatalytic reaction taking place at the surface of the semiconductor. The variation of pH affects TiO_2 surface speciation due to the amphoteric (point of zero charge at pH~6.5) nature of titania particles. Under acidic or alkaline conditions the surface of titania can be protonated or deprotonated, respectively. Also, the electronic state of the substrate molecule in the reaction media will depend on its acidic properties, namely pKa. The effect of the pH on the reaction rate can be interpreted in terms of electrostatic interactions between charged TiO_2 particles and the substrate. This in turn affects the adsorption process, important since the photocatalytic reactions are believed to be surface processes.

For photocatalytic reactions using TiO_2 slurries, pH conditions has also been reported to have an influence on the dispersion of the semiconductor particles in suspension, and therefore on the photodegradation rate [43].

1.7.1.4 Temperature

The overall process of photocatalytic degradation is not too sensitive to temperature. The degradation rate dependency on temperature is reflected by the low activation energy (5–20 kJ mol^{-1}) compared with ordinary thermal reactions [44]. Due to photonic activation, the photocatalytic systems do not require heating and can operate at room temperature. This absence of heating is very attractive for processes carried out in aqueous medium, especially for water purification, because there is no need to waste energy in heating water, which has a high heat capacity.

1.7.1.5 Oxygen pressure

In liquid phase reactions, it becomes difficult to study the influence of oxygen partial pressure because the reaction is polyphasic. It is generally assumed that oxygen adsorbs on titania from the liquid phase, where it is dissolved following Henry's law [7]. If oxygen is regularly supplied, it can be assumed that its coverage at the surface of TiO_2 is constant and its contribution can be integrated in the apparent rate constant.

Dissolved oxygen is strongly electrophilic and thus an increase of its content probably reduces unfavorable electron/hole recombination routes. However, higher concentrations lead to a downturn of the reaction rate, which can be attributed to the fact that the TiO_2 surface becomes highly hydroxylated inhibiting the adsorption of the pollutant at the active sites [45].

1.7.1.6 Photon flux

The radiant flux (φ), which is proportional to the light intensity, constitutes a very important parameter in the design of the reactor and in the choosing of the light source. Photocatalytic degradation rates have been found to follow two distinct regimes with respect to the radiant flux: a first-order regime for low photon flux and a half-order regime for high intensities [46]. In the former regime, the electron/hole pairs are consumed more rapidly by chemical reactions than by recombination reactions, whereas in the half-order regime, the electron/hole recombination is the dominant process.

1.7.2 TiO_2 structural and morphological properties

1.7.2.1 TiO_2 crystal structure

Titanium dioxide in the anatase form is generally accepted to be the most active polymorph. This better efficiency is attributed to a higher degree of hydroxylation of anatase when compared with rutile phase. Also, the higher surface area of anatase TiO_2 is pointed as one of the properties that contribute to its superior efficiency.

Even though, some studies have revealed that pure anatase not always lead to the best photocatalytic performance [47]. These findings were discussed in terms of the presence of rutile phase may introduce mesoporosity and a wider pore size distribution to the resultant catalyst. The catalytic activity may be a combined effect of the pore size, the pore size distribution and the appropriate crystal plane on which adsorption takes place.

1.7.2.2 Surface area

The surface area of a solid catalyst is directly related to the concentration of active sites for adsorption and reaction. A large surface area can be a determining factor in certain photodegradation reactions, since the adsorption of large amounts of substrate and oxygen promotes the reaction rate. However, powders with high surface areas are usually associated with large amounts of crystal lattice defects, facilitating the recombination of the photo-generated electron/hole pairs, leading to a poor photocatalytic activity [48]. It has been reported that the photocatalytic activity of amorphous titania is negligible indicating that crystallinity is an important requirement [49]. Therefore, a balance between surface area and crystallinity must be found in order to obtain the maximum photoactivity.

1.7.2.3 Particle dimensions

Particle size and ultimately, crystallite dimensions play an important role in the photoactivity of the semiconductor, since the electron/hole recombination process was showed to be particle size dependent [50]. It is known that in nanometer-size range, the physical and chemical properties of the semiconductors are modified, when compared to bulk size dimensions [51]. Small variations in particle size leads to great modifications in surface/bulk ratio, thus modifying the significance of volume and surface electron/hole recombination processes. Generally it is assumed that the smaller is the particle (in a nanometer range), the higher is the efficiency of the photocatalytic process. However, if the TiO_2 crystallite size is extremely reduced, in the range of a few nanometers, lattice defects can lead to an increase in the electron/hole recombination.

Additionally, particle size is an important parameter for heterogeneous catalysis in general since it directly impacts the specific surface area of a catalyst. With a smaller particle size, the number of active surface sites increases, and so does the surface charge carrier transfer rate in photocatalysis.

Some studies revealed that the photocatalytic efficiency does not monotonically increase with decreasing particle size, and there exists an optimal particle size of a few nanometers (3–10 nm) for pure nanocrystalline TiO_2 photocatalyst [50]. Nevertheless, as for other properties, an optimum value may be discussed only in the context of the used catalyst, organic compound and process parameters.

1.8 Photochemical technology

The development of water treatment systems based on heterogeneous photocatalysis is an area of major technical importance. The main challenge consists in the design of efficient photocatalytic reactors for intermediate and large-scale use, as demanded by industrial and commercial applications [52]. In the design of photochemical reactors some aspects have to be taking into account: the selection of the radiation source including output power, source efficiency, spectral distribution, shape, dimensions, etc.; the design of reactor geometry with respect to the irradiation source; the design of reactor irradiation devices such as reflectors and mirrors, their construction materials, shape, dimensions and cleaning procedures.

Photocatalytic reactors for water treatment can be classified according to their design characteristics namely the state of the catalyst in the reactor (slurry or immobilized photoreactors), the type of irradiation source (natural or artificial) and the position of the light source (immersed or external). In a photochemical reactor the catalyst can be either suspended or attached to a support. In photocatalytic slurry reactors, the catalyst particles are suspended in the fluid phase (Fig. 1.7a). This type of reactor is the most popular for photocatalytic water treatment applications. Some of the advantages of the use of slurry photoreactors include the fairly uniform catalyst distribution, minimum catalyst fouling effects and practically no mass transfer limitations. However, in this type of configuration light scattering can occur, lowering the efficiency of the treatment process. In addition, a post-

process of catalyst separation is needed to isolate the catalyst particles from the treated water.

Immobilized photocatalytic reactors (Fig. 1.7b) allow the continuous use of the photocatalyst, eliminating the problem of the catalyst post-separation. In this type of reactors the catalyst can be coated on the reactor wall around the light source or be immobilized in fixed supports such as glass beads [53], polymers [54], cellulose fibers [55], etc. Main drawbacks of the use of this kind of reactors are the possibility of mass transfer limitations, catalyst fouling or wash-out, low surface to volume ratio and significant pressure drop.

Slurry photocatalytic systems usually show largest photocatalytic activity when compared to immobilized photocatalytic reactors [56].

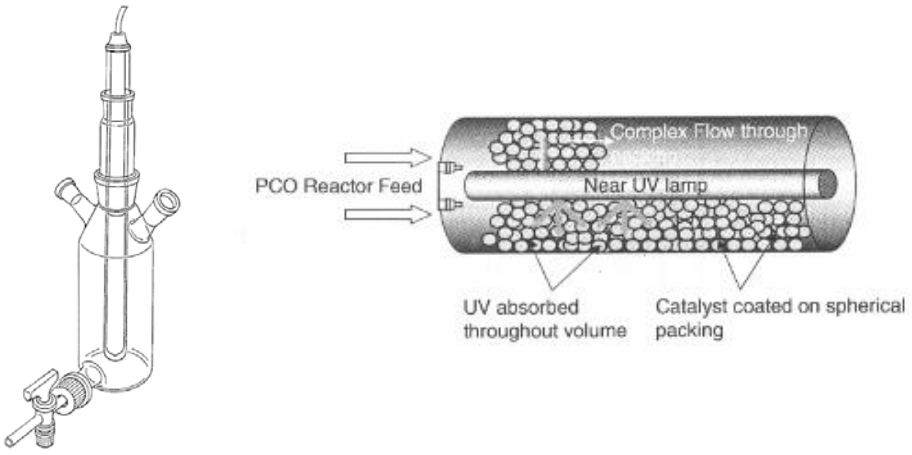

Figure 1.7 Photocatalytic reactors: (a) slurry reactor (source: *Heraeus* catalogue); (b) annular packed-bed reactor [52].

Efforts have been made to overcome photon and mass transfer limitations associated to traditional photocatalytic reactors. Therefore, not so conventional photoreactors such as optical fiber/hollow tube, monolith, spinning disc and microreactors have been investigated for their use in photocatalysis [57]. Increasing attention has being taken to recently developed photocatalytic microreactors (Fig. 1.8). The main advantage of this type of reactor is the high surface to volume ratio. In the case of photocatalytic reactions this implies efficient catalytic exposure to radiation and maximized reagent/catalyst contact. The small size of the channel also provides greater control over variables such as temperature and flow rates, due

to the fast heat and mass transfer, and the presence of laminar flow. The light source itself can also be UV-LED, thus miniaturizing the whole photocatalytic set-up. Obvious drawback is the relatively small throughput of microreactors.

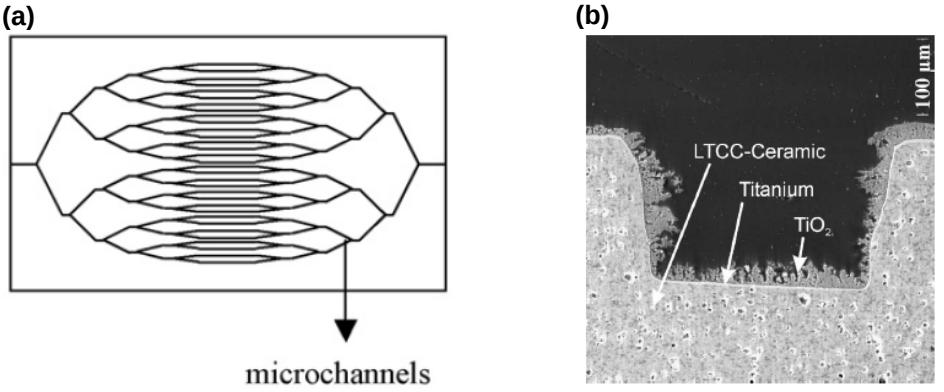

Figure 1.8 Photocatalytic microreactor: (a) overview of the microchannels [57]; (b) SEM micrograph of the cross-section of a microchannel [58].

Artificial radiation sources used in photocatalytic processes can be classified according to the emission spectra, power and geometry. Most common artificial light sources are arc lamps, incandescent lamps, fluorescent lamps and lasers [45]. Mercury vapor arc lamps are the most popular sources in photocatalytic applications. In this type of lamps, the mercury atoms are excited by means of an electric discharge between two electrodes, emitting light when returning to the ground state. The relative intensity of the emission lines depends on the pressure of the mercury vapor in the lamps. Three main types or mercury arc lamps are used: low pressure, medium pressure and high pressure.

In the low pressure mercury arc lamps the mercury pressure is between 10^{-3} and 10 mm Hg. These lamps have an emission line centered at 253.7 nm, which corresponds to the resonance line of mercury.

In medium and high pressure lamps, the mercury pressure varies between 1 and 100 atm, approximately. In these conditions, the mercury atoms are excited to different energy levels, resulting in the emission in a wide spectral range, from ultraviolet to visible.

When choosing the adequate light source for a certain application, three fundamental aspects have to be taken into account, being discussed in the

following. Firstly, in order to the photocatalytic reaction takes place, the emitted radiation has to be absorbed by the irradiated material. Therefore, the selection of the light source is dependent of the absorption spectra of the photocatalyst and/or the substrate to be degraded. The power of the lamp is the second item to be analyzed. This specification determines the flow of emitted photons and therefore, the photocatalytic reaction rate. The irradiation sources are commercially classified by their nominal electric power which does not correspond to their radiant power. A fraction of the electric power is normally dissipated as heat during the working period. The third factor to be taken in consideration is the geometrical configuration of the light source, which must fit the reactor geometry.

Instead of artificial light sources, solar radiation can also be used for photocatalytic reactions. The challenge is to collect and convert this dilute and intermittent energy to forms that are convenient and economical or to use solar photons in place of those from lamps, especially in countries with high insolation levels, in which Portugal is included (Fig. 1.9).

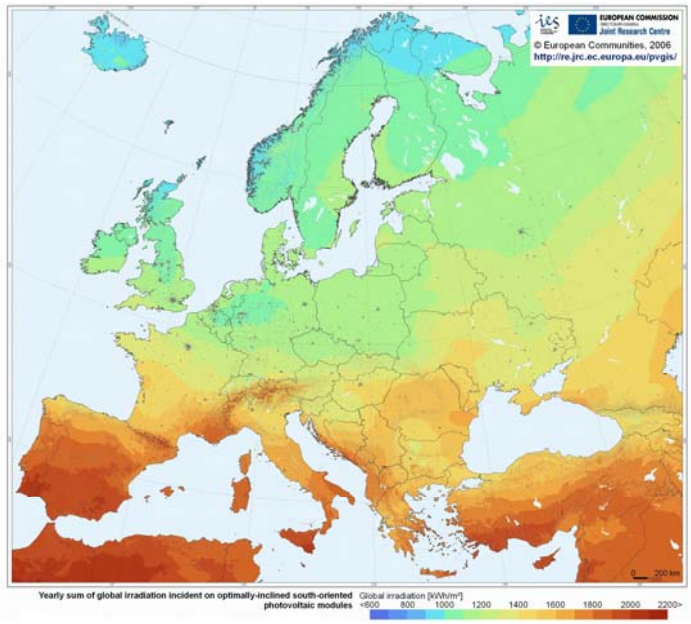

Figure 1.9 Yearly sum of global irradiation incident in European countries [59]. Global irradiation varying from less than 600 kWh/m^2 (dark blue) to more than 2200 kWh/m^2 (dark red).

Based on the photochemical properties of TiO_2, various types of reactors and solar collectors have been developed. One of the most impressive examples of the application of solar radiation for photocatalytic water treatment in a large scale is Plataforma Solar de Almeria in Spain [60]. There, compound parabolic collector (CPC) photoreactors, constituted by cylindrical tubes surrounded by static non-concentrator collectors, are used to treat contaminated water (Fig. 1.10).

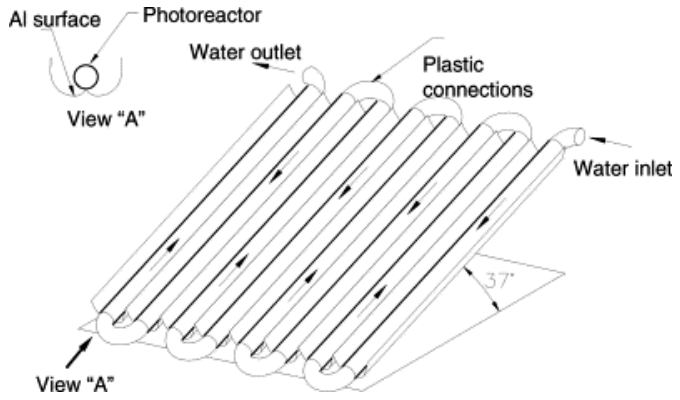

Figure 1.10 Scheme of the CPC photoreactor [60].

CPC photoreactor is of very simple conception, easy to operate and low installation and operation costs are required. The reflector design enables almost all the UV-radiation arriving at the CPC aperture (not only direct, but also diffuse) to be collected and available to the process in the reactor. The light reflected by the CPC is distributed around the back of the tubular photoreactor so that most of the reactor tube is illuminated. All these factors contribute to the excellent efficiency of this reactor configuration for photocatalytic applications [60]. Solar photocatalysis was baptized as "Heliophotocatalysis" by Jean-Marie Herrmann [7], the author of numerous scientific studies on photocatalysis.

1.9 Combination of photocatalysis with chemical and physical operations

To improve the overall performance of the photoprocess, heterogeneous photocatalysis has been combined with physical or chemical operations, which affect the chemical kinetics and/or the overall efficiency. This combination can either increase the photoefficiency and decrease the reaction time in respect to the

separated operations; or decrease the cost in respect to heterogeneous photocatalysis alone, generally in terms of light energy.

The application of heterogeneous photocatalysis may be divided in two main categories [61]: heterogeneous photocatalysis coupled with an operation that affects the photocatalytic mechanism thus improving the efficiency of the photocatalytic process; or heterogeneous photocatalytic processes coupled with an operation that does not affect the photocatalytic mechanism but improves the efficiency of the overall process. In the first, the coupling can be with ultrasonic irradiation, photo-Fenton reaction, ozonation or electrochemical treatment, while in the second option, photocatalytic processes can be coupled with biological treatment, membrane reactor, membrane photoreactor or physical adsorption.

1.10 Trends to improve TiO_2 activity

The overall photocatalytic activity of a particular semiconductor system for a stated purpose is measured by several factors including the stability of the semiconductor under illumination, the efficiency of the photocatalytic process and the wavelength of response. One of the most active fields of research in heterogeneous photocatalysis using semiconductor particles is the development of a system capable of using natural sunlight to degrade organic and inorganic pollutants in wastewater.

Although titanium dioxide is considered the catalyst of excellence in photocatalysis applications, in particular in the degradation of organic pollutants, three major limitations are normally quite restrictive to its efficient use: a) low photonic yield of the degradation process; b) a bandgap energy of 3.2 eV (corresponding to a wavelength of 388 nm) requiring excitation in the UV region for activation of the process, which is less than 10% of the overall solar intensity [13] (Fig. 1.11); c) in the case of liquid phase treatment, the use of suspensions requires a final step to separate the photocatalyst from the treated water.

Furthermore, the photocatalytic activity of TiO_2 largely depends on its surface and structural properties such as crystal structure, surface area, particle size distribution, porosity, bandgap and surface hydroxyl density.

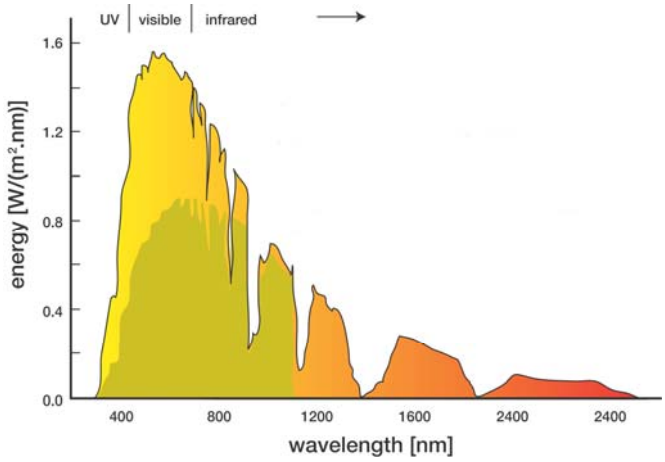

Figure 1.11 The solar spectrum.

In recent years a great deal of effort has been devoted to improve TiO_2 photocatalytic efficiency. For accomplish this purpose the main areas of activity are [62]:

i. incorporation of energy levels into the bandgap of titania;
ii. changing the life time of charge carriers;
iii. substitution of the Ti^{4+} with a cation of the same size;
iv. shifting the conduction band and/or valence band to enable photoexcitation at lower energies.

The major practices involve catalyst modification by doping metal and non-metal ions into the TiO_2 lattice, dye photosensitization, deposition of noble metals, mixing with other semiconductors and addition of inert supports.

1.10.1 TiO_2 doping

The chemical composition of TiO_2 can be altered by doping the semiconductor with metal and non-metal elements. Doping the semiconductor with transition metals may lead to an enhanced efficiency of the photocatalytic systems. Several studies dealing with this subject have been published, with titania being doped with several metal ions such as Sn^{4+}, Au^{3+}, Bi^{3+}, Mg^{2+}, Ba^{2+}, etc [63-66]. The main objective of doping is to induce a batho-chromic shift, *i.e.*, a decrease of the bandgap or introduction of intra-bandgap states, which results in more visible light absorption. The dopant ions may be adsorbed on the semiconductor catalyst, they

may be incorporated into the interior of the TiO_2 particle, or they may form separate oxide phases. The dopant ions can work as hole and electron traps or they can mediate interfacial charge transfer. Once incorporated into the interior of the titania particle, the dopant ions may occupy either lattice (substitutional) or interstitial sites. The site where the electron gets trapped greatly affects the redox chemistry of the doped semiconductor. A dopant ion might act as an electron trap, and this may in fact lead to a lengthening in the lifetime of the generated charge carriers, resulting in an enhancement in the photoactivity of the catalyst. However if an electron is trapped in a deep trapping site, it will have a longer lifetime, but it may also have lower redox potential, which may result in a decrease in the photoefficiency.

The effect of the addition of the dopant metal is largely influenced by its concentration in the TiO_2 matrix. As the concentration of the dopant increases, the space-charge region becomes narrower, with the electron/hole pairs within this region being efficiently separated by the large electric field before recombination. On the other hand, when the concentration is high, the space-charge region becomes very narrow and the penetration of light into TiO_2 greatly exceeds the space-charge layer. Therefore, the recombination of photogenerated electron/hole pairs in the semiconductor increases, because there is no driving force to separate them. Consequently, it can be said that there is an optimum concentration for doping ions [64, 66]. Nevertheless, some studies have demonstrated that in some cases electron/hole recombination is as fast or even faster than undoped TiO_2 [67]. p-Type dopants (heterocations of valences lower than Ti^{4+}) may act as acceptor centers, which trap photoelectrons and, once negatively charged, attract holes, thus forming recombination centers. On the opposite, n-type dopants (heterocations with valences higher than Ti^{4+}) may act as donor centers. By increasing the concentration of conduction electrons, they also favor electron/hole recombination, which is detrimental for the photoefficiency.

Various non-metal elements, such as B, C, N, V and S have been successfully doped into TiO_2 nanomaterials [68-70]. The bulk or surface modification of titania by these elements generates localized electronic states (surface states) close to the valence band edge, producing a red-shift in the semiconductor absorption.

1.10.2 Metal deposition

In photocatalysis the addition of a metal to a semiconductor can change the photocatalytic process by changing the semiconductor surface properties. If the work function of the metal is higher than that of titania, electrons are removed from the TiO_2 particles in the vicinity of each metal particle. This results in the formation of a Schottky barrier at each metal-semiconductor region, which leads to a decrease in the electron/hole recombination, as well as to an efficient charge separation [13]. As a consequence of the improved separation of electrons and holes, metal deposition on the TiO_2 surface enhances photocatalytic reactions by accelerating the transfer of electrons to dissolved oxygen molecules. Therefore, deposition of group III metals, oxygen reduction catalysts, or noble metals on the photocatalyst surface, should increase the electron transfer rate to oxygen and thereby the quantum yield. Also, it was observed that there is an optimum metal content above which the efficiency of the photocatalytic process actually decreases. At these conditions, the metal particles can act as recombination centers, thereby decreasing the activity of TiO_2.

The enhancement in TiO_2 reactivity was first observed for the photoconversion of H_2O to H_2 and O_2 using the Pt/TiO_2 system [71]. There are many examples in the literature of the doping of titania with metals such as Ag, Pd, Cr, Fe, Cu, Pt, etc. [72-75].

1.10.3 Surface sensitization

Surface sensitization of a wide bandgap semiconductor photocatalyst like TiO_2 through chemisorbed or physisorbed dyes/metal complexes is able to increase the efficiency of the excitation process. Also, photosensitization of a semiconductor can expand the used wavelength range by excitation of the sensitizer followed by charge transfer between the excited dye and the semiconductor conduction band.

Depending on its redox environment, the dye is able to donate (in most cases) or receive an electron, improving electron/hole separation. If the oxidative energy level of the excited state of the dye molecule with respect to the conduction band energy level of the semiconductor is favorable, *i.e.* more negative, then the dye molecule can transfer the electron to the conduction band of the semiconductor. The surface acts as a quencher accepting an electron form the excited dye molecule.

The electron can in turn be transferred to reduce an organic acceptor molecule adsorbed on the surface or react with surface adsorbed O_2 to yield $O_2^{\bullet -}$, which can undergo protonation to form $HO_2^{\bullet}$. Both radicals are capable to initiate the degradation of organic substrates.

Although there are some studies with dye/metal complex sensitized TiO_2 for photocatalytic degradation reactions [76, 77], is in the field of energy production that TiO_2 dye sensitization plays it most important role [78, 79]. Dye-sensitized solar cells have attracted a great deal of interest because of their relatively higher efficiency and low cost compared with conventional inorganic photovoltaic devices. The most efficient dye-sensitized solar cells to date are based on ruthenium-containing metallorganic dyes adsorbed on nanocrystalline TiO_2, the best of which have been reported to convert solar energy to electrical energy with an efficiency of 10–11% [80, 81].

1.10.4 Dual semiconductor systems

The coupling of two semiconductors, possessing different energy levels for their corresponding conduction and valence bands, provides a more efficient charge separation, an increase in the life time of the charge carriers and an enhanced interfacial charge transfer to adsorbed substrates. A possible way out consists in coupling a large bandgap semiconductor with a smaller bandgap semiconductor presenting suitable potential energies. For example, in CdS/TiO_2 the photogenerated electrons in CdS are transferred into the TiO_2 particles while the holes remain in the CdS particle. This not only helps for charge separation by isolating electrons and holes in two distinct particles but at the same time, allows the extension of the photoresponse of the photocatalyst in the visible [82].

Two different mechanisms can occur: only one semiconductor is illuminated and the second is non-activated or both are illuminated. In the first case, a photoelectron generated on the activated semiconductor with a more negative conduction band is injected into the conduction band of the inactivated semiconductor, while the photo-hole remains on the activated one. When both semiconductors are illuminated, electrons and holes are transferred from one semiconductor to another. As a result, electrons are accumulated at the lower lying conduction band of one semiconductor, while the holes accumulate at the valence band of the other semiconductor.

Coupled semiconductors have been used intensively for organic degradation in both aqueous and gas phase, including TiO_2/CdS, TiO_2/SnO_2, TiO_2/ZnO and TiO_2/WO_3 [82, 83]. In general, the coupled systems exhibit higher degradation rate as well as the increased extent of degradation.

1.10.5 TiO_2 composite catalysts

Different supports and immobilization techniques have been investigated for TiO_2 catalysts. Composite TiO_2 based materials can be obtained either by coupling the previously prepared TiO_2 with a support or by *in situ* generation. The first route can be performed by using various techniques such as spray coating, immobilization in a polymer matrix and electrophoretic deposition in various supports. The second route consists in the coating of a support and simultaneous TiO_2 synthesis by sol-gel technique, chemical vaporization of $TiCl_4$, etc.

The strategies focused on supported TiO_2 are developed in order to:

i. immobilize the TiO_2 photocatalyst;
ii. increase the illuminated specific catalyst area;
iii. increase the adsorption capacity and the surface area of the photocatalyst;
iv. increase the activity by creating synergies between TiO_2 and the support;
v. facilitate the separation of the catalyst, when using slurry type reactors.

The first two demands result from the requirement to use the photocatalyst in a continuous process, when utilization of TiO_2 powders is technologically impracticable.

The small particle size of titania particles leads to high filtration costs, hindering its industrial application. For this reason, the synthesis of TiO_2-based composite photocatalysts with high activity and effective separation properties simultaneously constitutes a priority topic. If we can add to these characteristics the capacity of the support to interact with titania producing a beneficial effect in its photo-efficiency, then a catalyst with special features for photocatalytic degradation processes will be obtained.

High surface area materials have been used to prepare TiO_2 composite catalysts, since they can work as co-adsorbents in the photocatalytic reaction process. Materials such as silica [84, 85], alumina [86], zeolites [87], mesoporous molecular sieves [88], clays [89], activated carbon [34, 90, 91], carbon fibers [92, 93] and carbon nanotubes [94-98], have been used to prepare TiO_2-based composite catalysts.

Among these materials, carbon nanotubes have attracted considerable attention in recent years. Carbon nanotubes have recently been determined to be more attractive catalyst supports than activated carbons, because their combination of electronic, adsorption, mechanical and thermal properties [99]. Several studies have shown that carbon nanotubes-TiO_2 composite catalysts prepared by different techniques such as impregnation [100], hydrolysis in supercritical ethanol [101], chemical vapor deposition [102] hydrothermal and sol-gel methods [96-98, 103], exhibit better photoactivities than pure TiO_2 under UV or visible light illumination. The assumable reasons for these phenomena can be explained by the role of carbon nanotubes as photosensitizers for visible-light response and, at the same time, as photoinduced electron traps, drastically reducing the electron/hole recombination. A detailed study about carbon nanotube-TiO_2 composite catalysts for the photocatalytic degradation of aromatic pollutants under visible irradiation will be presented in this work.

1.11 Aim of this work and thesis outline

Treatment systems for water and air based in semiconductor heterogeneous photocatalysis represent an area of major technical importance in our days. The use of TiO_2 nanoparticles for the catalytic degradation of water pollutants was recently recognized by an international panel to be one of the top ten applications of nanotechnology, most likely to benefit developing countries [104]. However, heterogeneous photocatalytic systems based in TiO_2 catalysts show some limitations that reduce their impact in the domain of environmental protection. Two of the most important limitations of the photocatalytic process are the low photonic yield and the little efficiency under visible light ($300\ nm < \lambda < 600\ nm$). Those limitations have recently been the source of the great development in the area of the production and characterization of TiO_2-based photocatalysts, capable of being efficiently used under visible irradiation or showing a higher photochemical yield in

the near UV. In this sense, TiO_2 intrinsic parameters like particle and crystallite dimensions, crystalline nature and hydroxylation degree will be object of study. Being aware of the importance of these findings for environmental applications, mainly in regions with high solar exposition, the main objectives of the present research work are the following:

i. Synthesis and characterization of nanostructured TiO_2 based photocatalysts;
ii. Utilization of several materials as supports for TiO_2 nanoparticles in order to increase the photo-efficiency of the semiconductor;
iv. Photocatalytic oxidation of organic pollutants in aqueous suspensions using the prepared catalysts under different irradiation wavelengths;
v. Description of the photocatalytic oxidation mechanisms.

The extensive characterization of the developed photocatalytic systems (catalysts, organic pollutants and operational parameters), opens the possibility of its utilization in larger scale applications. The present work is based mainly in the utilization of high resolution techniques for the characterization of the synthesized materials and *in situ* monitoring of the photocatalytic oxidation reactions, by identification and quantification of main intermediates and reaction products.

The present thesis is organized in eight chapters divided by five main parts. This introductory chapter is contained in Part I. Part II, containing Chapters 2 and 3, reports the production, characterization and use of nanocrystalline TiO_2 materials for photocatalytic application. The development of TiO_2 based composite catalysts is described in the third part, constituted by Chapter 4. Part IV deals with the preparation, characterization and testing of carbon nanotube-TiO_2 composite catalysts in the photocatalytic degradation of several aromatic molecules. These results are presented in Chapters 5 and 6. Part V deals with the suggestions for future work and conclusions, presented in Chapters 7 and 8. A detailed description is presented in the following.

In Chapter 2 is described the synthesis of nanocrystalline TiO_2 catalysts using an acid catalyzed sol-gel method. Materials are extensively characterized by spectroscopic, microscopic and thermogravimetric techniques. The effect of the calcination temperature in the physical-chemical properties of the obtained materials is discussed.

Materials described in Chapter 2 were used in the photocatalytic degradation of phenol under UV irradiation and results concerning this subject are shown in Chapter 3. The effect of operational parameters on the efficiency of the

photodegradation process is discussed namely catalysts concentration, pH of the medium, phenol initial concentration, photon flux, presence of oxidant species and oxygen partial pressure. A kinetic and mechanistic study based on the detected intermediates is proposed.

Chapter 4 reports the synthesis, characterization and use of nanostructured TiO_2-based materials prepared using different materials: zeolite NaY, mesoporous molecular sieves MCM41 and MCM48, activated carbon, activated carbon fibers and multi-walled carbon nanotubes. The degradation of phenol using the prepared composite catalysts under visible light is described in this chapter.

Detailed characterization of carbon nanotube-TiO_2 composite materials is presented in Chapter 5. Results on the photocatalytic degradation of phenol under visible light using nanocomposites with different carbon nanotube content, surface chemistries and irradiation wavelengths are presented in this chapter. Also, results on the degradation of mono-substituted benzene derivatives are presented.

Chapter 6 reports the photocatalytic degradation of several mono-substituted phenols using a carbon nanotube-TiO_2 composite catalyst and the effect of operational parameters in the degradation process efficiency.

An explorating study on the photocatalytic oxidation of clofibric acid, a current lipid regulator drug, under visible irradiation using nanocrystalline sol-gel TiO_2 catalysts is described in Chapter 7, as possible initiator for future work.

Finally, Chapter 8 is dedicated to the concluding remarks and suggestions for future work.

1.12 References

[1] Water withdrawal by sector in the regions of the world, *http://www.unescap.org/stat/data/syb2007/26-Water-use-syb2007.asp*. United Nations ESCAP, accessed at 2008/08/07.

[2] Commission of the European Communities. *Directive of the European Parliament and of the Council on environmental quality Standards in the field of water policy and amending Directive 2000/60/EC. COM(2006) 397* final, Brussels, July 2006.

[3] R. Andreozzi, V. Caprio, A. Insola, R. Marotta, *Advanced oxidation processes (AOP) for water purification and recovery*, Catal. Today. 53 (1999) 51-59.

[4] M.A. Fox, M.T. Dulay, *Heterogeneous photocatalysis*, Chem. Rev. 93 (1993) 341-357.

[5] A. Fujishima, X. Zhang, D.A. Tryk, *Heterogeneous photocatalysis: from water photolysis to applications in environmental cleanup*, Int. J. Hydrog. Energy. 32 (2007) 2664-2672.

[6] P.R. Gogate, A.B. Pandit, *A review of imperative technologies for wastewater treatment I: oxidation technologies at ambient conditions*, Adv. Emviron. Res. 8 (2004) 501-551.

[7] J.M. Herrmann, *Heterogeneous photocatalysis: State of the art and present applications*, Top. Catal. 34 (2005) 49-65.

[8] A. Mills, S. LeHunte, *An overview of semiconductor photocatalysis*, J. Photochem. Photobiol. A: Chem. 108 (1997) 1-35.

[9] G. Palmisano, V. Augugliaro, M. Pagliaro, L. Palmisano, *Photocatalysis: a promising route for 21st century organic chemistry*, Chem. Commun. (2007) 3425-3437.

[10] A. Fujishima, K. Honda, *Electrochemical photolysis of water at a semiconductor electrode*, Nature. 238 (1972) 37-38.

[11] J.H. Carey, J. Lawrence, H.M. Tosine, *Photodechlorination of PCB's in the presence of titanium dioxide in aqueous suspensions* Bull. Environ. Contam. Toxicol. 16 (1976) 697-701.

[12] S.E. Braslavsky, *Glossary of terms used in photochemistry 3rd Edition (IUPAC Recommendations 2006)*, Pure Appl. Chem. 79 (2007) 293-465.

[13] A.L. Linsebigler, G.Q. Lu, J.T. Yates, *Photocatalysis on TiO_2 surfaces - principles, mechanisms, and selected results*, Chem. Rev. 95 (1995) 735-758.

[14] D.S. Bhatkhande, V.G. Pangarkar, A. Beenackers, *Photocatalytic degradation for environmental applications - a review*, J. Chem. Technol. Biotechnol. 77 (2002) 102-116.

[15] O. Carp, C.L. Huisman, A. Reller, *Photoinduced reactivity of titanium dioxide*, Prog. Solid State Chem. 32 (2004) 33-177.

[16] D. Beydoun, R. Amal, G. Low, S. McEvoy, *Role of nanoparticles in photocatalysis*, Jounal of Nanoparticle Research. 1 (1999) 439-458.

[17] B. Neppolian, H.C. Choi, S. Sakthivel, B. Arabindoo, V. Murugesan, *Solar/UV-induced photocatalytic degradation of three commercial textile dyes*, J. Hazard. Mater. 89 (2002) 303-317.

[18] E. Reck, M. Richards, *TiO_2 manufacture and life cycle analysis*, Pigm. Resin. Technol. 28 (1999) 149-157.

[19] H. Sun, C. Wang, S. Pang, X. Li, Y. Tao, H. Tang, M. Liu, *Photocatalytic TiO_2 films prepared by chemical vapor deposition at atmosphere pressure*, J. Non-Cryst. Solids. 354 (2008) 1440-1443.

[20] C. Giolli, F. Borgioli, A. Credi, A.D. Fabio, A. Fossati, M.M. Miranda, S. Parmeggiani, G. Rizzi, A. Scrivani, S. Troglio, A. Tolstoguzov, A. Zoppi, U. Bardi, *Characterization of TiO_2 coatings prepared by a modified electric arc-physical vapour deposition system*, Surf. Coat. Technol. 202 (2007) 13-22.

[21] I. Oja, A. Mere, M. Krunks, R. Nisumaa, C.H. Solterbeck, M. Es-Souni, *Structural and electrical characterization of TiO_2 films grown by spray pyrolysis*, Thin Solid Films. 515 (2006) 674-677.

[22] X. Zhao, X. Liu, C. Ding, P.K. Chu, *Effects of plasma treatment on bioactivity of TiO_2 coatings*, Surf. Coat. Technol. 201 (2007) 6878-6881.

[23] I. Turkevych, Y. Pihosh, M. Goto, A. Kasahara, M. Tosa, S. Kato, K. Takehana, T. Takamasu, G. Kido, N. Koguchi, *Photocatalytic properties of titanium dioxide sputtered on a nanostructured substrate*, Thin Solid Films. 516 (2008) 2387-2391.

[24] X. Weng, P. Fisher, M. Skowronski, P.A. Salvador, O. Maksimov, *Structural characterization of TiO_2 films grown on $LaAlO_3$ and $SrTiO_3$ substrates using reactive molecular beam epitaxy*, J. Cryst. Growth. 310 (2008) 545-550.

[25] N.K. Huang, D.Z. Wang, Z. Lu, L.B. Lin, *X-Ray photoelectron-spectroscopy characterization of TiO_2 films deposited by dynamic ion-beam mixing*, Surf. Coat. Technol. 70 (1994) 69-71.

[26] J.H. Lee, Y.S. Yang, *Effect of hydrolysis conditions on morphology and phase content in the crystalline TiO_2 nanoparticles synthesized from aqueous $TiCl_4$ solution by precipitation*, Mater. Chem. Phys. 93 (2005) 237-242.

[27] M. Bellardita, M. Addamo, A. Di Paola, L. Palmisano, *Photocatalytic behaviour of metal-loaded TiO_2 aqueous dispersions and films*, Chem. Phys. 339 (2007) 94-103.

[28] M.C. Hidalgo, M. Aguilar, M. Maicu, J.A. Navío, G. Colón, *Hydrothermal preparation of highly photoactive TiO_2 nanoparticles*, Catal. Today. 129 (2007) 50-58.

[29] R.C. Xie, J.K. Shang, *Morphological control in solvothermal synthesis of titanium oxide*, J. Mater. Sci. 42 (2007) 6583-6589.

[30] M. Andersson, A. Kiselev, L. Osterlund, A.E.C. Palmqvist, *Microemulsion-mediated room-temperature synthesis of high-surface-area rutile and its photocatalytic performance*, J. Phys. Chem. C. 111 (2007) 6789-6797.

[31] Y. Kitamura, N. Okinaka, T. Shibayama, O.O.P. Mahaney, D. Kusano, B. Ohtani, T. Akiyama, *Combustion synthesis of TiO_2 nanoparticles as photocatalyst*, Powder Technol. 176 (2007) 93-98.

[32] B.R. Sankapal, S.D. Sartale, M.C. Lux-Steiner, A. Ennaoui, *Chemical and electrochemical synthesis of nanosized TiO_2 anatase for large-area photon conversion*, C. R. Chim. 9 (2006) 702-707.

[33] Y.V. Kolen´ko, A.V. Garshev, B.R. Churagulov, S. Boujday, P. Portes, C. Colbeau-Justin, *Photocatalytic activity of sol-gel derived titania converted into nanocrystalline powders by supercritical drying*, J. Photochem. Photobiol. A: Chem. 172 (2005) 19-26.

[34] W.D. Wang, C.G. Silva, J.L. Faria, *Photocatalytic degradation of Chromotrope 2R using nanocrystalline TiO_2/activated-carbon composite catalysts*, Appl. Catal. B: Environ. 70 (2007) 470-478.

[35] T. Tong, J. Zhang, B. Tian, F. Chen, D. He, *Preparation of Fe^{3+}-doped TiO_2 catalysts by controlled hydrolysis of titanium alkoxide and study on their photocatalytic activity for methyl orange degradation*, J. Hazard. Mater. 155 (2008) 572-579.

[36] S. Sivakumar, C.P. Sibu, P. Mukundan, P.K. Pillai, K.G.K. Warrier, *Nanoporous titania-alumina mixed oxides - an alkoxide free sol-gel synthesis*, Mater. Lett. 58 (2004) 2664-2669.

[37] K. Pan, Q. Zhang, Q. Wang, Z. Liu, D. Wang, J. Li, Y. Bai, *The photoelectrochemical properties of dye-sensitized solar cells made with TiO_2 nanoribbons and nanorods*, Thin Solid Films. 515 (2007) 4085-4091.

[38] Y.X. Zhang, G.H. Li, Y.X. Jin, Y. Zhang, J. Zhang, L.D. Zhang, *Hydrothermal synthesis and photoluminescence of TiO_2 nanowires*, Chem. Phys. Lett. 365 (2002) 300-304.

[39] J.M. Macak, H. Tsuchiya, A. Ghicov, K. Yasuda, R. Hahn, S. Bauer, P. Schmuki, *TiO_2 nanotubes: Self-organized electrochemical formation, properties and applications*, Curr. Opin. Solid State Mat. Sci. 11 (2007) 3-18.

[40] Y.C. Zhu, C.X. Ding, *Oriented growth of nano-TiO_2 whiskers*, Nanostruct. Mater. 11 (1999) 427-431.

[41] A. Mills, N. Elliott, G. Hill, D. Fallis, J.R. Durrant, R.L. Willis, *Preparation and characterisation of novel thick sol-gel titania film photocatalysts*, Photochem. Photobiol. Sci. 2 (2003) 591-596.

[42] M.R. Hoffmann, S.T. Martin, W.Y. Choi, D.W. Bahnemann, *Environmental applications of semiconductor photocatalysis*, Chem. Rev. 95 (1995) 69-96.

[43] A.C. van Dyk, A.M. Heyns, *Dispersion stability and photo-activity of rutile (TiO_2) powders*, J. Colloid Interface Sci. 206 (1998) 381-391.

[44] D. Chen, A.K. Ray, *Photocatalytic kinetics of phenol and its derivatives over UV irradiated TiO_2*, Appl. Catal. B: Environ. 23 (1999) 143-157.

[45] A.M. Braun, M.T. Maurette, E. Oliveros, *Photochemical Technology*, ed. J.W. Sons (1991), Chichester, England.

[46] D.F. Ollis, *Kinetics of liquid phase photocatalyzed reactions: an illuminating approach*, J. Phys. Chem. B. 109 (2005) 2439-2444.

[47] R.R. Bacsa, J. Kiwi, *Effect of rutile phase on the photocatalytic properties of nanocrystalline titania during the degradation of p-coumaric acid*, Appl. Catal. B: Environ. 16 (1998) 19-29.

[48] J.A. Ayllón, A. Figueras, S. Garelik, L. Spirkova, J. Durand, L. Cot, *Preparation of TiO_2 powder using titanium isopropoxide decomposition in a plasma enhanced chemical vapor deposition (PECVD) reactor*, J. Mater. Sci. Lett. 18 (1999) 1319-1321.

[49] B. Ohtani, Y. Ogawa, S. Nishimoto, *Photocatalytic activity of amorphous-anatase mixture of titanium(IV) oxide particles suspended in aqueous solutions*, J. Phys. Chem. B. 101 (1997) 3746-3752.

[50] Z. Zhang, C.-C. Wang, R. Zakaria, J.Y. Ying, *Role of particle size in nanocrystalline TiO_2-based photocatalysts*, J. Phys. Chem. B. 102 (1998) 10871-10878.

[51] X. Li, X. Quan, C. Kutal, *Synthesis and photocatalytic properties of quantum confined titanium dioxide nanoparticle*, Scr. Mater. 50 (2004) 499-505.

[52] H.d. Lasa, B. Serrano, M. Salaices, *Photocatalytic Reaction Engineering* (2005), New York Springer.

[53] C.-S. Chiou, J.-L. Shie, C.-Y. Chang, C.-C. Liu, C.-T. Chang, *Degradation of di-n-butyl phthalate using photoreactor packed with TiO_2 immobilized on glass beads*, J. Hazard. Mater. 137 (2006) 1123-1129.

[54] Y. Zhiyong, D. Laub, M. Bensimon, J. Kiwi, *Flexible polymer TiO_2 modified film photocatalysts active in the photodegradation of azo-dyes in solution*, Inorg. Chim. Acta. 361 (2008) 589-594.

[55] B. Mounir, M.N. Pons, O. Zahraa, A. Yaacoubi, A. Benhammou, *Discoloration of a red cationic dye by supported TiO_2 photocatalysis*, Journal of Hazardous Materials. 148 (2007) 513-520.

[56] G. Mascolo, R. Comparelli, M.L. Curri, G. Lovecchio, A. Lopez, A. Agostiano, *Photocatalytic degradation of methyl red by TiO_2: comparison of the efficiency of immobilized nanoparticles versus conventional suspended catalyst*, J. Hazard. Mater. 142 (2007) 130-137.

[57] T. Van Gerven, G. Mul, J. Moulijn, A. Stankiewicz, *A review of intensification of photocatalytic processes*, Chem. Eng. Process. 46 (2007) 781-789.

[58] R. Gorges, S. Meyer, G. Kreisel, *Photocatalysis in microreactors*, J. Photochem. Photobiol. A: Chem. 167 (2004) 95-99.

[59] Yearly sum of global irradiation incident in European countries, *http://re.jrc.ec.europa.eu/pvgis/countries/europe.htm#Europe*, European Comission - Joint Research Centre, accessed at 2008/08/07.

[60] S. Malato, J. Blanco, A. Vidal, C. Richter, *Photocatalysis with solar energy at a pilot-plant scale: an overview*, Appl. Catal. B: Environ. 37 (2002) 1-15.

[61] V. Augugliaro, M. Litter, L. Palmisano, J. Soria, *The combination of heterogeneous photocatalysis with chemical and physical operations: A tool for improving the photoprocess performance*, J. Photochem. Photobiol. C: Photochem. Rev. 7 (2006) 127-144.

[62] U.I. Gaya, A.H. Abdullah, *Heterogeneous photocatalytic degradation of organic contaminants over titanium dioxide: A review of fundamentals, progress and problems*, J. Photochem. Photobiol. C: Photochem. Rev. 9 (2008) 1-12.

[63] Y.A. Cao, W.S. Yang, W.F. Zhang, G.Z. Liu, P.L. Yue, *Improved photocatalytic activity of Sn^{4+} doped TiO_2 nanoparticulate films prepared by plasma-enhanced chemical vapor deposition*, New J. Chem. 28 (2004) 218-222.

[64] F.B. Li, X.Z. Li, *Photocatalytic properties of gold/gold ion-modified titanium dioxide for wastewater treatment*, Appl. Catal. A: Gen. 228 (2002) 15-27.

[65] N. Venkatachalam, M. Palanichamy, V. Murugesan, *Sol-gel preparation and characterization of alkaline earth metal doped nano TiO_2: Efficient photocatalytic degradation of 4-chlorophenol*, J. Mol. Catal. A: Chem. 273 (2007) 177-185.

[66] J. Yu, S. Liu, Z. Xiu, W. Yu, G. Feng, *Combustion synthesis and photocatalytic activities of Bi^{3+}-doped TiO_2 nanocrystals*, J. Alloy. Compd. 461 (2008) L17-L19.

[67] B.A. Smith, D.M. Waters, A.E. Faulhaber, M.A. Kreger, T.W. Roberti, J.Z. Zhang, *Preparation and ultrafast optical characterization of metal and semiconductor colloidal nano-particles*, J. Sol-Gel Sci. Technol. 9 (1997) 125-137.

[68] M. Bettinelli, V. Dallacasa, D. Falcomer, P. Fornasiero, V. Gombac, T. Montini, L. Romanò, A. Speghini, *Photocatalytic activity of TiO_2 doped with boron and vanadium*, J. Hazard. Mater. 146 (2007) 529-534.

[69] C. Burda, Y.B. Lou, X.B. Chen, A.C.S. Samia, J. Stout, J.L. Gole, *Enhanced nitrogen doping in TiO_2 nanoparticles*, Nano Lett. 3 (2003) 1049-1051.

[70] D.B. Hamal, K.J. Klabunde, *Synthesis, characterization, and visible light activity of new nanoparticle photocatalysts based on silver, carbon, and sulfur-doped TiO_2*, J. Colloid Interface Sci. 311 (2007) 514-522.

[71] S. Sato, J.M. White, *Photo-Decomposition of Water over Pt-TiO_2 Catalysts*, Chem. Phys. Lett. 72 (1980) 83-86.

[72] N. Sobana, M. Muruganadham, M. Swaminathan, *Nano-Ag particles doped TiO_2 for efficient photodegradation of Direct azo dyes*, J. Mol. Catal. A: Chem. 258 (2006) 124-132.

[73] C.-G. Wu, C.-C. Chao, F.-T. Kuo, *Enhancement of the photo catalytic performance of TiO_2 catalysts via transition metal modification*, Catal. Today. 97 (2004) 103-112.

[74] J. Araña, J.M. Doña-Rodríguez, O. González-Díaz, E. Tello Rendón, J.A. Herrera Melián, G. Colón, J.A. Navío, J. Pérez Peña, *Gas-phase ethanol photocatalytic degradation study with TiO_2 doped with Fe, Pd and Cu*, J. Mol. Catal. A: Chem. 215 (2004) 153-160.

[75] G.N. Kryukova, G.A. Zenkovets, A.A. Shutilov, M. Wilde, K. Günther, D. Fassler, K. Richter, *Structural peculiarities of TiO_2 and Pt/TiO_2 catalysts for the photocatalytic oxidation of aqueous solution of Acid Orange 7 Dye upon ultraviolet light*, Appl. Catal. B: Environ. 71 (2007) 169-176.

[76] J. Moon, C.Y. Yun, K.-W. Chung, M.-S. Kang, J. Yi, *Photocatalytic activation of TiO_2 under visible light using Acid Red 44*, Catal. Today. 87 (2003) 77-86.

[77] Z. Wang, W. Mao, H. Chen, F. Zhang, X. Fan, G. Qian, *Copper(II) phthalocyanine tetrasulfonate sensitized nanocrystalline titania photocatalyst: Synthesis in situ and photocatalysis under visible light*, Catal. Commun. 7 (2006) 518-522.

[78] C. Li, X. Yang, R. Chen, J. Pan, H. Tian, H. Zhu, X. Wang, A. Hagfeldt, L. Sun, *Anthraquinone dyes as photosensitizers for dye-sensitized solar cells*, Sol. Energy Mater. Sol. Cells. 91 (2007) 1863-1871.

[79] X. Ma, J. Hua, W. Wu, Y. Jin, F. Meng, W. Zhan, H. Tian, *A high-efficiency cyanine dye for dye-sensitized solar cells*, Tetrahedron. 64 (2008) 345-350.

[80] M.K. Nazeeruddin, A. Kay, I. Rodicio, R. Humphrybaker, E. Muller, P. Liska, N. Vlachopoulos, M. Gratzel, *Conversion of light to electricity by cis-X2bis(2,2'-Bipyridyl-4,4'-Dicarboxylate)Ruthenium(Ii) charge-transfer sensitizers ($X = Cl^-, Br^-, I^-, Cn^-$, and Scn^-) on nanocrystalline TiO_2 electrodes*, J. Am. Chem. Soc. 115 (1993) 6382-6390.

[81] A.S. Polo, M.K. Itokazu, N.Y. Murakami Iha, *Metal complex sensitizers in dye-sensitized solar cells*, Coord. Chem. Rev. 248 (2004) 1343-1361.

[82] Y. Bessekhouad, N. Chaoui, M. Trzpit, N. Ghazzal, D. Robert, J.V. Weber, *UV-vis versus visible degradation of Acid Orange II in a coupled CdS/TiO_2 semiconductors suspension*, J. Photochem. Photobiol. A: Chem. 183 (2006) 218-224.

[83] C.-F. Lin, C.-H. Wu, Z.-N. Onn, *Degradation of 4-chlorophenol in TiO_2, WO_3, SnO_2, TiO_2/WO_3 and TiO_2/SnO_2 systems*, J. Hazard. Mater. 154 (2008) 1033-1039.

[84] M.-J. López-Muñoz, R.v. Grieken, J. Aguado, J. Marugán, *Role of the support on the activity of silica-supported TiO_2 photocatalysts: Structure of the TiO_2/SBA-15 photocatalysts*, Catal. Today. 101 (2005) 307-314.

[85] P. Pucher, M. Benmami, R. Azouani, G. Krammer, K. Chhor, J.F. Bocquet, A.V. Kanaev, *Nano-TiO_2 sols immobilized on porous silica as new efficient photocatalyst*, Appl. Catal. A: Gen. 332 (2007) 297-303.

[86] A.R. Torres, E.B. Azevedo, N.S. Resende, M. Dezotti, *A comparison between bulk and supported TiO_2 photocatalysts in the degradation of formic acid*, Braz. J. Chem. Eng. 24 (2007) 185-192.

[87] A. Bhattacharyya, S. Kawi, M.B. Ray, *Photocatalytic degradation of orange II by TiO2 catalysts supported on adsorbents*, Catal. Today. 98 (2004) 431-439.

[88] X. Wang, W. Lian, X. Fu, J.-M. Basset, F. Lefebvre, *Structure, preparation and photocatalytic activity of titanium oxides on MCM-41 surface*, J. Catal. 238 (2006) 13-20.

[89] J. Ménesi, L. Körösi, É. Bazsó, V. Zöllmer, A. Richardt, I. Dékány, *Photocatalytic oxidation of organic pollutants on titania-clay composites*, Chemosphere. 70 (2008) 538-542.

[90] A.H. El-Sheikh, A.P. Newman, H. Al-Daffaee, S. Phull, N. Cresswell, S. York, *Deposition of anatase on the surface of activated carbon*, Surf. Coat. Technol. 187 (2004) 284-292.

[91] B. Tryba, A.W. Morawski, M. Inagaki, *A new route for preparation of TiO_2-mounted activated carbon*, Appl. Catal. B: Environ. 46 (2003) 203-208.

[92] Z. Liuxue, L. Peng, S. Zhixing, *Photocatalysis anatase thin film coated PAN fibers prepared at low temperature*, Mater. Chem. Phys. 98 (2006) 111-115.

[93] R. Yuan, R. Guan, P. Liu, J. Zheng, *Photocatalytic treatment of wastewater from paper mill by TiO_2 loaded on activated carbon fibers*, Colloid Surf. A: Physicochem. Eng. Asp. 293 (2007) 80-86.

[94] Q. Huang, L. Gao, *Immobilization of rutile TiO_2 on multiwalled carbon nanotubes*, J. Mater. Chem. 13 (2003) 1517-1519.

[95] A. Jitianu, T. Cacciaguerra, R. Benoit, S. Delpeux, F. Béguin, S. Bonnamy, *Synthesis and characterization of carbon nanotubes-TiO_2 nanocomposites*, Carbon. 42 (2004) 1147-1151.

[96] W. Wang, P. Serp, P. Kalck, J.L. Faria, *Photocatalytic degradation of phenol on MWNT and titania composite catalysts prepared by a modified sol-gel method*, Appl. Catal. B: Environ. 56 (2005) 305-312.

[97] W. Wang, P. Serp, P. Kalck, J.L. Faria, *Visible light photodegradation of phenol on MWNT-TiO_2 composite catalysts prepared by a modified sol-gel method*, J. Mol. Catal. A: Chem. 235 (2005) 194-199.

[98] W. Wang, P. Serp, P. Kalck, C.G. Silva, J.L. Faria, *Preparation and characterization of nanostructured MWCNT-TiO_2 composite materials for photocatalytic water treatment applications*, Mater. Res. Bull. 43 (2008) 958-967.

[99] P. Serp, M. Corrias, P. Kalck, *Carbon nanotubes and nanofibers in catalysis*, Appl. Catal. A: Gen. 253 (2003) 337-358.

[100] Y. Yu, J.C. Yu, C.-Y. Chan, Y.-K. Che, J.-C. Zhao, L. Ding, W.-K. Ge, P.-K. Wong, *Enhancement of adsorption and photocatalytic activity of TiO_2 by using carbon nanotubes for the treatment of azo dye*, Appl. Catal. B: Environ. 61 (2005) 1-11.

[101] G. An, W. Ma, Z. Sun, Z. Liu, B. Han, S. Miao, Z. Miao, K. Ding, *Preparation of titania/carbon nanotube composites using supercritical ethanol and their photocatalytic activity for phenol degradation under visible light irradiation*, Carbon. 45 (2007) 1795-1801.

[102] Y. Ou, J.D. Lin, S.M. Fang, D.W. Liao, *MWNT-TiO_2: Ni composite catalyst: A new class of catalyst for photocatalytic H_2 evolution from water under visible light illumination*, Chem. Phys. Lett. 429 (2006) 199-203.

[103] C.Y. Yen, Y.F. Lin, C.H. Hung, Y.H. Tseng, C.C. Ma, M.C. Chang, H. Shao, *The effects of synthesis procedures on the morphology and photocatalytic activity of multi-walled carbon nanotubes/TiO_2 nanocomposites*, Nanotechnology. 19 (2008) 11.

[104] F. Salamanca-Buentello, D.L. Persad, E.B. Court, D.K. Martin, A.S. Daar, P.A. Singer, *Nanotechnology and the Developing World*, PLoS Med. 2 (2005) 300-303.

Part II

Nanocrystalline TiO_2 catalysts

Chapter 2

Synthesis and characterization of nanocrystalline TiO_2 produced by an acid catalyzed sol-gel method

Titanium dioxide powder is prepared following an acid catalyzed sol-gel method starting from titanium isopropoxide. The xerogel calcination temperature is used to control surface and morphological properties of the material. Lower calcination temperatures result in materials with smaller crystallite sizes and higher surface areas. At temperature below 723K crystalline anatase is identified as the only phase present. Higher calcination temperatures induce phase transformation from anatase to more thermodynamically stable rutile phase. At 973K only rutile phase is obtained. Crystallite size is found to increase with calcination temperature, whereas surface area decreases. Materials are characterized by thermogravimetric analysis, differential scanning calorimetry, N_2 adsorption-desorption isotherm measurements, atomic force microscopy, transmission electron microscopy, powder X-ray diffraction, X-ray photoelectron spectroscopy, diffuse reflectance infrared and UV-Vis spectroscopy.

2.1 Introduction

It has been recognized that TiO_2 photocatalytic efficiency is related to surface and structural properties of the semiconductor such as crystal structure, surface area, particle size distribution, porosity, bandgap and surface hydroxyl density. In addition, resistance to mechanical stress may be important to industrial applications. Particle size is of primary importance in heterogeneous catalysis, because is directly related to the efficiency of a catalyst through the definition of its specific surface area. The smaller the particles are the larger is their surface to volume ratio, which leads to large specific surface areas. Additionally, if particle size is reduced and the nanoscale dimension approached, new interesting electronic, optical, and catalytic properties start to develop, which in many instances differ markedly from those of the bulk materials. As for commercial and industrial applications supported TiO_2 nanoparticles could offer increased surface area, facilitate interfacial charge transfer and avoid supplementary separation steps in heterogeneous catalysis.

The sol-gel method is one of the most used techniques to synthesize powdered TiO_2. The alkoxide route catalyzed in acid medium is known to lead to the formation of pure crystalline powders [1]. The physical-chemical properties of the so obtained TiO_2 are found to be directly related to preparation parameters such as type of Ti(IV)-alkoxide precursor, solvent, aging time and calcination temperature [2, 3].

In the present work is described the production of TiO_2 nanocrystalline powders from Ti(IV) isopropoxide by an acid catalyzed sol-gel method. Calcination temperature was used to control several properties including crystal structure, phase composition, surface area and particle size. The different stages of the process are thoroughly monitored and relevant spectroscopic, microscopic and calorimetric data for nanocrystalline sol-gel TiO_2 is presented.

2.2 Experimental

2.2.1 Titanium dioxide preparation

TiO_2 was prepared by an acid-catalyzed sol-gel method from an alkoxide precursor. The preparation was performed at room temperature as described in the following. An ethanol solution 0.5M in $Ti(OC_3H_7)_4$ (Aldrich 97%) was stirred for

30 minutes and then acidified with 0.8% v/v nitric acid (HNO_3, Fluka 65 wt.%). The solution was loosely covered and kept stirring until the homogeneous gel formed. The gel was aged in air for one week. The resulting xerogel was ground into a fine powder and dried at room temperature. The powder was divided in several batches and calcined at different temperatures (573 to 973K) in a nitrogen flow for 2 hours.

2.2.2 Catalysts characterization

The thermal behavior of the materials was investigated by thermogravimetric (TG) and differential scanning calorimetry (DSC) analysis, using a Mettler TA 4000 instrument equipped with a TG 50, DSC 27-HP and TC 11-TA system. The runs were carried out under nitrogen flow using a heating rate of 5 K min^{-1}.

N_2 adsorption-desorption isotherms were measured on a Coulter Omnisorp 100 CX instrument. All samples were first degassed in vacuum at 423K before analysis. The BET specific area was calculated from the nitrogen adsorption data in the relative pressure range from 0.01 to 0.15.

Powder XRD patterns were obtained on a Philips X'Pert MPD diffractometer (Cu Kα = 0.15406 nm). Diffraction patterns were collected in the range 20º – 60º (2θ) with a step size of 0.02º.

XPS (X-Ray photoelectron spectroscopy) study was performed with an electron spectroscopy for chemical analysis (ESCA) VG Scientific ESCALAB 200A spectrometer using monochromatized Mg K X-ray radiation (15 keV, 300W). The pressure in the analysis chamber was less than 10^{-7} Pa. The powdered samples were glued in carbon adhesive tape and fixed to sample holder for performing the analysis. Charging effects were corrected using C 1s level (285.0 eV) as reference.

Atomic force microscopy (AFM) images were obtained by means of a Multimode NanoScope IVa (Veeco Metrology) using tapping mode measurement technique. Powder samples were dispersed in ethanol and then a drop of the suspension was placed in a glass plate and dried in vacuum atmosphere.

Transmission electron microscopy (TEM) analysis was performed on a Leica LEO 906E instrument operating at a 120 kV accelerating voltage. The samples were previously dispersed in ethanol, and after sonication the suspensions were deposited on a 400 mesh copper grid covered with a formvar film.

Diffuse reflection spectroscopy enables the analysis of powder materials with little or no sample preparation. Many substances at their natural state, specially powders but also any solid with a rough surface, exhibit diffuse reflection, *i. e.*, incident light is scattered in all directions, unlike specular reflection where the angle of incidence equals the angle of reflection. Diffuse reflectance spectra are in practice complex, because of spectral distortions caused by the mixing of both absorbance and reflectance features owing to contributions from transmission, internal, and specular components in the measured radiation. Hence, diffuse reflectance spectra are affected by particle size, packing, and dilution of the sample. The diffuse reflectance (R_∞) of a diluted sample of infinite thickness (*i. e.*, a sample for each an increase in thickness does not appreciably change the spectrum) is linearly related to the concentration (c) of the sample, as given by the Kubelka-Munk equation:

$$f(R_\infty) = \frac{(1-R_\infty)^2}{2R_\infty} = \frac{2.303ac}{s} \tag{2.1}$$

where a is the absorptivity and s in the scattering coefficient. Because the scattering coefficient depends on both particle size and degree of packing, the linearity of the Kubelka-Munk function can only be assured if particle size and packing method are strictly controlled. If these conditions are maintained, quantitative analysis can be performed by using this technique.

Diffuse reflection infrared Fourier transformed (DRIFT) spectroscopic analysis of the solid materials was performed on a Nicolet 510P FTIR Spectrometer, with a KBr beam splitter for mid-IR range and a DTGS with KBr windows equipped with a special beam collector (COLLECTOR from Spectra Tech), fixed on a plate for consistent experimental conditions. The interferograms were converted by the instrument software (OMINC) to equivalent absorption units in the Kubelka–Munk scale.

The UV-Vis diffuse reflectance spectra (200-800 nm) of the powder samples were recorded on a JASCO V-560 UV-Vis spectrophotometer, with a double monochromator, double beam optical system. The spectrophotometer was

equipped with an integrating sphere attachment (JASCO ISV-469). The powders were not diluted in any matrix to avoid a decrease of the absorbance. The reflectance spectra were converted by the instrument software (JASCO) to equivalent absorption Kubelka–Munk units.

2.3 Results and discussion

Nanocrystalline TiO_2 was obtained by hydrolysis starting from titanium isopropoxide. In acidified ethanol solution the alkoxide is hydrolyzed (Eq. 2.2) and then condensation of the polymeric chains (≡Ti-OH and ≡Ti-OC_3H_7) takes place (Eqs. 2.3 and 2.4). Acid catalyzed hydrolysis provides control over the rate of this step avoiding TiO_2 precipitation.

$$\equiv Ti - OC_3H_7 \xrightarrow{HNO_3} \equiv Ti - OH \tag{2.2}$$

$$\equiv Ti - OH + C_3H_7O - Ti \equiv \longrightarrow \equiv Ti - O - Ti \equiv + C_3H_7OH \tag{2.3}$$

$$\equiv Ti - OH + HO - Ti \equiv \longrightarrow \equiv Ti - O - Ti \equiv + H_2O \tag{2.4}$$

The resulting xerogel is thermally treated under nitrogen flow. The mass loss and heat release from xerogel samples during calcination was followed by thermal analysis (Fig. 2.1).

As shown in Fig. 2.1a, differential thermogravimetric (DTG) curve of TiO_2 xerogel presents one intense band at 373K and a broad band centered around 553K. The corresponding peaks could be observed in DSC profiles (Fig. 2.1b). The former can be attributed to the evaporation of remained ethanol and adsorbed water, which corresponds to an endothermic process. The second band is ascribed to the exothermal crystallization of the amorphous gel to anatase form. The glass transition point can be observed around 650K, ascribed to the inflection of the DSC curve at this temperature. The strong and well-defined exothermic peak centered at 800K corresponds to the anatase to rutile phase transition [4].

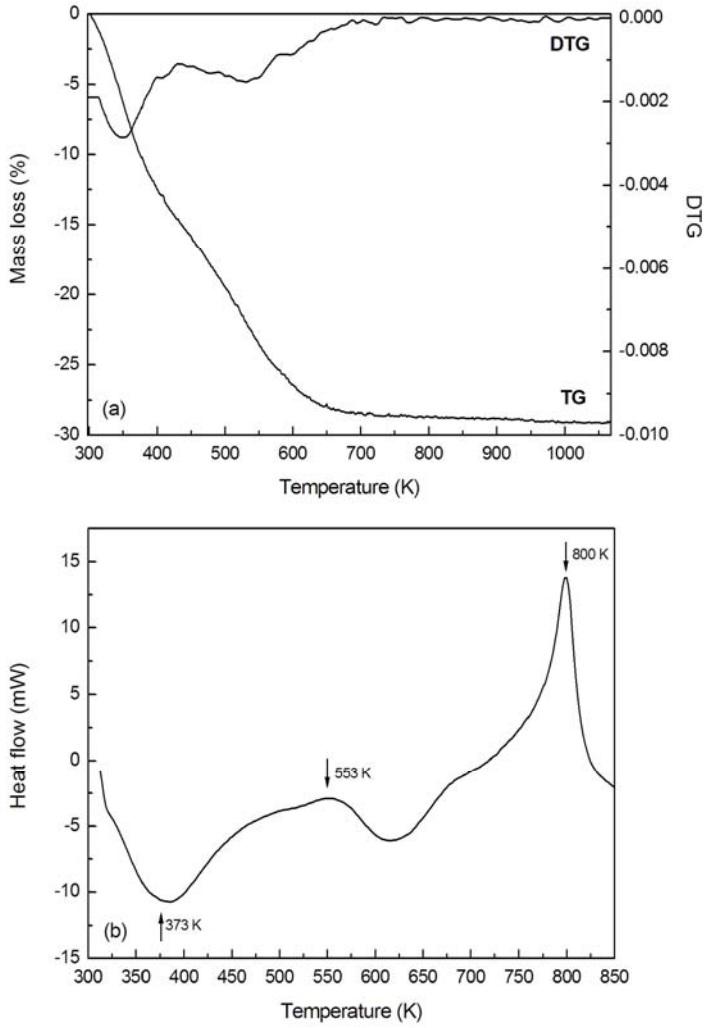

Figure 2.1 Xerogel evolution during calcination process: (a) TG/DTG profile and (b) DSC profile.

The synthesized materials were characterized by diffuse reflectance infrared Fourier transform spectroscopy (Fig. 2.2). This technique applied to homogeneous fine particles and powders provides information about the surface chemical structure. Depending on the environment of the sample some additional information can be obtained concerning the adsorption of probe molecules on the surface. The bands observed under laboratory conditions (normal pressure and room temperature) lead to the group assignments listed in Table 2.1.

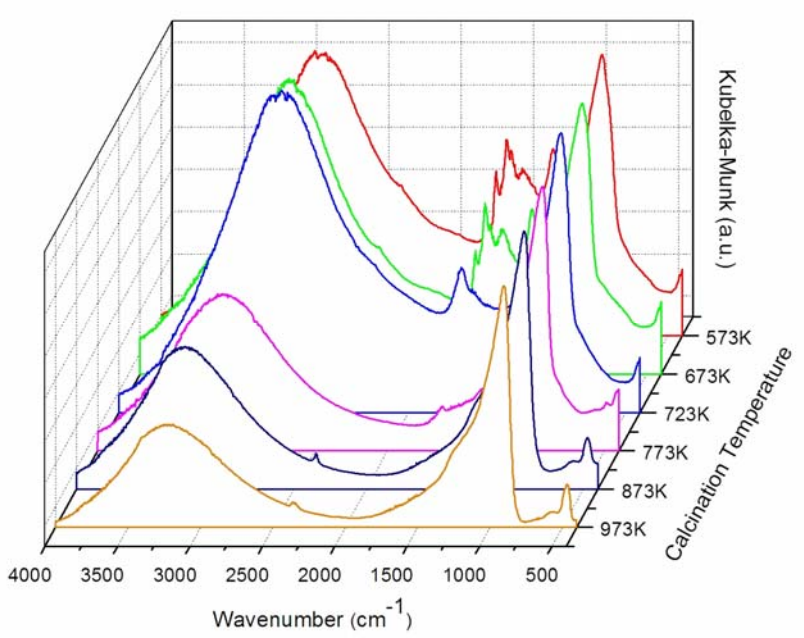

Figure 2.2 DRIFT spectra of TiO_2 obtained at different calcination temperature.

Common to all spectra is a broad band located between 2500 and 3800 cm^{-1}, attributed to the stretching vibrations of hydrogen-bonded surface water molecules and hydroxyl groups [5]. This is confirmed by the presence of some weak bands around 1620 and 1685 cm^{-1} caused by bending vibration of coordinated water as well as from the Ti–OH group [6, 7]. For higher calcination temperature these bands tend to disappear as a result of the removal of these hydroxyl groups from the TiO_2 surface.

Samples obtained on calcination at temperatures higher than 723K show a peak around 490 cm^{-1}, corresponding to the Ti–O vibration in the rutile crystalline phase [8].

At 900–950 cm^{-1} there is band, also common to all spectra, typical of TiO_2 material. For calcination temperature lower than 723K this band peaks at 950 cm^{-1}. As the calcination temperature increases, phase transition from anatase to rutile occurs and the peak shifts towards lower wavenumbers. For TiO_2 produced at 873 and 973K, consisting mostly on rutile crystallites, the peak is centered at 900 cm^{-1}. This phenomenon can be attributed to the modification of the crystalline arrangement of the materials as calcination temperature is changed.

Table 2.1 Assignments of observed peaks in the DR infrared spectrum of TiO_2.

Wavenumber (cm^{-1})	**Assignment**	**References**
2500 – 3800 (very strong, broad)	ν (H_2O and Ti–OH)	[5], [9], [10]
1620 and 1685 (strong)	δ (H_2O and Ti–OH)	[6], [7], [9]
900 – 950 (very strong, broad)	Triangular peroxy titanyl group 	[7], [11]
506	ν (Ti–O)	[7], [8]
448	δ (Ti–O)	[7], [8]

The crystal phase of TiO_2 was studied by powder X-ray diffraction. The XRD patterns of titania obtained at different calcination temperature are shown in Fig. 2.3. At temperature below 723K only anatase crystalline phase is detected. Anatase to rutile transformation occurs between 723 and 773K thermal treatments. At temperatures above 723K there is a mixture between anatase and rutile phases. At 973K only the rutile phase is observed. It can also be noticed that for lower calcination temperature diffraction peaks are relatively broad, particularly for calcination at 573K. The peak broadening may be caused by the small crystallite size and by the presence of a certain portion of titania not yet crystallized. The crystallite dimensions (*d*) were calculated from the broadening of the (1 0 1) reflection for anatase and (1 1 0) reflection for rutile using Scherrer's equation:

$$d = \frac{k\ \lambda}{\beta\ \cos\theta} \tag{2.5}$$

where *k* is a constant that depends on the crystallite shape (0.9, with the assumption of spherical particles) [12, 13], λ is the X-ray wavelength, β is the full width at half maximum of the selected peak and θ is the Bragg's angle of diffraction for the peak.

The rutile to anatase ratio was determined from the relation [14]:

$$x_A = \left(1 + 1.26\frac{I_R}{I_A}\right)^{-1} \tag{2.6}$$

where x_A is the anatase fraction in the catalyst, I_R and I_A are the integral intensities of the (1 1 0) and (1 0 1) peaks of rutile and anatase, respectively.

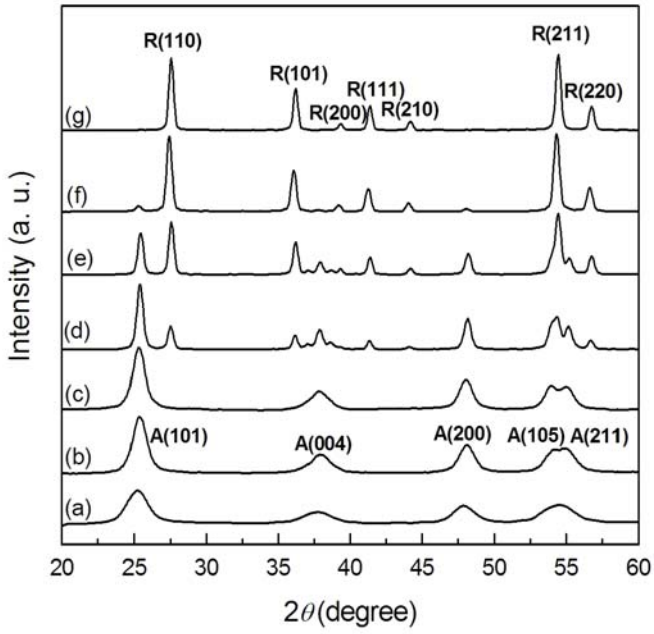

Figure 2.3 X-ray diffraction patterns of TiO_2 obtained at different calcination temperatures: (a) 573K, (b) 673K, (c) 723K, (d) 773K, (e) 823K, (f) 873K, and (g) 973K.

The crystallite sizes and the corresponding anatase phase contents are listed in Table 2.2. It's known that temperature greatly affects the structure and size of TiO_2 crystals. The crystallite sizes of both anatase and rutile forms increased with calcination temperature. Thermal treatment of TiO_2 gels at higher temperature accelerates phase transformation from thermodynamically metastable anatase to more stable and condensed rutile phase. As mentioned above, the gel presents hydroxyl groups on the surface that are removed during heating treatment. As the dehydration process occurs, crystallites grow to dimensions larger than those of the original particles.

TEM micrographs of the catalysts obtained at 673K and 973K are shown in Figs. 2.4a and 2.4b, respectively. Crystallites with dimensions similar to the calculated by XRD data could be observed.

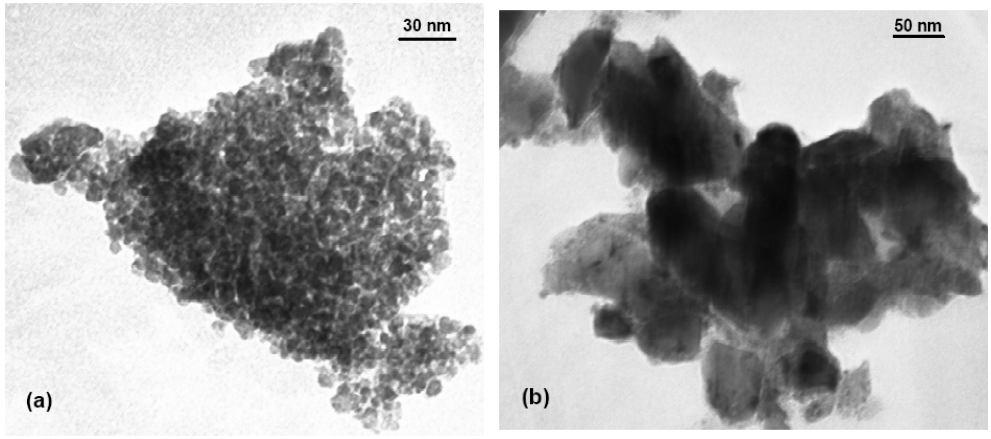

Figure 2.4 TEM micrographs of TiO_2 materials obtained at 673K (a) and 973K (b).

Anatase and rutile crystalline structures are constituted by TiO_2^{6-} octahedrons arranged in tetragonal unit cell geometry [15]. The two crystal structures differ by the distortion of each octahedron and the assembly patterns of the octahedral chains. In anatase, octahedrons are coupled by their vertices while in rutile the edges are connected. The determination of the crystal lattice parameters for tetragonal geometry (*a* and *c*) were carried using the following expression [16]:

$$\frac{1}{d_{hkl}^2} = \frac{h^2 + k^2}{a^2} + \frac{l^2}{c^2} \tag{2.7}$$

where d_{hkl} is the interplane distance and *hkl* are the plane indices. The lattice parameters were determined by selecting two diffractogram lines and solving the equations system. Lattice constants for TiO_2 obtained at 673K (pure anatase) were a = 0.3806 nm and c = 0.9404 nm and for TiO_2 calcined at 973K (pure rutile), a = 0.4578 nm and c = 0.2967 nm. These values are in good agreement with the ones referred in literature [17], confirming the crystalline nature of the synthesized materials.

Nitrogen adsorption isotherms at 77K were used for determination of surface area of the TiO_2 samples. The results, listed in Table 2.2, show the dependence of the surface area on the TiO_2 calcination temperature. Higher the

temperature, lower the surface area. Materials obtained at the lower temperature 573K exhibited a surface area of 134 m^2 g^{-1}. As the temperature increases, the surface area gradually decreases, reaching 3 m^2 g^{-1} at temperature higher than 873K. This results from the increase in the crystallite dimensions.

The adsorption-desorption isotherm of sample obtained at 673K is shown in Fig. 2.5a. The curve shape reveals a type IV isotherm behavior [18].

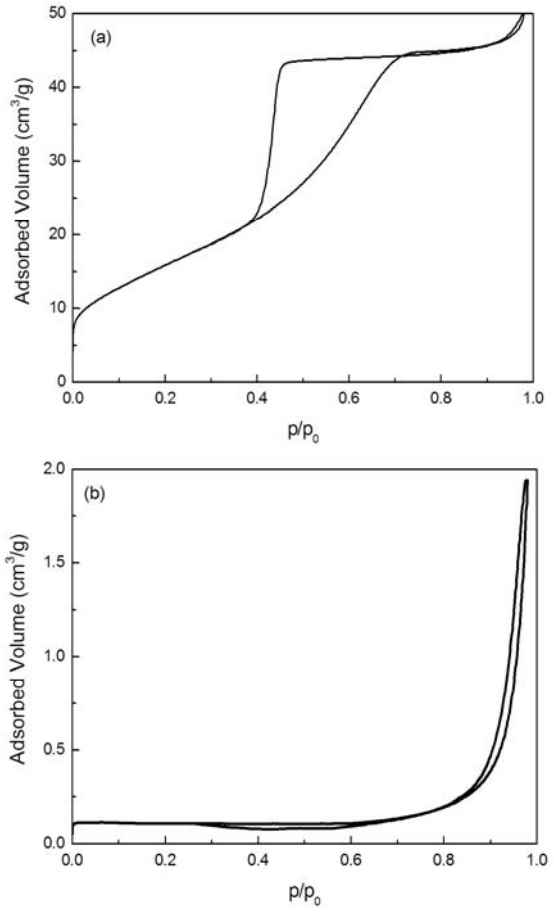

Figure 2.5 N_2 adsorption-desorption isotherm at 77K of TiO_2 obtained at 673K (a) and 973K (b).

At relative pressure between 0.4 and 0.8, the curve exhibits a hysteresis loop (type H2) indicating a mesoporous texture of a solid consisting of agglomerates of spherical particles [18, 19]. The mesoporosity was confirmed by applying α_S method using an isotherm of a non-porous material (TiO_2 Degussa P25) as standard. The calculated microporous volume was considered negligible. A similar behavior was observed for TiO_2 obtained at calcination temperatures lower

than 823K. As mentioned earlier, samples obtained at 873 and 973K showed very low surface area. Adsorption-desorption isotherm obtained for TiO_2 calcined at 973K (Fig. 2.5b) is characteristic of a non-porous material. Therefore, for TiO_2 produced at these higher temperatures, the calculated surface area corresponds to the geometrical area of the powdered particles.

Using diffuse reflectance (DR) UV-Vis spectroscopy we characterized the electronic structure of the TiO_2 nanoparticles. The anatase to rutile transformation is visible by the change on the DR UV-Vis spectra of the solids (Fig. 2.6).

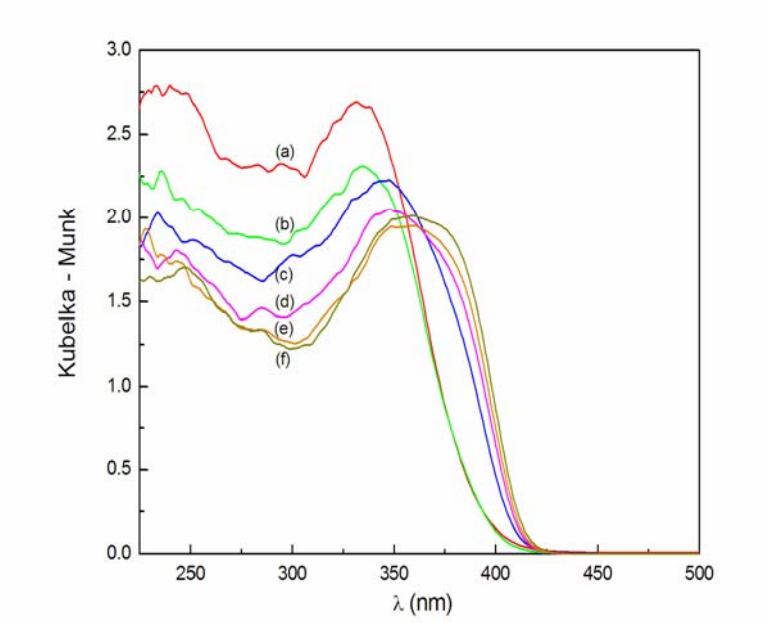

Figure 2.6 Diffuse reflectance UV-Vis spectra of TiO_2 obtained at: (a) 573K, (b) 673K, (c) 773K, (d) 823K, (e) 873K, and (f) 973K.

On decreasing the calcination temperature, the absorption edge moved towards shorter wavelengths (blue shift), which corresponds to an increase in the band gap energy. This shift is much more pronounced for samples calcined at 573 and 673K, consisting only in anatase phase. The characteristic band of nanocrystalline anatase at 335 nm can be observed for these materials and progressively disappear as temperature increases.

The absorption edges were determined by extrapolating the horizontal and vertical portions of the curves and defining the edge as the wavelength of intersection [20]. The absorption edges and the calculated band gap energies are given in Table 2.2. For samples calcined at 673K (pure anatase) and at 973K (pure

rutile) the band gap energies were 3.17 and 3.00 eV, respectively, in agreement with 3.20 and 3.02 eV referred in the literature [15].

The absorption threshold present in all spectra is attributed to a O^{2-}:Ti^{4+} charge transfer of TiO_2 [21]. There is no indication of reduced titania sites, because no significant absorption is observed in the visible region, characteristic of d-d transitions.

Table 2.2 Anatase (d_A) and rutile (d_R) crystallite dimensions, surface area (S), anatase content (x_A), absorption edge (AE) and bandgap energy (E_g) of the TiO_2 samples obtained at different calcination temperatures (T_c).

T_c (K)	d_A (nm)	d_R (nm)	S (m^2 g^{-1})	x_A (%)	AE (nm)	Eg (eV)
573	5.7	-	134	100	389	3.19
673	8.5	-	107	100	391	3.17
723	10	-	84	100	403	3.08
773	14	20	26	69	410	3.03
823	23	24	13	38	412	3.01
873	37	39	3	5	413	3.00
973	-	39	3	0	413	3.00

The significant shift in the profiles to lower energies as the calcination temperature increases must be associated to the grow of titania particles during the transition from quantum-sized to bulk-sized particles as confirmed by the AFM images (Fig. 2.7).

The dimensions of the TiO_2 particles obtained at 673K (Fig. 2.7a) revealed to be of a magnitude of 10 to 20 nm. The results are in line with the XRD results (Table 2.2), which show that these particles are mainly constituted by anatase crystallites. On the other hand, as we increase the calcination temperature the crystallites tend to agglomerate leading to the formation of bigger particles. In the case of TiO_2 obtained at 973K (Fig. 2.7b), the observed agglomerates are typically of a magnitude of one to two hundred nanometers. There are also visible crystallites with 30-40 nm, again in agreement with the XRD results.

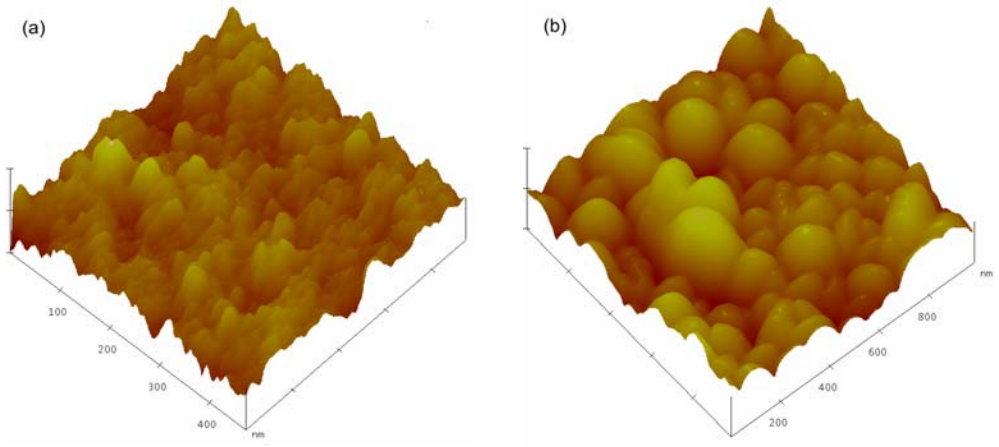

Figure 2.7 AFM images of TiO_2 particles (tapping mode) annealed at 673K (a) and 973K (b).

XPS measurements were performed for TiO_2 powders. Major characteristic transition peaks for Ti, O and C were found in the ESCA survey spectrum (Fig. 2.8a). The detected peaks are attributed to the Ti2p doublet, O 1s, C 1s and the correspondent Auger peaks Ti LMM, O KLL and C KLL. Note that the occurrence of C 1s and C KLL peaks is attributed to surface contamination since the samples were exposed to air before ESCA measurements. Also, a contribution by the adhesive tape, where the sample is hold, is expected.

Fig. 2.8b shows the XPS TiO_2 2p spectra of the powders obtained at 673 and 973K. The peaks at around 458 and 464 eV in the XPS spectra correspond to Ti $2p_{3/2}$ and Ti $2p_{1/2}$ of TiO_2, respectively [22]. Based on detailed analysis of TiO_2 $2p_{3/2}$, we can notice that the binding energy of Ti ion changes when TiO_2 powders are obtained at different calcination temperatures. The binding energy of Ti $2p_{3/2}$ for the powders obtained at 673K and 973K are 458.47 eV and 458.67 eV, respectively. It's well known that XPS spectra are very sensitive to the environment around atomic species. This change in binding energy is defined as a chemical shift. Since the sensitivity of the XPS apparatus is 0.10 eV, the difference of 0.20 eV between the powders produced at 673 and 973K can be attributed to the existence of oxygen vacancies around Ti^{4+} ion [23].

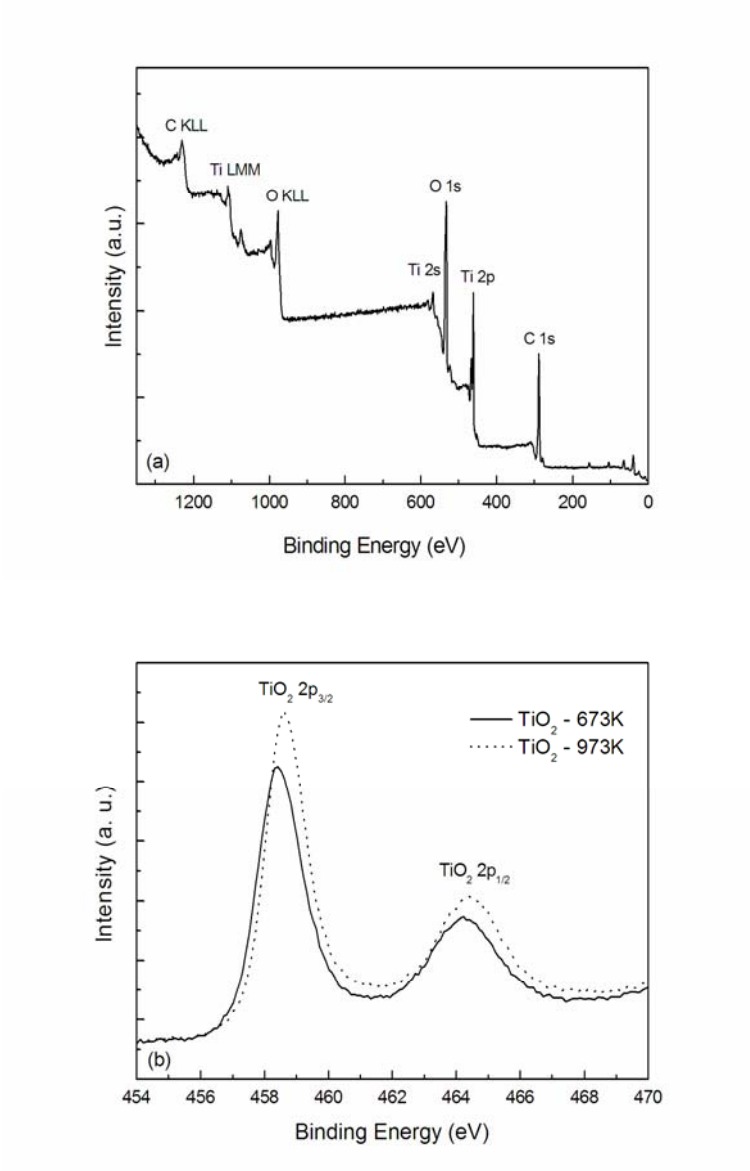

Figure 2.8 ESCA survey spectrum of TiO_2 calcined at 673K (a); XPS spectra of Ti 2p of TiO_2 samples obtained at 673 and 973K (b).

The titanium to oxygen atomic ratio was obtained by integration of Ti 2p and O 1s peaks considering the respective sensitivity factor. For sample calcined at 673K, the titanium to oxygen ratio is 1:1.67 indicating that TiO_2 nanoparticles have many surface oxygen vacancies that are generally considered when particles are very small.

2.4 Conclusions

The nitric acid catalyzed sol-gel method, using titanium(IV) isopropoxide as precursor leads to the formation of nanocrystalline TiO_2. The crystal structure and crystallite size were dependent on the thermal treatment within the range 573-973K. Figure 2.9 shows a resume of the phenomena taking place during calcination on that temperature range and its implications on the physical-chemical parameters that were focused in this study.

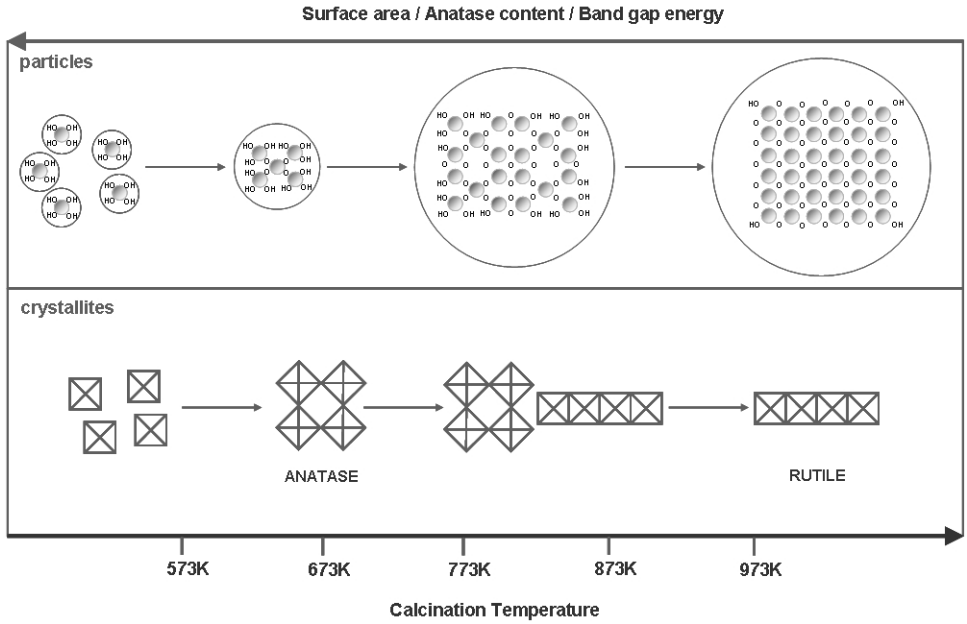

Scheme 2.1 Evolution of crystallite and particle dimension and composition with calcination temperature.

The crystallites dimension increases with calcination temperature. A concomitant decrease in the surface area of the synthesized materials is observed. At the lowest temperature there is a certain amount of non-crystalline material. The ratio anatase to rutile is also dependent on the temperature. Increasing the calcination temperature promotes phase transition from anatase to rutile. Up to temperatures of 723K only anatase can be identified. At 973K titanium dioxide consists in pure rutile phase. Anatase crystallites in the range 5 to 40 nm were observed, while for rutile crystallites the dimensions ranged from 20 to 40 nm. The band gap energy of the materials changes from 3.17 eV (pure anatase) to 3.00 eV (pure rutile), as the calcination temperatures increases, and the trend is not completely dependent on the ratio of anatase to rutile, with a geometric factor possibly playing a role.

2.5 References

[1] W. Wang, P. Serp, P. Kalck, J.L. Faria, *Photocatalytic degradation of phenol on MWNT and titania composite catalysts prepared by a modified sol-gel method*, Appl. Catal. B: Environ. 56 (2005) 305-312.

[2] H.-I. Hsiang, S.-C. Lin, *Effects of aging on the kinetics of nanocrystalline anatase crystallite growth*, Mater. Chem. Phys. 95 (2006) 275-279.

[3] S.S. Watson, D. Beydoun, J.A. Scott, R. Amal, *The effect of preparation method on the photoactivity of crystalline titanium dioxide particles*, Chem. Eng. J. 95 (2003) 213-220.nao o vi

[4] B.D. Stojanovic, Z.V. Marinkovic, G.O. Brankovic, E. Fidancevska, *Evaluation of kinetic data for crystallization of TiO_2 prepared by hydrolysis method*, J. Therm. Anal. Calorim. 60 (2000) 595-604.

[5] J.R.S. Brownson, M.I. Tejedor-Tejedor, M.A. Anderson, *Photoreactive anatase consolidation chracterized by FTIR spectroscopy*, Chem. Mat. 17 (2005) 6304-6310.

[6] Y. Gao, Y. Masuda, W.-S. Seo, H. Ohta, K. Koumoto, *TiO_2 nanoparticles prepared using an aqueous peroxotitanate solution*, Ceram. Int. 30 (2004) 1365-1368.

[7] G.V. Jere, C.C. Patel, *Infrared absorption studies on peroxy titanium sulphate*, Can. J. Chem.-Rev. Can. Chim. 40 (1962) 1576-1578.

[8] T. Busani, R.A.B. Devine, *Dielectric and infrared properties of TiO_2 films containing anatase and rutile*, Semicond. Sci. Technol. 20 (2005) 870-875.

[9] Y.V. Kolen´ko, A.V. Garshev, B.R. Churagulov, S. Boujday, P. Portes, C. Colbeau-Justin, *Photocatalytic activity of sol-gel derived titania converted into nanocrystalline powders by supercritical drying*, J. Photochem. Photobiol. A-Chem. 172 (2005) 19-26.

[10] J.-Y. Zhang, I.W. Boyd, B.J. O'Sullivan, P.K. Hurley, P.V. Kelly, J.-P. Sénateur, *Nanocrystalline TiO_2 films studied by optical, XRD and FTIR spectroscopy*, J. Non-Cryst. Solids. 303 (2002) 134-138.

[11] R. Comparelli, E. Fanizza, M.L. Curri, P.D. Cozzoli, G. Mascolo, R. Passino, A. Agostiano, *Photocatalytic degradation of azo dyes by organic-capped anatase TiO_2 nanocrystals immobilized onto subtrates*, Appl. Catal. B-Environ. 55 (2005) 81-91.

[12] H. Natter, M. Schmelzer, M.-S. Löffler, C.E. Krill, A. Fitch, R. Hempelmann, *Grain-growth kinetics of nanocrystalline iron studied in situ by synchrotron real-time X-ray diffraction*, J. Phys. Chem. B. 104 (2000) 2467-2476.

[13] Y. Xie, C. Yuan, *Visible-light responsive cerium ion modified titania sol and nanocrystallites for X-3B dye photodegradation*, Appl. Catal. B: Environ. 46 (2003) 251-259.

[14] R.A. Spurr, H. Myers, *Quantitative analysis of anatase-rutile mixtures with an X-Ray diffractometer*, Anal. Chem. 29 (1957) 760-762.

[15] O. Carp, C.L. Huisman, A. Reller, *Photoinduced reactivity of titanium dioxide*, Prog. Solid State Chem. 32 (2004) 33-177.

[16] T. Bezrodna, G. Puchkovska, V. Shymanovska, A. Hauser, *X-ray and AFM studies of polydisperse TiO_2 (anatase) particles*, J. Phys. Chem. Solids. 66 (2005) 1057-1063.

[17] U. Diebold, *The surface science of titanium dioxide*, Surf. Sci. Rep. 48 (2003) 53-229.

[18] K.S.W. Sing, D.H. Everett, R.A.W. Haul, L. Moscou, R.A. Pierotti, J. Rouquérol, T. Siemieniewska, *Reporting physisorption data for gas/solid systems with special reference to the determination of surface area and porosity*, Pure Appl. Chem. 57 (1985) 603-619.

[19] G. Leofanti, M. Padovan, G. Tozzola, B. Venturelli, *Surface area and pore structure of catalysts*, Catal. Today. 41 (1998) 207-219.

[20] P.L. Provenzano, G.R. Jindal, J.R. Sweet, W.B. White, *Flame-excited luminescence in the oxides Ta_2O_5, Nb_2O_5, TiO_2, ZnO and SnO_2*, J. Lumines. 92 (2001) 297-305.

[21] J.M.G. Amores, V.S. Escribano, M. Daturi, G. Busca, *Preparation, characterization and surface structure of coprecipitated high-area $Sr_xTiO_2+x(0<x<1)$ pouders*, J. Mater. Chem. 6 (1996) 879-886.

[22] J.F. Moulder, W.F. Stickle, P.E. Sobol, K.D. Bomben, *Handbook of X-Ray Photoelectron Spectroscopy*, ed. J. Chastain (1992), MN, USA, Perkin-Elmer Corporation.

[23] X. Li, X. Quan, C. Kutal, *Synthesis and photocatalytic properties of quantum confined titanium dioxide nanoparticle*, Scr. Mater. 50 (2004) 499-505.

Chapter 3

Photocatalytic degradation of phenol under UV irradiation using nanocrystalline TiO_2 catalysts

Nanocrystalline TiO_2 catalysts produced by an acid-catalyzed sol-gel method are tested in the photocatalytic degradation of phenol under ultraviolet (253.7 nm) light. The kinetics of the photo-oxidation of the organic molecule follow a pseudo-first order rate law. The effect of key parameters on the photo-efficiency of the process namely TiO_2 physical-chemical properties, catalyst loading, pH of the medium, initial phenol concentration, light intensity, oxygen partial pressure and presence of oxidant species are studied. In photo-degradation of phenol, pure anatase TiO_2 is more efficient than anatase/rutile or pure rutile. A modified Langmuir-Hinshelwood kinetic model is used considering a pseudo-steady state approach, in order to explain both, kinetic rate constant and adsorption equilibrium constant dependency on light intensity. Hydroquinone (p-hydroxyphenol) and catechol (o-hydroxyphenol) are the main intermediates of the photocatalytic reaction. These intermediates are believed to result from the reaction of phenol with photogenerated hydroxyl radicals. A possible degradation pathway is proposed.

3.1 Introduction

In this chapter, the study of the photocatalytic degradation of phenol under ultraviolet irradiation using nanocrystalline TiO_2 catalysts is described. The characterization of TiO_2 materials, produced by an acid catalyzed sol-gel method is given in detail in Chapter 2.

Several studies about photo-oxidation of phenol have already been published [1-3]. Moreover, phenol and phenolic derivatives are common compounds in industrial wastewaters [4-6] being refractory and recalcitrant species in conventional biological treatment processes. This type of pollutants is highly stable, toxic and carcinogenic, capable of causing considerable damage and threat to the ecosystem and human health. Therefore, phenol happens to be a very useful model compound for photocatalytic degradation studies.

Kinetics and mechanism of the photocatalytic oxidation of phenol in a slurry reactor was here investigated. Besides being of very simple conception, this type of reactors, where the catalyst is suspended in the liquid phase, are still the most popular. Main advantages are the easiness of handling, inexistence of mass transfer limitations and the very favorable surface to treated volume ratio, especially if nanostructured particles are used.

In order to fully characterize the photocatalytic process, parameters such as TiO_2 physical-chemical properties, catalyst loading, pH of the medium, phenol initial concentration, light intensity, oxygen partial pressure and presence of oxidant species are here investigated. A pseudo-steady state kinetic approach is presented having in consideration the light dependency of the Langmuir-Hinshelwood rate constant, k_{LH} and apparent adsorption constant, K_{LH}.

Having established optimal operation conditions for the photocatalytic oxidation of phenol using monochromatic (λ_{exc} = 253.7 nm) UV radiation, the applicability of the process using different TiO_2-based catalysts and distinct radiation sources could be performed, as described in the subsequent chapters.

3.2 Experimental

3.2.1 Catalysts preparation and characterization

The preparation procedure and characterization of the TiO_2 catalysts used in this study are described in Chapter 2, section 2.2. The different catalysts were labeled as TiO_2-X, where X is the calcination temperature at which they were prepared.

3.2.2 Equilibrium adsorption isotherm of phenol on TiO_2

Phenol solutions with concentrations varying between 10 mg l^{-1} and 300 mg l^{-1} were prepared and 50 ml aliquots of each solution were placed in 100 ml Erlenmeyer flasks. A TiO_2 sample (50 mg) was added at each solution. The suspensions were left to equilibrate in the dark under magnetic stirring for 24 hours, at 298K and natural pH conditions (pH=5.6). At the end of this period, samples were taken of each flask and were centrifuged for solid separation. Phenol equilibrium concentration in solution (C_e) was determined by HPLC analysis. The amount phenol adsorbed on TiO_2 (Q_e) was calculated by the difference between the initial and equilibrium concentration of the compound in solution divided by the concentration of the catalyst on the suspension. The adsorption equilibrium isotherm was given by the plot of C_e *versus* Q_e.

3.2.3 Determination of the point of zero charge

The point of zero charge of TiO_2 was determined by the procedure indicated in Ref. [7], as it follows: 50 ml aliquots of 0.01M NaCl solution were placed in 100 ml Erlenmeyer flasks. The pH was adjusted to values between 2 and 12 by addition of 0.1M HCl and 0.1M NaOH solutions ($pH_{initial}$). A 150 mg sample of TiO_2 was added at each flask. The suspensions were magnetically stirred for 24 hours at 298K. Finally, the pH was measured (pH_{final}) and plotted against the respective initial pH. The pH at which the curve crosses the line $pH_{initial} = pH_{final}$ is taken as the point of zero charge, pH_{pzc}.

3.2.4 Photocatalytic degradation of phenol

3.2.4.1 Photocatalytic reactor and light source

The experiments were carried out in a 1000 ml glass immersion photochemical reactor charged with 800 ml of solution/suspension. The reactor was equipped with an UV lamp, located axially and held in a quartz immersion tube (Fig. 3.1).

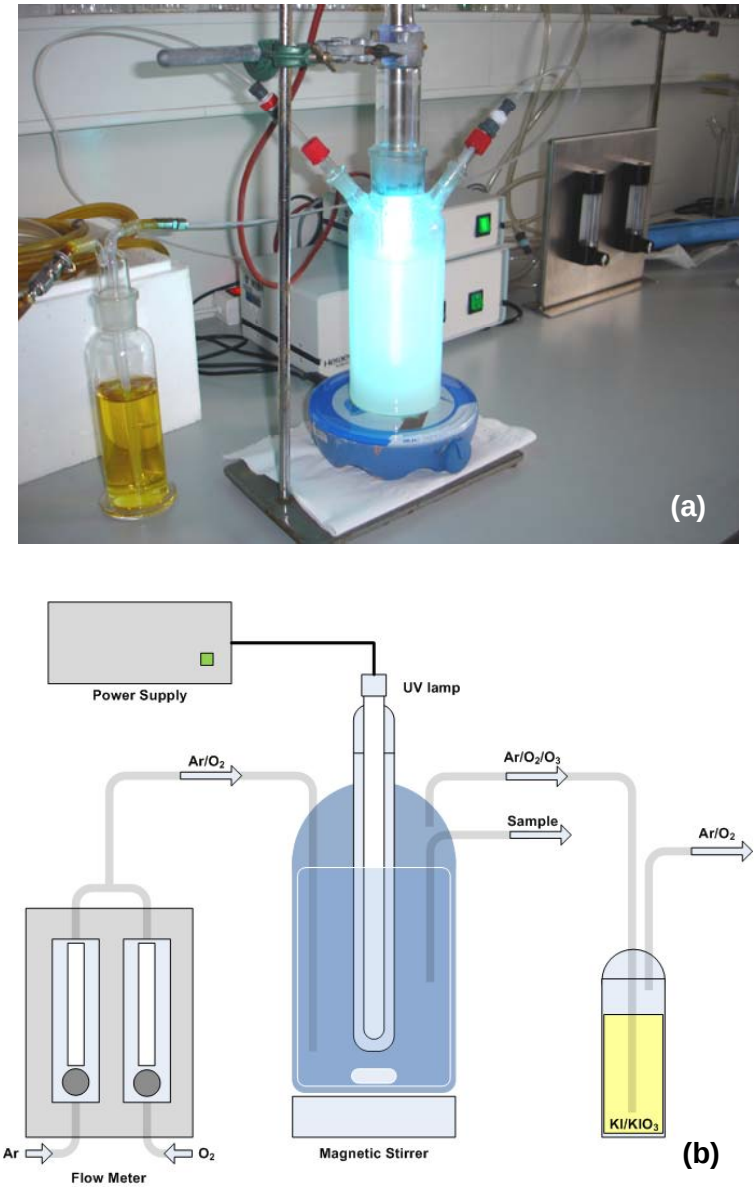

Figure 3.1 Photocatalytic reaction setup: (a) photograph; (b) scheme.

The radiation source was a Heraeus TNN 15/32 low-pressure mercury vapor lamp (3 W of nominal radiant flux) with an emission line at 253.7 nm (Fig. 3.2). The photon flux inside the photoreactor, measured by potassium ferrioxalate actinometry [8], was of 4.78×10^{-6} Einstein s^{-1}. When necessary, the photon flux was controlled by using a quartz-glass jacket around the light source with dye solutions of different concentration flowing inside of it.

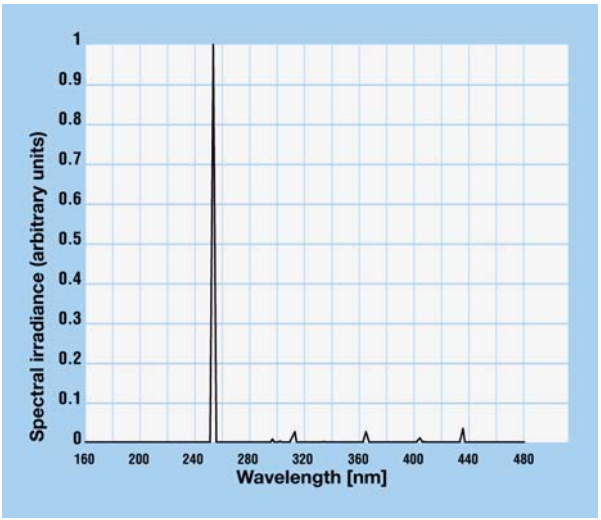

Figure 3.2 Spectral irradiance of Heraeus TNN 15/32 immersion lamp (manufacturer data).

The solution/suspensions were magnetically stirred. A gas feeding system was connected to the reactor, for bubbling through the reaction media a controlled flow of an oxygen/argon mixture at different partial pressures. Temperature of the reaction media was measured during the experiments varying between 298 and 301K.

The gas phase leaving the reactor, constituted by a mixture of argon, oxygen and ozone, this last resulting from the reaction of oxygen with UV light, was passed through a gas washing bottle filled with an iodide potassium solution. Ozone reacts with potassium iodide to form potassium iodate. The indigo colorimetric method was used to investigate the presence of dissolved ozone in solution [9]. The determined amount of dissolved ozone was considered negligible.

3.2.4.2 Photodegradation experiments

The photocatalytic activity of TiO_2 catalysts prepared at different calcination temperature was evaluated following phenol (Aldrich, redistilled 99+%) degradation in aqueous solution under ultraviolet irradiation (λ_{exc} = 253.7 nm) at natural pH conditions (pH=5.6) .

The UV-Vis spectrum of the aqueous solution of phenol at natural pH shows two absorption maxima at 210 and 270 nm (Fig. 3.3). The molar absorption coefficients (ε) are, respectively, 5853 and 1408 M^{-1} cm^{-1}.

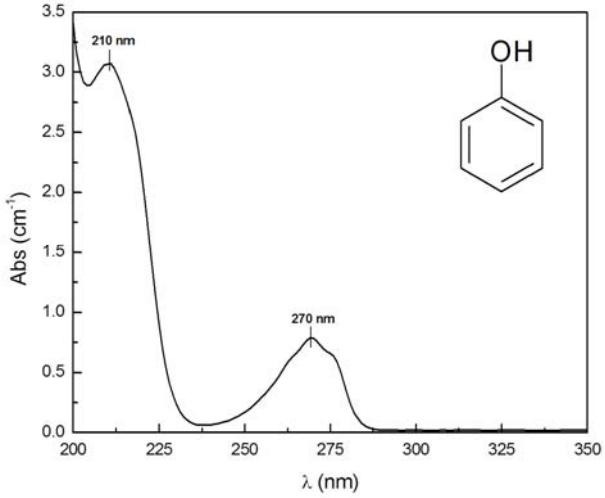

Figure 3.3 UV-Vis spectrum (50 mg l^{-1}; pH=5.6) and molecular structure of phenol.

In a typical experiment, the initial phenol concentration and the amount of suspended TiO_2 were set at 50.0 mg l^{-1} and 1.0 g l^{-1}, respectively. A 200 ml min^{-1} oxygen/argon (20% vol. of oxygen) stream was continuously supplied to the reactor. Before turning on the illumination, the suspensions were saturated with the gas mixture and magnetically stirred for 30 minutes to establish an adsorption-desorption equilibrium. Then, the suspensions were irradiated with UV light at constant stirring speed.

Samples were withdrawn regularly from the reactor and centrifuged for separation of any suspended solid, prior to analysis. The clean transparent solution was then analyzed by HPLC using a Hitachi Elite LaChrom liquid chromatograph equipped with an L-2450 diode array detector. The stationary phase consisted in a Purospher Star RP-18 endcapped column (250 mm × 4.6 mm, 5μm particles)

working at room temperature. The mobile phase was a mixture of water and methanol with a gradient concentration at a flow rate of 1.0 ml min^{-1}. For known compounds, the relationship between area and concentration was determined by using adequate standards. Total organic carbon (TOC) measurements were performed in a Shimadzu TOC-5000 analyzer.

3.2.4.3 Catalyst recovery and reuse

At the end of the photocatalytic reactions, the suspensions were filtered to recover the catalyst particles, which were rinsed with water and dried at 373K for 24 h. The recovered photocatalyst was then washed again with a mixture of distilled water and ethanol to remove any trace of adsorbed compounds. At the end of this operation, TiO_2 was again dried and reused in a new photocatalytic reaction.

3.3 Results and discussion

3.3.1 Influence of operational parameters on the photocatalytic degradation of phenol

Catalyst loading, substrate concentration, pH, presence of oxidant species and photonic flux are found to be crucial parameters in heterogeneous photocatalytic reactions [10]. Preliminary experiments revealed that photocatalytic oxidation of phenol follow a pseudo-first order kinetic model, as described by the following equation:

$$C_{PhOH} = C_{0,PhOH} e^{-k_{app} t} \tag{3.1}$$

where C_{PhOH} corresponds to phenol concentration, k_{app} is the apparent first order kinetic rate constant, t is the reaction time and $C_{0,PhOH}$ is the phenol concentration for $t = 0$ (at the instant that illumination is turned on).

Operational parameters were therefore evaluated comparing the values of k_{app}, obtained by non-linear regression, and total organic carbon removal.

3.3.1.1 Photocatalytic degradation of phenol using different TiO_2 catalysts

TiO_2 catalysts obtained by sol-gel method at different calcination temperature were tested in the photodegradation of phenol under UV irradiation. It is known that several factors, including surface area, crystal composition and crystal phase contribute to the photocatalytic efficiency of TiO_2 [11, 12].

Phenol degradation was followed by high performance liquid chromatography. Irradiation with UV light was carried out for four hours. For all catalysts, the total conversion of phenol was achieved at the end of the reaction.

Since phenol absorbs at 253.7 nm ($\varepsilon_{253.7\ nm}$ = 410 M^{-1} cm^{-1}), direct photolysis of the molecule should not be excluded when studying the degradation process by UV radiation.

From pure photochemical reaction resulted an apparent rate constant of 1.4×10^{-2} min^{-1}, while the higher k_{app} of 2.04×10^{-2} min^{-1} was obtained for TiO_2-673 (Table 3.1). Catalysts obtained at higher temperatures resulted on progressively lower kinetic rate constants. Catalyst TiO_2-973, constituted by pure rutile crystals, showed a k_{app} of 1.45×10^{-2} min^{-1}, which corresponds to a close to 30% reduction comparing with pure anatase catalyst produced at 673K.

Table 3.1 Phenol conversion at 2 hours of reaction (X_{2h}), TOC removal after 4 hours of irradiation ($X_{TOC,4h}$) and pseudo-first order kinetic rate constant (k_{app}) for the different photochemical and photocatalytic systems.

System	X_{2h} (%)	$X_{TOC,4h}$ (%)	k_{app} ($\times10^{-2}$ min^{-1})
UV	82	19	1.4 ± 0.1
UV/TiO_2-573	91	70	1.83 ± 0.04
UV/TiO_2-673	93	83	2.04 ± 0.07
UV/TiO_2-773	90	67	1.73 ± 0.03
UV/TiO_2-723	89	64	1.69 ± 0.03
UV/TiO_2-873	88	56	1.49 ± 0.06
UV/TiO_2-973	82	33	1.45 ± 0.08

Total organic carbon analysis provided valuable information about the efficiency of the photo-assisted processes. It is obvious that the presence of a catalyst improved the removal of organic compounds from the solutions. At the end of the photodegradation runs (4 hours of irradiation) it was observed a merely 19%

decrease in organic content for reaction without any catalyst and 83% of TOC removal for reaction in the presence of TiO_2-673. The fraction of non-mineralized organics probably corresponds to aliphatic acids, not detected by HPLC in these experimental conditions, such as lactic, acetic, formic, maleic, oxalic and others resulting from the aromatic ring opening [13, 14].

From an energetic point of view, the photonic efficiency of a photo-induced process can be quantified in terms of its quantum yield (Φ), *i.e.*, the number of molecules which react according to this process divided by the number of photons absorbed by the system during the same time [15]. The determination of the quantum yield consists is an important tool to compare the activity of different catalysts for the same reaction.

In terms of kinetics, the initial quantum yield (Φ_0) can be defined as the ratio of the reaction rate (r_0), in moles of molecules per second, to the efficient photonic flux (φ), in Einstein per second [10], according to:

$$\Phi_0 = \frac{r_0}{\varphi} \tag{3.2}$$

The quantum yield of a process may vary on a wide range according to the characteristics of the catalyst, the experimental conditions and especially the nature of the reactions under consideration. The photonic flux (φ) is related to the radiant power of the lamp used in the degradation experiments as well as the wavelength of radiation emission. In the present work, a low-pressure mercury lamp was used with the most important emission line at 253.7 nm, with a photon flux for this wavelength of 4.78×10^{-6} Einstein s^{-1}. The initial quantum yields for the photochemical and photocatalytic reactions with the different catalysts are compared in Fig. 3.4.

Results are consistent with the previous observations based on first-order kinetics rate constants and TOC removal. TiO_2-673 appear to be the most photo-efficient catalyst, with a quantum yield of 3.05%, while for the pure rutile TiO_2 material a quite lower quantum yield of 2.16% was obtained. The pure photochemical process revealed the worst photo-efficiency with a quantum yield of 2.09%

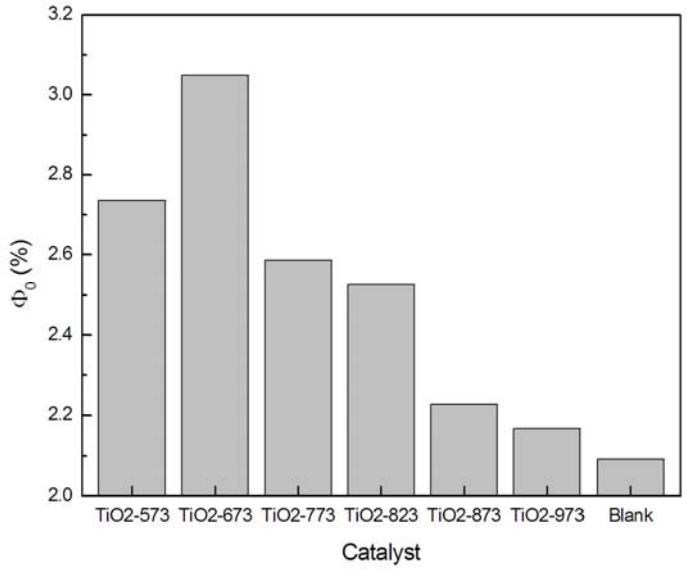

Figure 3.4 Initial quantum yields (Φ_0) for the different photochemical (Blank) and photocatalytic systems.

From these results it is obvious that the physical-chemical properties of the sol-gel TiO_2 materials play a crucial role on its photocatalytic performance.

Titanium dioxide obtained at 573K has the highest surface area and is mainly composed of anatase. Nevertheless, XRD measurements revealed broad peaks which indicate that the crystallization process is not complete. Amorphous titania is known to have low photocatalytic activity due to a high electron-hole recombination rate [16]. It was found that TiO_2 photocatalytic efficiency increases with calcination temperature up to 673K. The catalysts obtained at this temperature revealed to be the most active for photocatalytic degradation of phenol. For higher calcination temperature a progressive loss in photocatalytic efficiency was observed. The sample TiO_2-973 showed only little photocatalytic efficiency to decompose phenol. The decline in photoefficiency for higher calcination temperatures is attributed to the phase transformation from anatase to rutile. Simultaneously, the larger-sized titanium dioxide crystals resulted from higher temperatures also gives raise to a decrease in the photocatalytic performance of the semiconductor.

Because TiO_2-673 revealed itself as the most photo-efficient catalyst, it was used to optimize key parameters of the photodegradation of phenol under UV light.

3.3.1.2 Phenol adsorption on TiO_2-673

Adsorption followed by reaction in the adsorbed phase are the key steps in the heterogeneous photocatalytic process. Thus, is important to characterize the adsorption of phenol on nanocrystalline TiO_2. The equilibrium adsorption isotherm of phenol on TiO_2-673 was determined at room temperature (~298K) in natural pH conditions and is represented on Fig. 3.5.

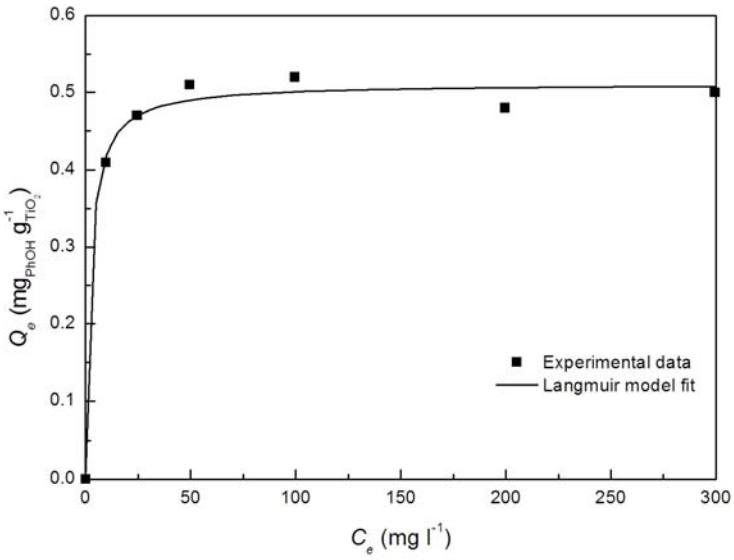

Figure 3.5 Adsorption equilibrium isotherm of phenol on TiO_2-673.

The experimental data has a good adherence to the equation of the Langmuir isotherm:

$$\theta = \frac{Q_e}{Q_m} = \frac{K_L C_e}{1 + K_L C_e} \tag{3.3}$$

where θ is the fraction of active sites for phenol adsorption, C_e and Q_e are the adsorptive equilibrium concentrations in the liquid and solid phases, respectively, Q_m is the maximum adsorption capacity and K_L is the adsorption equilibrium constant. K_L and Q_m parameters were calculated by non-linear fitting of the experimental data to Eq. 3.3 being of 4.27×10^4 M^{-1} and 5.44×10^{-6} mol g_{TiO2}^{-1}, respectively (R^2=0.992).

3.3.1.3 Catalyst loading

In order to avoid an ineffective excess of catalyst and to ensure a total absorption of efficient photons, the optimum mass of catalyst has to be found. In this study, TiO_2-673 concentration in the suspension was varied from 0.10 to 1.5 g l^{-1}. As shown in Table 3.2, k_{app} increased with the mass of catalyst up to a concentration of 1.0 g l^{-1}, confirming the heterogeneous nature of the photocatalytic process. This behavior reflects the increment of the active sites available for phenol adsorption and degradation. However, an increase on the catalyst loading to 1.5 g l^{-1} resulted in a decrease in the apparent rate constant, which can be attributed to a scattering effect due to the dispersion of UV radiation caused by the substantial amount of suspended photocatalyst. Furthermore, in these conditions, particles tend to agglomerate, making a significant fraction of the catalyst to be inaccessible to either adsorbing the molecules or absorbing the radiation, with consequent decrease in the active sites available for the catalytic reaction. The same tendency was observed for TOC removal.

Table 3.2 Apparent first-order kinetic rate constants and TOC removal after 4 hours of irradiation obtained for different TiO_2 concentrations.

C_{TiO2} (g l^{-1})	k_{app} ($\times 10^{-2}$ min^{-1})	$X_{TOC,4h}$ (%)
0.10	1.52±0.07	29
0.20	1.56±0.07	32
0.50	1.74±0.06	44
1.0	2.04±0.07	83
1.5	1.91±0.04	76

Following these observations, it was decided to keep the amount of TiO_2 at the optimum value of 1.0 g l^{-1} in subsequent photocatalytic degradation experiments.

3.3.1.4 Effect of pH

TiO_2 shows amphoteric behavior in aqueous media. The point of zero charge (pzc) of TiO_2-673, *i.e.* the point when the surface charge density is zero was found to be of 6.4, as shown in Fig. 3.6. This value corresponds to the pH at which

the straight line ($pH_{initial} = pH_{final}$) crosses the sigmoid curve (dashed line) passing through the experimental points.

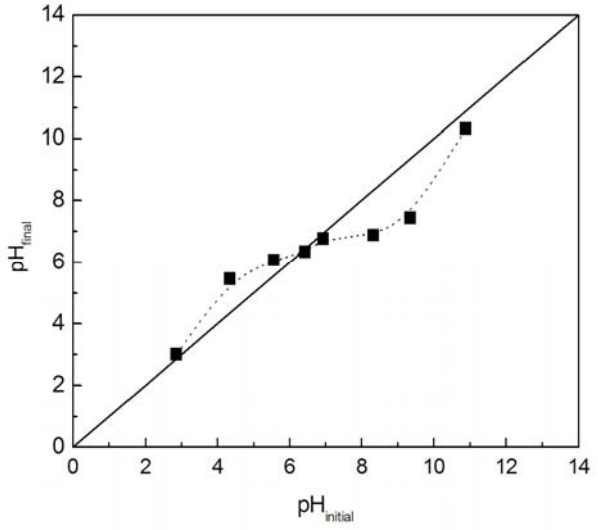

Figure 3.6 Determination of the point of zero charge of TiO_2-673.

At pH higher than pH_{pzc}, TiO_2 surface is negatively charged and TiO^- appears to be the predominant form (Fig. 3.7). For lower pH values, titania surface is in the protonated form ($TiOH_2^+$).

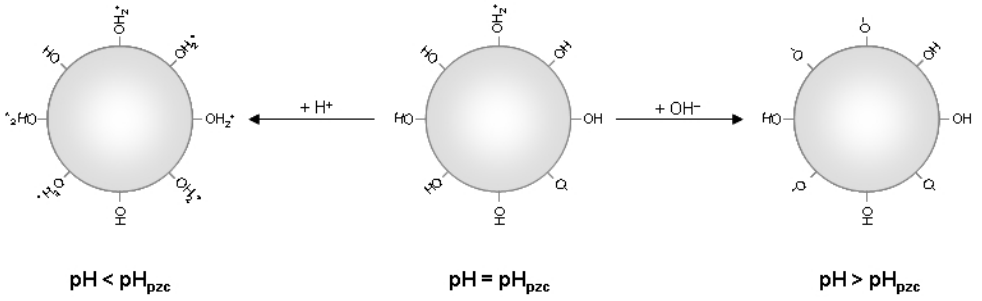

Figure 3.7 Effect of pH on surface charge of TiO_2.

Electric charge properties of both, catalyst and substrate, are found to play an important role on the adsorption process. Under aqueous media, phenol shows a pKa of 9.9 (at 25 ºC), which means that for pH<pKa, it is in the molecular form (C_6H_5OH) and at pH>pKa the molecule undergoes deprotonation becoming negatively charged ($C_6H_5O^-$). In order to study the effect of pH in the photocatalytic

degradation of phenol the initial pH of the suspensions was set at 3.0, 5.6 (natural pH) and 11.0 (Fig. 3.8).

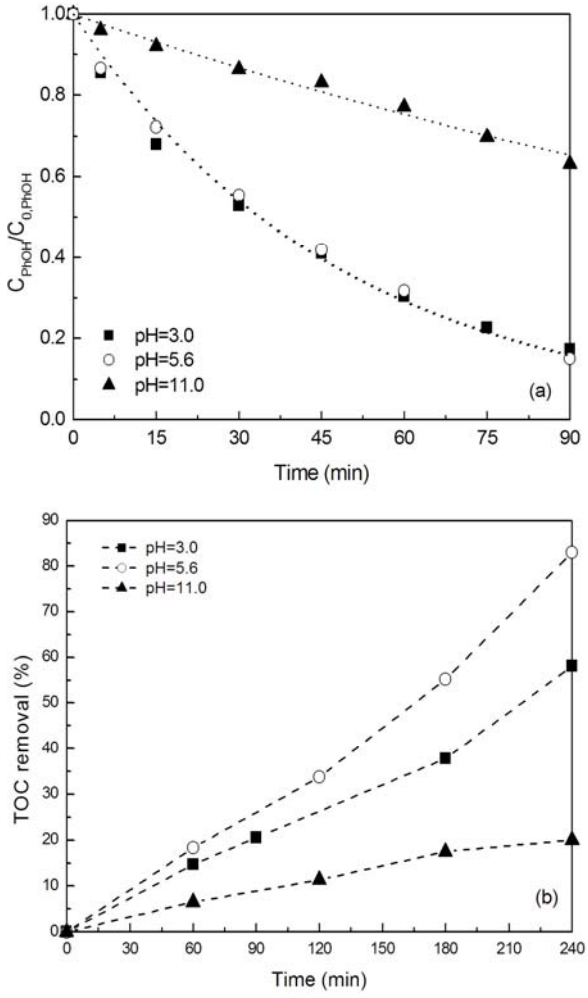

Figure 3.8 Effect of pH on phenol photocatalytic degradation (a) and TOC removal (b).

In terms of kinetics, basically no effect was observed when pH was decreased from 5.6 to 3.0 (Fig. 3.8a). Apparent first order kinetic rate constants were found to be of 2.04×10^{-2} min^{-1} and 2.06×10^{-2} min^{-1}, respectively. However, in what concerns to the mineralization of the organic compounds, the reaction at initial pH of 3.0 produced a lower TOC removal (Fig. 3.8b). At these acidic conditions the amount of HO^- groups in solution is much lower and therefore, there is a significant

decrease in the concentration of hydroxyl radicals available for the degradation of reaction intermediates. At the initial pH of 11.0, the photoefficiency of the process drastically decrease, and phenol removal becomes very slow, with a k_{app} of 4.70×10^{-3} min^{-1}. At these conditions, both catalyst and substrate are negatively charged, developing repulsive forces between them and therefore decreasing phenol adsorption.

3.3.1.5 Effect of photonic flux

For studying the influence of different light intensity in the photocatalytic degradation of phenol, a quartz jacket was placed around the irradiation source and inside of it a dye (C.I. Direct Green 26, $\varepsilon_{253.7nm}$=32 346 $M^{-1}cm^{-1}$) solution was circulating, acting as a light filter. Solutions of dye with different concentrations were used in order to absorb different fractions of light. Resultant radiation intensities were determined by ferrioxalate actinometry and are here presented as fractions of the initial flux (φ/φ_0), *i.e.*, the photonic flux obtained when water is passing throw the quartz jacket.

For the range of intensities studied, the apparent rate constant revealed to change linearly with the photonic flux (Fig. 3.9), which confirms the photoinduced nature of the catalytic process.

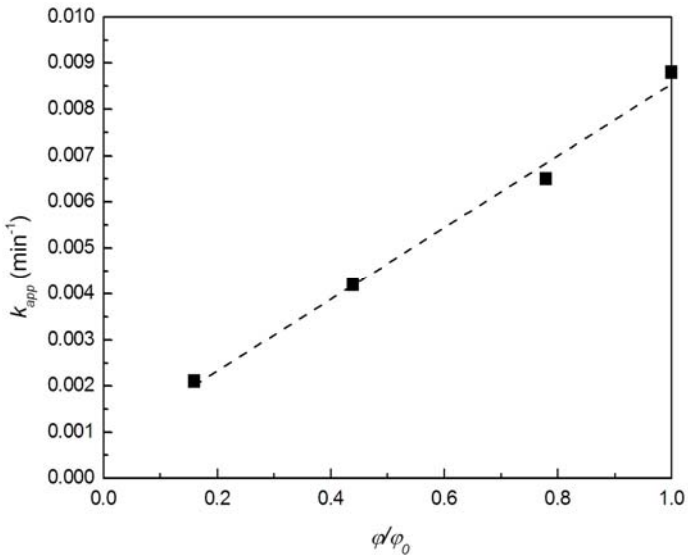

Figure 3.9 Apparent rate constant as a function of the photonic flux.

It is known that for high photonic flux, the instantaneous rate of formation of e^-/h^+ pairs become higher than photocatalytic reaction rate (r) and r become proportional to $\varphi^{1/2}$ [17]. Nevertheless, it is also known that the optimum light power utilization corresponds to the domain where r is proportional to φ [10].

3.3.1.6 Effect of oxygen partial pressure

The presence of an electron acceptor is essential to enhance the separation of photo-generated electrons and holes, improving the efficiency of the photocatalytic process. Oxygen dissolved in the solution is commonly employed as the electron acceptor.

The study of the effect of oxygen partial pressure on the photocatalytic degradation of phenol under UV irradiation was performed using nanocrystalline TiO_2-673 catalyst. The oxygen partial pressure was adjusted by diluting it in argon, and maintaining the overall flow rate at 200 ml min^{-1} for a total gas pressure of 1 atm. The initial phenol concentration was kept at 50 mg l^{-1} and the concentration of TiO_2-673 at 1 g l^{-1}. The comparison parameter was the apparent reaction rate constant (Fig. 3.10).

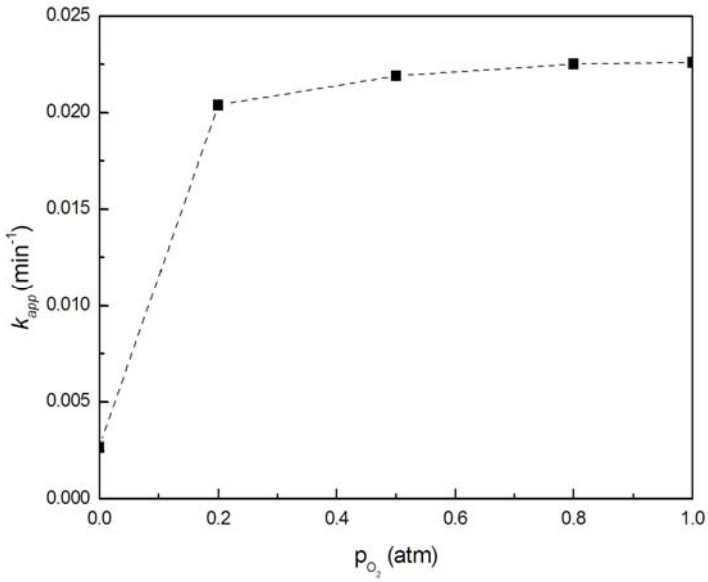

Figure 3.10 Effect of oxygen partial pressure on the apparent rate constant for the photocatalytic removal of phenol over TiO_2-673 under UV irradiation.

Results showed that the first-order rate constant increased with the oxygen partial pressure. The apparent rate constant reached about 90% of its maximum value at an oxygen partial pressure of 0.2 atm. This fact indicates that it is feasible to operate using air instead of pure oxygen for commercial application purpose.

It can be noticed that even in the absence of oxygen, when pure argon was bubbled through the suspension, degradation of phenol was still observed. At these conditions an apparent rate constant of 2.66×10^{-3} min^{-1} was obtained probably due to photolytic degradation of the organic compound. UV radiation itself has a tremendous oxidation potential (a 253.7 nm photon provides 4.89 eV) which is normally enough to interact with the electronic structure of the matter. However, in the absence of an electron acceptor the recombination of the electron/hole pairs is very fast inhibiting the photocatalytic process.

3.3.1.7 Effect of oxidant species

Photocatalytic reaction major energy wasting step consists in the recombination of photogenerated electrons and holes leading to the low quantum yield of the process. Electron/hole recombination can be minimized by adding a proper electron acceptor to the system.

Generally molecular oxygen, pure or in air, is used for this purpose. In order to compensate for the lack of oxygen caused either by consumption or slow oxygen mass transfer, the addition of inorganic oxidants to the semiconductor suspension such as H_2O_2, $KClO_3$, $Na_2S_2O_8$, $KBrO_3$ and KIO_4 must be considered [18-20]. These compounds show a positive effect on the rate of the photocatalytic oxidation of organic molecules in water by avoiding electron/hole recombination, as they act as electron acceptors. In the present study, hydrogen peroxide and sodium peroxydisulfate were tested as oxidizing agents in the photodegradation of phenol.

Hydrogen peroxide plays a dual role in photocatalytic reaction acting as electron acceptor, promoting the charge separation, being also able to decompose to produce $HO^{\bullet}$ radicals by absorption of light at 253.7 nm:

$$H_2O_2 + e^-_{cb} \longrightarrow HO^{\bullet} + HO^- \quad (3.4)$$

$$H_2O_2 \xrightarrow{h\upsilon} 2HO^{\bullet} \quad (3.5)$$

Hydroxyl radicals can as well be produced by reaction of H_2O_2 with superoxide radical anion as follows:

$$H_2O_2 + O_2^{\bullet -} \longrightarrow HO^{\bullet} + HO^{-} + O_2 \tag{3.6}$$

The addition of H_2O_2 to TiO_2 suspensions produced a significant enhancement on the kinetics of phenol photodegradation (Fig. 3.11) resulting an apparent rate constant of 2.16×10^{-1} min^{-1}, which correspond to an increase in k_{app} of a factor of about ten times. Total removal of phenol was observed at an irradiation time of less than 60 minutes. At that point, a 58% TOC removal was achieved and at the end of 4 hours of irradiation a 93% TOC decrease was observed, meaning a close to total mineralization.

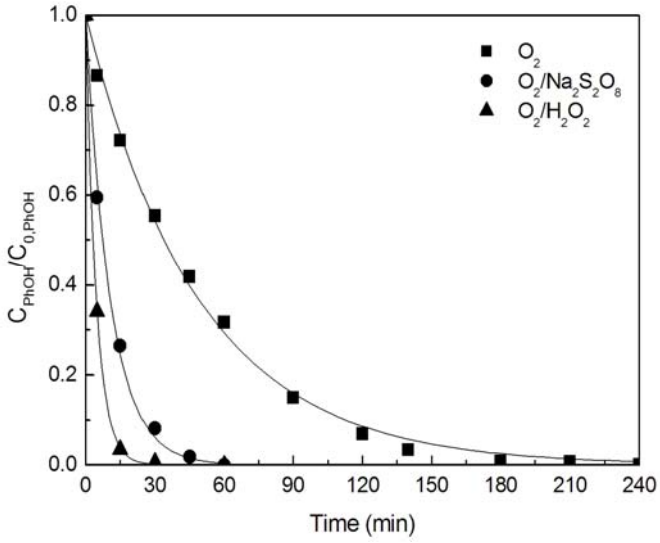

Figure 3.11 Effect of oxidants on photocatalytic degradation of phenol (C_{PhOH} = 50 mg l^{-1}; $C_{oxidant}$ = 1 g l^{-1}; gas flow rate = 200 ml min^{-1}; p_{O2} = 0.2 atm).

The introduction of peroxydisulfate anion also produced a beneficial effect on phenol degradation rate with a k_{app} of 9.31×10^{-2} min^{-1}. This positive effect is not only attributed to the promotion of semiconductor charge separation by reacting with conduction band electrons but also to the production of extremely oxidizing (E^0 = 2.6 eV) sulfate radicals capable of react with most organic molecules:

$$S_2O_8^{2-} \xrightarrow{h\upsilon} 2SO_4^{\bullet -} \tag{3.7}$$

$$S_2O_8^{2-} + e_{cb}^{-} \longrightarrow SO_4^{\bullet -} + SO_4^{2-} \tag{3.8}$$

$$SO_4^{\bullet -} + e_{cb}^- \longrightarrow SO_4^{2-} \quad (3.9)$$

$$SO_4^{\bullet -} + H_2O \longrightarrow HO^{\bullet} + SO_4^{2-} + H^+ \quad (3.10)$$

$$SO_4^{\bullet -} + R \longrightarrow SO_4^{2-} + intermediates \quad (3.11)$$

At the end of one hour of reaction, total removal of phenol was reached with a TOC reduction of 59% being of 94% at the end of 4 hours of irradiation.

3.3.1.8 Phenol concentration

Phenol concentration before dark adsorption period was varied from 10 to 50 mg l^{-1}. Results showed that for this range of concentrations the reaction rate gets slower as the initial amount of phenol in solution increases (Fig. 3.12).

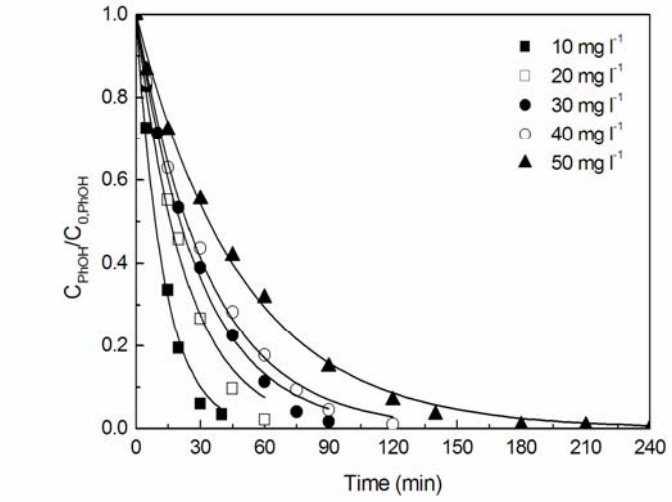

Figure 3.12 Effect of the initial concentration of phenol on the kinetics of the photocatalytic reaction.

The first-order apparent rate constant obtained for the reaction with the 10.0 mg l^{-1} phenol solution was of 9.32×10^{-2} min^{-1} while for the higher initial concentration (50.0 mg l^{-1}) a k_{app} of 2.04×10^{-2} min^{-1} was observed. As phenol concentration increases, more reactant and reaction intermediates are adsorbed on

the surface of the photocatalyst, therefore, the generation of hydroxyl radicals will be reduced since are only a fewer active sites for adsorption of hydroxyl anions.

The photocatalytic reaction rate dependency on the concentration of the organic substrate is generally well described by a Langmuir-Hinshelwood kinetic model [10]:

$$-r_A = k_{LH}\frac{K_{LH}C_A}{1+K_{LH}C_A} \tag{3.12}$$

where r_A is the rate of degradation of the organic compound A, and k_{LH} and K_{LH} are the apparent reaction rate and the apparent Langmuir adsorption constants, respectively.

The reaction mechanism usually considered for heterogeneous photocatalyzed reactions consist in two main steps: fast adsorption of the reactants on the catalyst surface (Eq. 3.13) and a slow step of reaction in the adsorbed phase of the organic compound and a photogenerated hydroxyl radical (Eq. 3.14), as follows:

$$A \underset{k_{-1}}{\overset{k_1}{\longleftrightarrow}} A_{ads} \tag{3.13}$$

$$A_{ads} \xrightarrow{k_{LH}} products \tag{3.14}$$

Although this is well established and greatly used for most of the authors to describe the kinetics of photo-oxidation reactions, some considerations have to be taking into account.

It has been recognized that k_{LH} and K_{LH} are light intensity dependent [21-24]. K_{LH} in a photocatalytic oxidation reaction has not the same meaning as the K_L dark adsorption constant. In a photo-induced reaction, the number of active catalyst sites is much fewer than the total surface adsorption sites. Thus, the K_{LH} value measured under illumination does not characterize the generally accessible surface probed by dark adsorption measurements. Another fact is that the active sites exist only under illumination and the species involved do not exist appreciably in the dark. Additionally, the determining rate step (Eq. 3.14) involves the reaction of the adsorbed substrate with a photogenerated $HO^{\bullet}$ radical. Since the latter will be a function of absorbed light intensity, which in turn will be proportional to the

incident light intensity (I), it follows that k_{LH} will also be a function of absorbed light intensity:

$$k_{LH} = \alpha\ I^{\beta} \tag{3.15}$$

where α is a proportionality constant and β is equal to 1.0 or 0.5 at low and high absorbed light intensities, respectively. A pseudo-steady state approach has recently been proposed [22-25] introducing the previously mentioned considerations. Therefore, the surface coverage of the organic compound (A) is given by:

$$\theta_A = \frac{K_{LH} C_A}{1 + K_{LH} C_A} \tag{3.16}$$

with

$$K_{LH} = \frac{1}{K_{LH,diss}} = \frac{k_1}{k_{-1} + \alpha I^{\beta}} \tag{3.17}$$

and $K_{LH,diss}$ being the apparent dissociation constant.

Thus, the general intensity dependence of the photocatalyzed reaction is given by:

$$-r_A = k_{LH}\theta_A = \frac{k_{LH} C_A}{K_{LH,diss} + C_A} \tag{3.18}$$

This pseudo-steady state approach predicts that both k_{LH} and $K_{LH,diss}$ depend on the intensity of absorbed light [23]. In this study, k_{LH} and K_{LH} constants were determined for two light intensities correspondent to a photon flux of 4.78×10^{-6} and 2.05×10^{-6} Einstein s^{-1} (Table 3.3).

Table 3.3 Langmuir-Hinshelwood parameters, k_{LH} and K_{LH} as a function of the photonic flux, φ.

φ ($\times10^{-6}$ Einstein s^{-1})	k_{LH} ($\times10^{-5}$ M min^{-1})	K_{LH} ($\times10^{4}$ M^{-1})
4.78	1.099	1.520
2.05	0.554	2.825

Results showed that k_{LH} is directly proportional to the photon flux while K_{LH} decreased for higher light intensity. As photon flux increases, the number of photogenerated $HO^{\bullet}$ radicals rise up accelerating the oxidation of the substrate molecules. Simultaneously, the increase of surface active species such as electrons, holes and $HO^{\bullet}$ radicals lead to a decrease in the available sites for adsorption of the primary molecule and therefore a decrease in K_{LH}. The adsorption equilibrium constants determined under illumination showed lower values than K_L, the adsorption constant in dark conditions. This means that only a small part of the adsorption sites play a role in the photocatalytic process.

3.3.2 Product analysis and reaction mechanism

HPLC analysis performed during the photocatalytic runs revealed that, despite the catalyst used, the primary reaction intermediates are single-substituted hydroxyl derivates, indicating that $HO^{\bullet}$ radicals are the key species involved in the oxidation process. Catechol (CT; 2-hydroxyphenol) and hydroquinone (HQ; 4-hydroxyphenol) were detected as main intermediates, which is in agreement with the orientating properties of phenol's hydroxyl group. Photocatalytic oxidation of benzene-substituted substrates containing electron donor groups, such as phenol, generate *ortho* and *para* mono-hydroxy derivatives as primary intermediates [26]. Trace concentrations of benzoquinone (in equilibrium with hydroquinone) were also detected. Thus, a simplified reaction mechanism is proposed (Scheme 3.1).

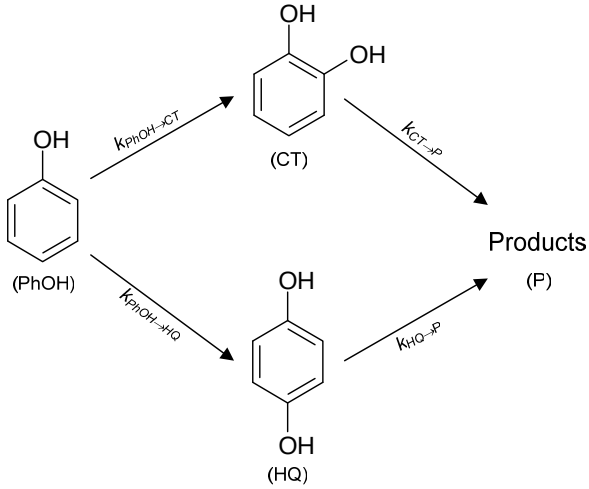

Scheme 3.1 Simplified mechanism for phenol degradation.

A kinetic model was developed taking into account the following observations: a) phenol concentration decays following a pseudo-first order rate law, reaching at the end of the photocatalytic run essentially zero concentration; b) the concentration of the main reaction intermediates initially rise and then decrease until almost complete disappearance at the same time of complete phenol conversion; c) TOC decrease follows a zero order kinetic rate, indicating that for short reaction times there is already a high portion of organic compound that has been mineralized. Assuming all reactions to be first order, the rate expression of phenol, catechol and hydroquinone can be expressed as follows:

$$\frac{dC_{PhOH}}{dt} = -(k_{PhOH\rightarrow CT} + k_{PhOH\rightarrow HQ})C_{PhOH} \quad (3.19)$$

$$\frac{dC_{CT}}{dt} = k_{PhOH\rightarrow CT}C_{PhOH} - k_{CT\rightarrow P}C_{CT} \quad (3.20)$$

$$\frac{dC_{HQ}}{dt} = k_{PhOH\rightarrow HQ}C_{PhOH} - k_{HQ\rightarrow P}C_{HQ} \quad (3.21)$$

being $k_{PhOH\rightarrow CT}$, $k_{PhOH\rightarrow HQ}$, $k_{CT\rightarrow P}$ and $k_{HQ\rightarrow P}$ the first order apparent rate constants for the formation and consumption of phenol, catechol and hydroquinone as represented in Scheme 3.1. The first order ordinary differential equations were solved using MatLab and non-linearly regressed with experimental data to obtain the kinetic rate constants (Table 3.4). The rate of photocatalytic removal for phenol ($k_{PhOH\rightarrow CT}$ + $k_{PhOH\rightarrow HQ}$) follows the same tendency of k_{app} obtained by non-linear curve fitting of the experimental data from phenol abatement to Eq. 3.1.

Table 3.4 First order apparent rate constants, k ($\times 10^{-2}$ min^{-1}), for the photocatalytic oxidation of phenol using different TiO_2 catalysts.

Catalyst	$k_{PhOH\rightarrow CT}$	$k_{PhOH\rightarrow HQ}$	$k_{CT\rightarrow P}$	$k_{HQ\rightarrow P}$
UV	0.58	0.90	1.86	1.30
UV/TiO_2-573	0.88	0.98	1.58	2.27
UV/TiO_2-673	1.29	0.72	1.58	2.27
UV/TiO_2-723	1.28	0.60	1.23	1.33
UV/TiO_2-773	1.27	0.59	1.15	1.24
UV/TiO_2-873	1.20	0.54	1.00	1.12
UV/TiO_2-973	0.97	0.45	0.89	1.03

Concentration profiles (experimental and model fit) for phenol, catechol and hydroquinone obtained during the photocatalytic oxidation reactions using TiO_2-673 and TiO_2-973 are showed in Figs. 3.13a and 3.13b, respectively.

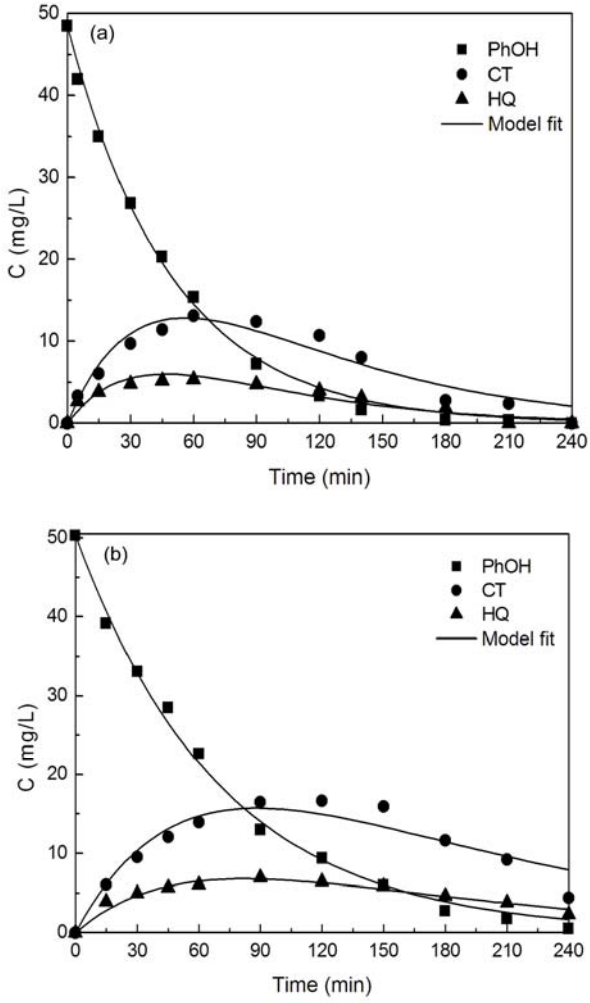

Figure 3.13 Concentration profiles of PhOH, CT and HQ and model fit for the photocatalytic degradation of phenol using TiO_2-673 (a) and TiO_2-973 (b) as catalysts.

As rutile fraction increases, phenol, catechol and hydroquinone formation and disappearance rate constants tend to decrease as a result of the loss of activity of the photocatalysts. The higher percentage of rutile phase and higher crystal particle dimension contribute both for the decrease on the photoefficiency of the

catalysts, inhibiting the formation of $HO^{\bullet}$ radicals and slowing down the degradation of the intermediate species.

The good adherence of the experimental points to the theoretical model is strongly supportive of the proposed mechanism.

3.3.3 Reutilization tests

Catalyst deactivation is one of the drawbacks on the application of TiO_2 to photocatalytic degradation of organic pollutants, mainly due to the strong adsorption of the original compound and/or by-products on the active sites of the catalyst surface [27-29]. The slight yellowish color of the used catalyst after photocatalytic degradation reactions may indicate the effects of chemisorption and chemisorbed species reconstruction processes on the degradation mechanism. These occurrences can be investigated from the DRIFT spectra of fresh TiO_2 and used catalysts after photocatalytic degradation reaction (Fig. 3.14).

Comparing the spectrum of the pure TiO_2 with that of the same material after the 30 min period of dark adsorption (assigned in Fig. 3.14 as t=0 h), it is visible the difference due to the adsorption of phenol. New bands ascribed to aromatic molecules can be observed in the region 1600–1000 cm^{-1} [28, 30]. The bands at 1278, 1375 and 1501 cm^{-1} correspond to the C–O stretching, O–H bending and C=C stretching vibrations of phenol molecule, respectively. The broad band present in the neat TiO_2 spectrum at around 3000 cm^{-1} attributed to the stretching vibrations of titania hydroxyl groups appears to be weaker in the adsorbed phenol spectrum and a deviation towards higher wavenumbers is observed. A broad band centered at 3250 cm^{-1} due to the O–H stretching vibration of phenol is now observed.

After illumination is turned on, and as reaction takes place, a progressive loss in the resolution of the spectra in the 1600–1000 cm^{-1} region is observed, which can be attributed to the degradation of the aromatic molecule. Parallel to this degradation, there is also a change in the vibrational structure of the TiO_2, as the bands at 1685 and 1280 cm^{-1} are getting less defined. Additionally, a significant and progressive reduction of the broad band located between 2500 and 3800 cm^{-1} is observed due to both phenol degradation and titania O–H surface groups removal during the photocatalytic reaction.

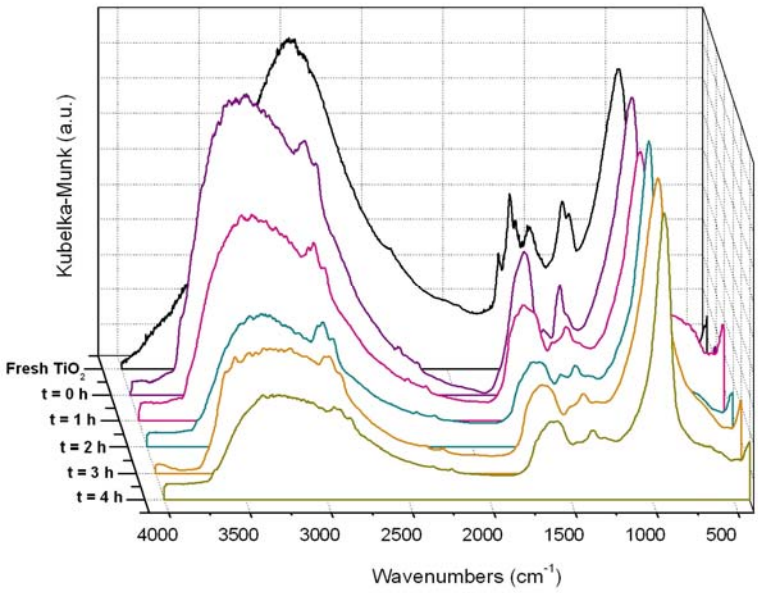

Figure 3.14 DRIFT spectra of the catalyst TiO_2-673 during several steps in the photocatalytic experiment.

After the photocatalytic degradation experiment, the recovered catalysts were reused in another two resumed photocatalytic experiments with fresh aqueous solutions of phenol. It was observed that the rate constants decreased in the two subsequent reactions by about 18% for each reutilization. Also a loss in the ability for TOC removal was observed (Table 3.5).

Table 3.5 Phenol conversion at 2 hours of reaction (X_{2h}), TOC removal after 4 hours of irradiation ($X_{TOC,4h}$) and pseudo-first order kinetic rate constant (k_{app}) for the photocatalytic degradation of phenol using fresh and recovered TiO_2.

Experiment	X_{2h} (%)	$X_{TOC,4h}$ (%)	k_{app} ($\times 10^{-2}$ min^{-1})
1st run	93	83	2.04 ± 0.07
2nd run	92	78	1.67 ± 0.05
3rd run	78	55	1.28 ± 0.04

At the end of the second reutilization of the catalyst only a 55% decrease in the organic content was observed being of 83% when the catalyst was used for the first time. This decline of the kinetics is ascribed to the presence of adsorbed species on the active sites of the catalyst surface and to the change on the catalyst

surface properties. Both factors account for the reduction of the number of available photoactive sites.

3.4 Conclusions

Nanocrystalline TiO_2 produced by an acid catalyzed sol-gel method can be successfully used as catalyst in the photo-oxidation of phenol under ultraviolet irradiation. Pure anatase TiO_2 is found to be more active than rutile containing catalysts. As calcination temperature of the xerogel increases, anatase to rutile phase transition occurs and crystallites tend to agglomerate from quantum to bulk-size particles with the progressive loss of activity of the catalyst.

The photocatalytic process is influenced by several operating factors such as catalyst loading, initial phenol concentration, pH of the medium, irradiation intensity, oxygen partial pressure and presence of oxidant species. Optimal operation conditions were found at natural pH using 1.0 g l^{-1} TiO_2-673 suspensions aerated with a 0.2 atm oxygen flow.

A pseudo-steady state approach applied to the Langmuir-Hinshelwood model is used to explain the dependency of the kinetics on the initial concentration of substrate and on illumination intensity. As photon flux increase, an increase in the kinetic rate constant is observed with a decrease on the adsorption rate constant.

Hydroquinone and catechol are detected as the main intermediates resulting form the attack of hydroxyl radical in the *para* and *ortho* positions of phenol molecule, respectively. Kinetics of consumption and formation reactions of substrate and intermediates fit well a first order rate law.

The reutilization of the catalyst resulted in a loss on its efficiency. A reduction on the catalyst ability for mineralization of the organic compounds was also observed. This loss on the photo-efficiency of the catalyst after being used in a degradation reaction is attributed to the presence of adsorbed species and to the change in the catalyst surface properties.

3.5 References

[1] H. Chun, W. Yizhong, T. Hongxiao, *Destruction of phenol aqueous solution by photocatalysis or direct photolysis*, Chemosphere. 41 (2000) 1205-1209.

[2] Z. Guo, R. Ma, G. Li, *Degradation of phenol by nanomaterial TiO_2 in wastewater*, Chem. Eng. J. 119 (2006) 55-59.

[3] A. Sobczynski, L. Duczmal, W. Zmudzinski, *Phenol destruction by photocatalysis on TiO_2: an attempt to solve the reaction mechanism*, J. Mol. Catal. A: Chem. 213 (2004) 225-230.

[4] W. Gernjak, M.I. Maldonado, S. Malato, J. Caceres, T. Krutzler, A. Glaser, R. Bauer, *Pilot-plant treatment of olive mill wastewater (OMW) by solar TiO_2 photocatalysis and solar photo-Fenton*, Sol. Energy. 77 (2004) 567-572.

[5] H.T. Gomes, J.L. Figueiredo, J.L. Faria, *Catalytic wet air oxidation of olive mill wastewater*, Catal. Today. 124 (2007) 254-259.

[6] M.C. Yeber, J. Rodriguez, J. Freer, N. Duran, H.D. Mansilla, *Photocatalytic degradation of cellulose bleaching effluent by supported TiO_2 and ZnO*, Chemosphere. 41 (2000) 1193-1197.

[7] J. Rivera-Utrilla, I. Bautista-Toledo, M.A. Ferro-Garcia, C. Moreno-Castilla, *Activated carbon surface modifications by adsorption of bacteria and their effect on aqueous lead adsorption*, J. Chem. Technol. Biotechnol. 76 (2001) 1209-1215.

[8] H.J. Kuhn, S.E. Braslavsky, R. Schmidt, *Chemical actinometry*, Pure Appl. Chem. 76 (2004) 2105-2146.

[9] M.H. Franson, A.D. Eaton, L.S. Clesceri, A.E. Greenberg, *Standard Methods for the Examination of Water and Wastewater*. 21st Edition ed. American Public Health Association, American Water Works Association and Water Environment Federation (2005), Washington D.C.

[10] J.M. Herrmann, *Heterogeneous photocatalysis: State of the art and present applications*, Top. Catal. 34 (2005) 49-65.

[11] G. Colon, J.M. Sanchez-Espana, M.C. Hidalgo, J.A. Navio, *Effect of TiO_2 acidic pre-treatment on the photocatalytic properties for phenol degradation*, J. Photochem. Photobiol. A: Chem. 179 (2006) 20-27.

[12] R.J. Tayade, R.G. Kulkarni, R.V. Jasra, *Photocatalytic degradation of aqueous nitirobenzene by nanocrystalline TiO_2*, Ind. Eng. Chem. Res. 45 (2006) 922-927.

[13] B. Tryba, A.W. Morawski, M. Inagaki, M. Toyoda, *The kinetics of phenol decomposition under UV irradiation with and without H_2O_2 on TiO_2, Fe-TiO_2 and Fe-C-TiO_2 photocatalysts*, Appl. Catal. B: Environ. 63 (2006) 215-221.

[14] Z. Wang, W. Cai, X. Hong, X. Zhao, F. Xu, C. Cai, *Photocatalytic degradation of phenol in aqueous nitrogen-doped TiO_2 suspensions with various light sources*, Appl. Catal. B: Environ. 57 (2005) 223-231.

[15] A.M. Braun, M.T. Maurette, E. Oliveros, *Photochemical Technology*, ed. J.W. Sons (1991), Chichester, England.

[16] B. Ohtani, Y. Ogawa, S.-i. Nishimoto, *Photocatalytic activity of amorphous-anatase mixture of titanium(IV) oxide particles suspended in aqueous solutions*, Journal of Physical Chemistry B. 101 (1997) 3746-3752.

[17] A. Mills, J. Wang, D.F. Ollis, *Dependence of the kinetics of liquid-phase photocatalyzed reactions on oxygen concentration and light intensity*, J. Catal. 243 (2006) 1-6.

[18] M. Kositzi, A. Antoniadis, I. Poulios, I. Kiridis, S. Malato, *Solar photocatalytic treatment of simulated dyestuff effluents*, Sol. Energy. 77 (2004) 591-600.

[19] L. Ravichandran, K. Selvam, M. Swaminathan, *Effect of oxidants and metal ions on photodefluoridation of pentafluorobenzoic acid with ZnO*, Sep. Purif. Technol. 56 (2007) 192-198.

[20] A.M.T. Silva, E. Nouli, N.P. Xekoukoulotakis, D. Mantzavinos, *Effect of key operating parameters on phenols degradation during H_2O_2-assisted TiO_2 photocatalytic treatment of simulated and actual olive mill wastewaters*, Appl. Catal. B: Environ. 73 (2007) 11-22.

[21] A.V. Emeline, V. Ryabchuk, N. Serpone, *Factors affecting the efficiency of a photocatalyzed process in aqueous metal-oxide dispersions: Prospect of distinguishing between two kinetic models*, J. Photochem. Photobiol. A: Chem. 133 (2000) 89-97.

[22] A. Mills, J. Wang, D.F. Ollis, *Kinetics of liquid phase semiconductor photoassisted reactions: Supporting observations for a pseudo-steady-state model*, J. Phys. Chem. B. 110 (2006) 14386-14390.

[23] D.F. Ollis, *Kinetics of Liquid Phase Photocatalyzed Reactions: An Illuminating Approach*, J. Phys. Chem. B. 109 (2005) 2439-2444.

[24] D.F. Ollis, *Kinetic disguises in heterogeneous photocatalysis*, Top. Catal. 35 (2005) 217-223.

[25] S. Brosillon, L. Lhomme, C. Vallet, A. Bouzaza, D. Wolbert, *Gas phase photocatalysis and liquid phase photocatalysis: Interdependence and influence of substrate concentration and photon flow on degradation reaction kinetics*, Appl. Catal. B: Environ. 78 (2008) 232-241.

[26] G. Palmisano, M. Addamo, V. Augugliaro, T. Caronna, A.D. Paola, E.G. López, V. Loddo, G. Marcì, L. Palmisano, M. Schiavello, *Selectivity of hydroxyl radical in partial oxidation of aromatic compounds in heterogeneous photocatalysis*, Catal. Today. 122 (2007) 118-127.

[27] J. Arana, J.A.H. Melian, J.M.D. Rodriguez, O.G. Diaz, A. Viera, J.P. Pena, P.M.M. Sosa, V.E. Jimenez, *TiO_2-photocatalysis as a tertiary treatment of naturally treated wastewater*, Catal. Today. 76 (2002) 279-289.

[28] J. Arana, E.T. Rendon, J.M.D. Rodriguez, J.A.H. Melian, O.G. Diaz, J.P. Pena, *High concentrated phenol and 1,2-propylene glycol water solutions treatment by photocatalysis - Catalyst recovery and re-use*, Appl. Catal. B: Environ. 30 (2001) 1-10.

[29] L.X. Cao, Z. Gao, S.L. Suib, T.N. Obee, S.O. Hay, J.D. Freihaut, *Photocatalytic oxidation of toluene on nanoscale TiO_2 catalysts: Studies of deactivation and regeneration*, J. Catal. 196 (2000) 253-261.

[30] B.H. Stuart, *Infrared Spectroscopy: Fundamentals and Applications*. E-book ed. Analytical techniques in the sciences (2004), Chichester, West Sussex, England, J. Wiley.

Part III

Nanostructured TiO_2 composite catalysts

Chapter 4

Nanostructured TiO_2 based materials for visible-light-driven photocatalysis

In this chapter the preparation of TiO_2-based composites is reported. Materials are prepared by combining titania with several materials including, activated carbon, activated carbon fibers, multi-walled carbon nanotubes, mesoporous molecular sieves, MCM41 and MCM48, and zeolite NaY. The synthesized materials are characterized by thermogravimetric analysis, N_2 adsorption-desorption isotherm measurements, X-ray diffraction, scanning electron microscopy and diffuse reflectance UV-Vis spectroscopy. The photocatalytic degradation of phenol is chosen as a model reaction to evaluate the photocatalytic activities of the composite catalysts under visible irradiation. The photoassisted oxidation results are compared in terms of the kinetics of the process and total organic carbon removal. The role of the introduced materials in the photocatalytic behavior of the composite catalysts is discussed by means of the mechanism of the photocatalytic degradation reaction. The increase of the efficiency of the photocatalytic process using the biphasic composite materials in relation to the pure TiO_2 is quantified in terms of a synergy factor.

4.1 Introduction

In photocatalytic reactions, catalysts are generally suspended in the liquid phase using slurry reactors [1, 2]. Main disadvantage consists in the necessity of a post-separation process to isolate the catalyst particles.

By the other hand, immobilization of the photocatalyst in a fixed support [3-5] does not pose the problem of additional catalyst post-separation. Immobilized catalyst photoreactor systems can operate in a continuous regime and if an adequate catalyst support is used they can benefit of some synergetic effects to improve photo-efficiency. However, mass transfer limitations are an issue to take in consideration, as well as the possibility of catalyst fouling and/or wash out.

When TiO_2 is used as catalyst in slurry reactors, usual shortcomings of the process are filtration of titania fine particles and effective absorption of radiation, particularly in the visible range of the spectrum. In order to facilitate the use of TiO_2 as photocatalyst, immobilization on a suitable substrate is desired. Therefore, a great deal of effort has been taken to increase the photoefficiency by dispersing TiO_2 nanoparticles on high surface area materials. In addition it was found that a beneficial effect in the photocatalytic activity of TiO_2 can be obtained by introducing different materials such as silica [6-8], alumina [9, 10], materials derived from carbon [11-16], zeolites [17-20] and mesoporous molecular sieves [20-22], due to their unique pore structure, adsorption, acidity and electronic properties.

In the present study, TiO_2 prepared by an acid-catalyzed sol-gel method was combined with several materials including activated carbon (AC), activated carbon fibber (ACF), multi-walled carbon nanotubes (CNT), mesoporous molecular sieves (MCM41 and MCM48) and zeolite NaY. The photocatalytic degradation of phenol was chosen as model reaction to evaluate the photocatalytic activities of the developed catalysts under visible radiation.

4.2 Experimental

4.2.1 Catalysts preparation

Composite catalysts were produced by combining TiO_2 with several different materials: siliceous molecular sieves (hexagonal MCM41 and cubic MCM48), synthesized hydrothermally according to the procedure outlined elsewhere [23]; zeolite NaY (Grace Davison GmbH); activated carbon (AC) NORIT ROX 0.8 (NORIT Nederland B.V.), produced by steam activation and acid washed; phenolic based activated carbon fiber (ACF) Kuractive FR15 (Kuraray Chemical) and multi-walled carbon nanotubes (CNT) synthesized by catalytic decomposition of CH_4, purchased from Shenzhen Nanoport Co. Ltd (manufacturer data: purity > 95%, diameter < 10 nm; length = 5 – 15 μm).

Composite catalysts were prepared by means of a modified acid-catalyzed sol-gel method from an alkoxide precursor. The mass ratio between the different materials and TiO_2 phases was maintained at 1:5. The preparation of the TiO_2-based composites was performed at room temperature as following: 0.1 mol of titanium isopropoxide ($Ti(OC_3H_7)_4$, Aldrich 97%) was dissolved in 200 ml of ethanol (Panreac p.a.). The solution was stirred magnetically for 30 min, and then 1.56 ml of nitric acid (Fluka 65 wt.%) was added. Subsequently, certain amount of material was introduced into the $Ti(OC_3H_7)_4$ ethanol solution. The mixture was loosely covered and kept stirring until a homogenous gel formed. The gel was aged in air for several days. Then, the xerogel was crushed into a fine powder (particle size < 100 μm) and dried at room temperature. The powder was calcined at 673K in a flow of nitrogen for 2 h. Catalysts are named as X-TiO_2, where X corresponds to the material which titania was combined with.

For comparison purposes commercial TiO_2 Degussa P25 (Degussa Portuguesa) was used, without any modification. This material consists mainly of anatase (~80%) with a BET surface area of 55 $m^2\ g^{-1}$ and a mean particle size of 30 nm (manufacturer data).

4.2.2 Catalysts characterization

Characterization of TiO_2-loaded catalysts was performed by thermogravimetric analysis, N_2 adsorption-adsorption isotherm measurements at

77K, powdered X-ray diffraction and diffuse reflectance UV-Vis spectroscopy, following the procedures described in Chapter 2, section 2.2.2.

Scanning electron microscopy (SEM) was performed in a high resolution (Schottky) FEI Quanta 400FEG microscope. Elemental analysis was determined by energy dispersive X-ray spectroscopy (EDX) in an EDAX Genesis X4M apparatus. For both techniques, the powders were placed in a sample holder using a carbon tape. In order to increase its conductivity, MCM41-TiO_2, MCM48-TiO_2 and NaY-TiO_2 composites were coated by gold sputtering.

4.2.3 Photocatalytic degradation of phenol

4.2.3.1 Photocatalytic reactor and light source

The experiments were carried out in a 1000 ml glass immersion photochemical reactor charged with 800 ml of solution/suspension. The reactor was equipped with an UV-Visible lamp, located axially and held in a quartz immersion tube (Fig. 4.1).

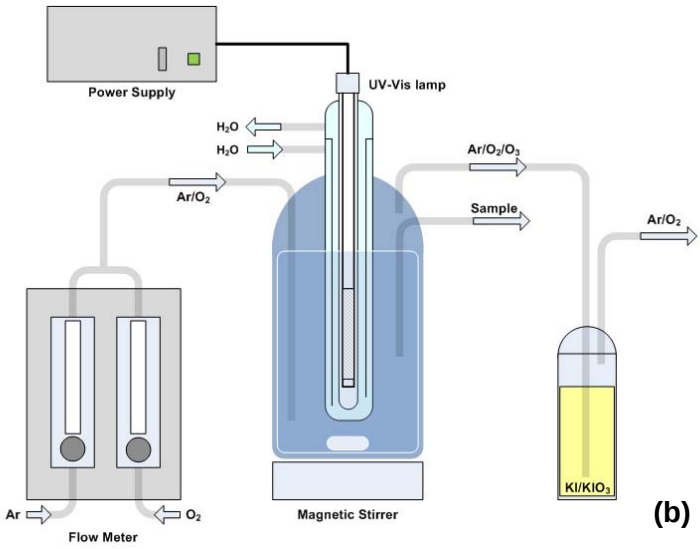

Figure 4.1 Photocatalytic reaction setup: (a) photograph; (b) scheme.

The radiation source was a Heraeus TQ 150 medium-pressure mercury vapor lamp with the more intense lines at λ_{exc} of 254, 313, 366, 436, 546 and 578 nm (Fig. 4.2).

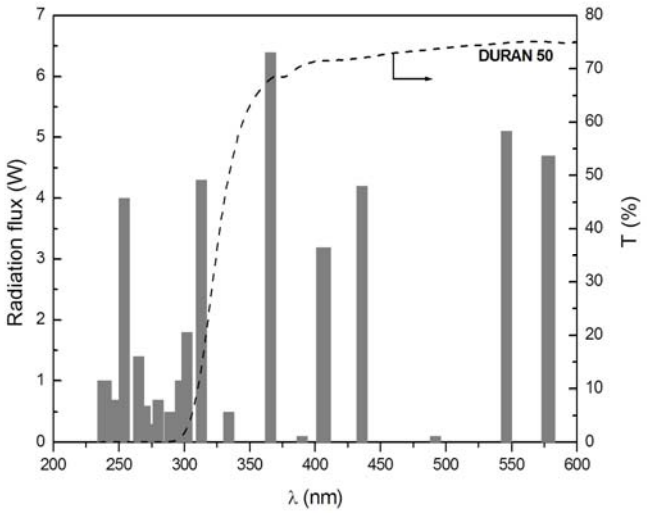

Figure 4.2 Radiation flux of Heraeus TQ 150 immersion lamp and transmission spectrum of the DURAN 50 filter.

The lamp was located axially and held in a quartz immersion tube. The UV radiation ($\lambda < 300$ nm) was filtered using a DURAN 50® glass jacket where water

was circulating to cool the irradiation source and cancel the infrared radiation, thus preventing any heating of the suspension.

The solution/suspensions were magnetically stirred. The gas feeding system was the same that was used for the UV system described in Chapter 3, section 3.2.4.1. Temperature of the reaction media was kept at 298 ± 3K by the water cooling jacket placed around the radiation source.

4.2.3.2 Photodegradation experiments

Photocatalytic activities of the synthesized materials were evaluated by phenol (Aldrich redistilled, 99+%) degradation in aqueous media under visible irradiation. The experiments were carried out in a glass immersion photochemical reactor charged with 800 ml of solution/suspension.

The initial phenol concentration was set at 50 mg l^{-1}. The amount of suspended TiO_2 was kept at 1 g l^{-1}, with the corresponding concentration of composite catalyst of 1.2 g l^{-1}. Experimental runs were carried out at natural pH conditions. A gaseous mixture of oxygen and argon (20% *vol.* O_2) was continuously bubbled during the experiments. Suspensions were left to equilibrate in the dark for 30 minutes before the light was turned on. The bulk concentration of phenol was determined at this point for each experiment and denoted $C'_{0,PhOH}$. Reactions were extended for 9 hours.

Samples were withdrawn regularly from the reactor and centrifuged for separation of the catalyst. The clean transparent solution was then analyzed by UV-Vis spectroscopy. The full spectrum (200-800 nm) of each sample was recorded on a JASCO V-560 UV–Vis spectrophotometer (double monochromator and double beam optical system) and the absorbance at characteristic phenol band at 270 nm was followed. Reaction intermediates of selected reactions were detected by high performance liquid chromatography. Total organic carbon measurements were performed at controlled reaction times.

4.3 Results and discussion

4.3.1 Catalysts characterization

The evolution of the xerogel samples during calcination could be obtained by thermogravimetric analysis. TG and DTG curves, here shown for NaY-TiO_2 (Fig. 4.3a) and AC-TiO_2 (Fig. 4.3b), revealed that apart from the material used to produce the TiO_2-based composites, similar evolution profiles are observed.

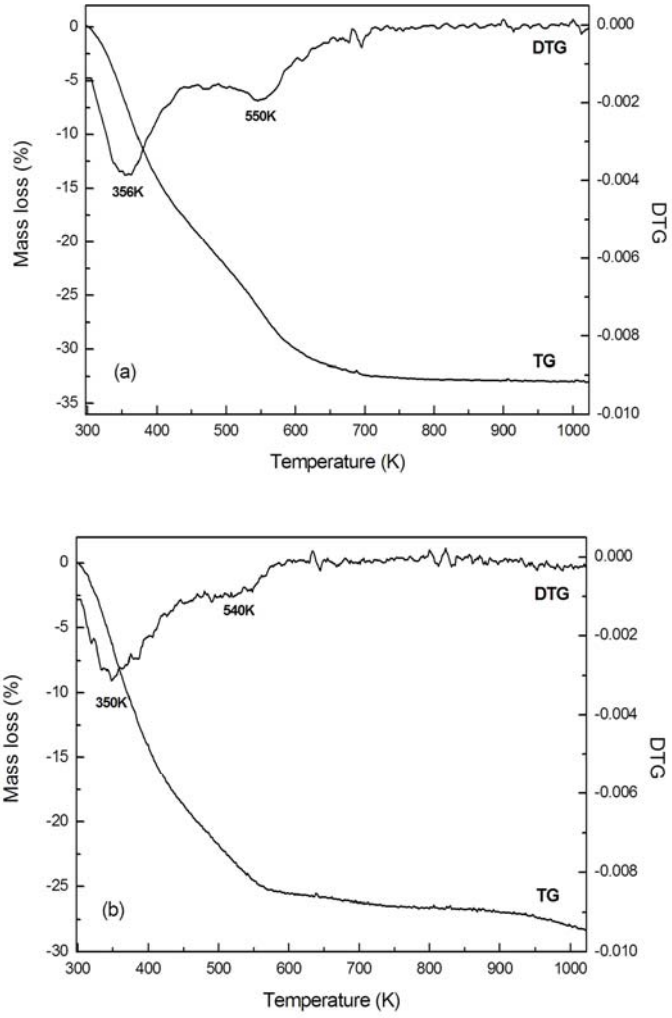

Figure 4.3 Thermogravimetric analysis of (a) NaY-TiO_2 and (b) AC-TiO_2 xerogels in nitrogen.

DTG curves present one intense band at approximately 350K and one broad band at around 550K, which can be attributed to the evaporation the alcohol solvent

and the decomposition of titanium isopropoxide during TiO_2 crystallization process, respectively. In the case of AC-TiO_2 material, TG profile indicate a mass loss up to 673K of a total 26%, followed by less than 3% loss up to a temperature of 1023K. For NaY-TiO_2 xerogel, these mass losses were of 32% and 1%, respectively. TG analysis of the composite catalysts revealed that calcination at 673K doesn't provide any degradation of the support materials.

XRD patterns reveal that only anatase phase can be identified for the prepared catalysts (Fig 4.4a). The rutile and brookite phases of TiO_2 are not observed.

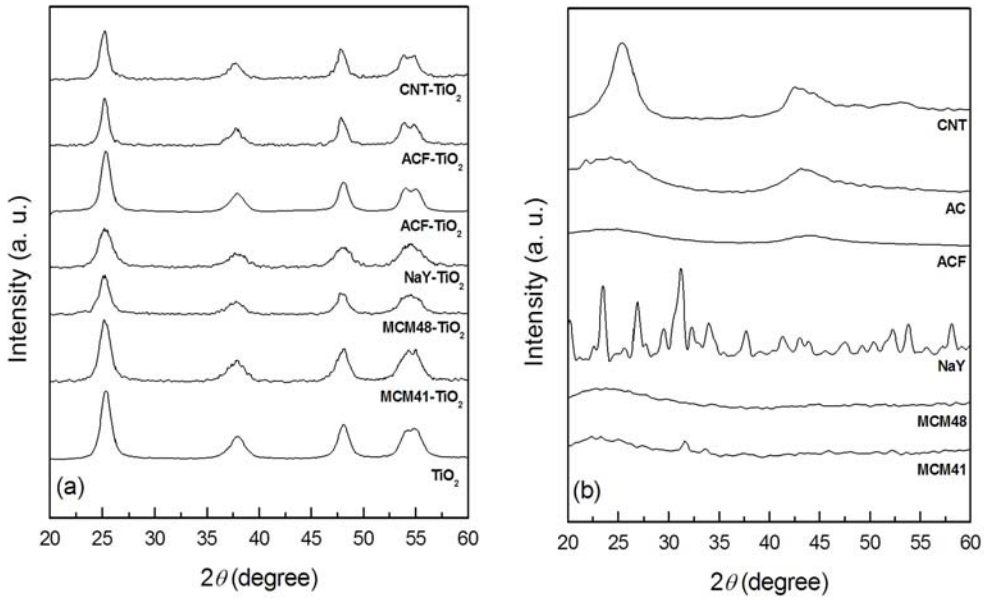

Figure 4.4 XRD patterns of: (a) TiO_2-based composite catalysts; (b) different materials (X) used to produce X-TiO_2.

It is noteworthy that the characteristic peaks of the different materials can hardly been identified from the patterns of composite materials (Fig. 4.4b).

The anatase crystallite dimensions were estimated using Scherrer's equation (Eq. 2.5) from the (2 0 0) line broadening of TiO_2 (2θ = 48.1º), where there is hardly any interference from the different supports (Table 4.1). The dimensions of anatase crystallites in the composite catalysts and of bare titania appear to be comparable. In fact, estimated crystallite sizes on composite catalysts

are even lower than for titania, which suggests that the introduction of the different supports avoid TiO_2 particle agglomeration.

Table 4.1 Surface area (S), calculated surface area (S_{calc}) and anatase crystal size (d_A) of TiO_2 loaded materials.

Catalyst	S (m^2 g^{-1})	S_{calc} (m^2 g^{-1})	d_A (nm)
TiO_2	107	---	8.5
MCM41	660	---	---
MCM41-TiO_2	138	201	6.9
MCM48	954	---	---
MCM48-TiO_2	208	251	7.3
NaY	698	---	---
NaY-TiO_2	139	207	8.0
AC	1047	---	---
AC-TiO_2	173	267	8.4
ACF	1280	---	---
ACF-TiO_2	244	306	8.3
CNT	185	---	---
CNT-TiO_2	131	120	8.3

As expected the composite catalysts exhibit higher surface area than neat TiO_2. With the exception of CNT-TiO_2, the surface areas of the composite catalysts are lower than those estimated theoretically (S_{calc}) in proportion to the TiO_2 and support contents, suggesting the formation of a common interface between the two solid phases. This contact surface was confirmed by scanning electron microscopy (Fig. 4.5).

The synthesized composites showed distinct morphologies depending on the material which TiO_2 was combined with. Generally, an intimate contact between TiO_2 and the different substrates can be observed, with the two phases blending together.

Micrographs of MCM41-TiO_2 (Fig. 4.5a) and MCM48-TiO_2 (Fig. 4.5b) composite materials show MCM41 and MCM48 spheroid particles mixed together with TiO_2 phase. NaY-TiO_2 composite is constituted by TiO_2 crystallite aggregates placed outside the external surface of NaY granules (Fig. 4.5c).

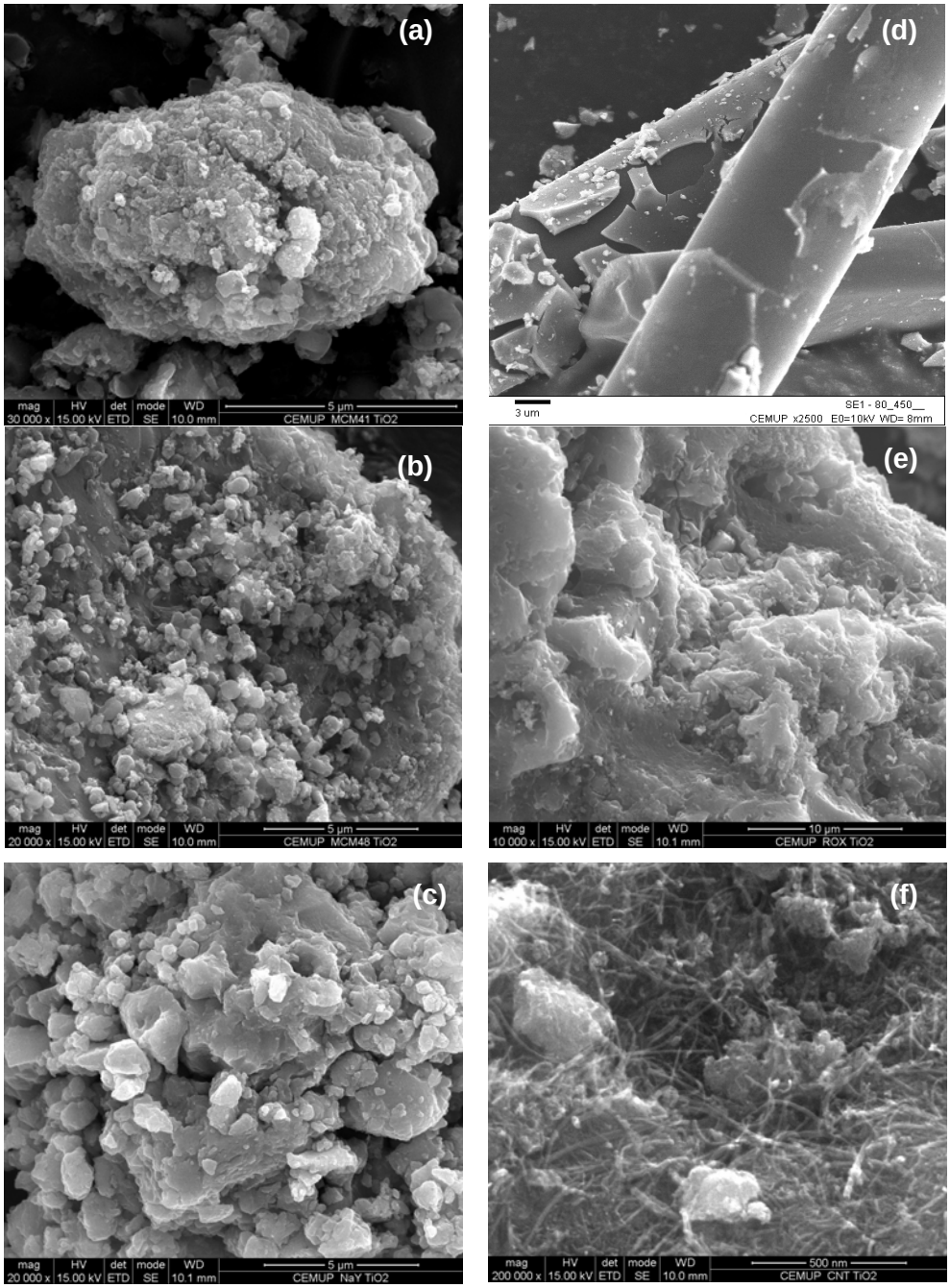

Figure 4.5 SEM micrographs of the X-TiO_2 composite materials: (a) MCM41-TiO_2; (b) MCM48-TiO_2; (c) NaY-TiO_2; (d) ACF-TiO_2; (e) AC-TiO_2; (f) CNT-TiO_2.

In the case of ACF-TiO_2 (Fig. 4.5d), a non-uniform titania layer is observed on the carbon fiber surface, while in AC-TiO_2 composite catalyst (Fig. 4.5e) TiO_2 particles with small size are settled in the outside surface of AC substrate. CNT-TiO_2 SEM image (Fig 4.5f) shows relatively homogeneous CNT embedding in the TiO_2 matrix with little agglomeration of TiO_2 particles.

Following the characterization above, morphologies of the composite materials suggest different types of interaction between TiO_2 and the different substrates.

EDX spectra of the carbon materials-TiO_2 composites confirm only the presence of C, O and Ti elements (Figs. 4.6d, 4.6e and 4.6f). MCM41-TiO_2 and MCM48-TiO_2 EDX analysis show the presence of silicon, titanium and oxygen. In the case of NaY-TiO_2 catalyst, besides Ti and O, also Na, Si and Al from NaY zeolite constitution were detected. Additionally, the EDX spectra of the composite catalysts showed on Figs. 4.6a, 4.6b and 4.6c reveal the presence of carbon, probably due to the carbon tape used to fix the sample, and gold from the film sputtered in order to improve the conductivity of those materials.

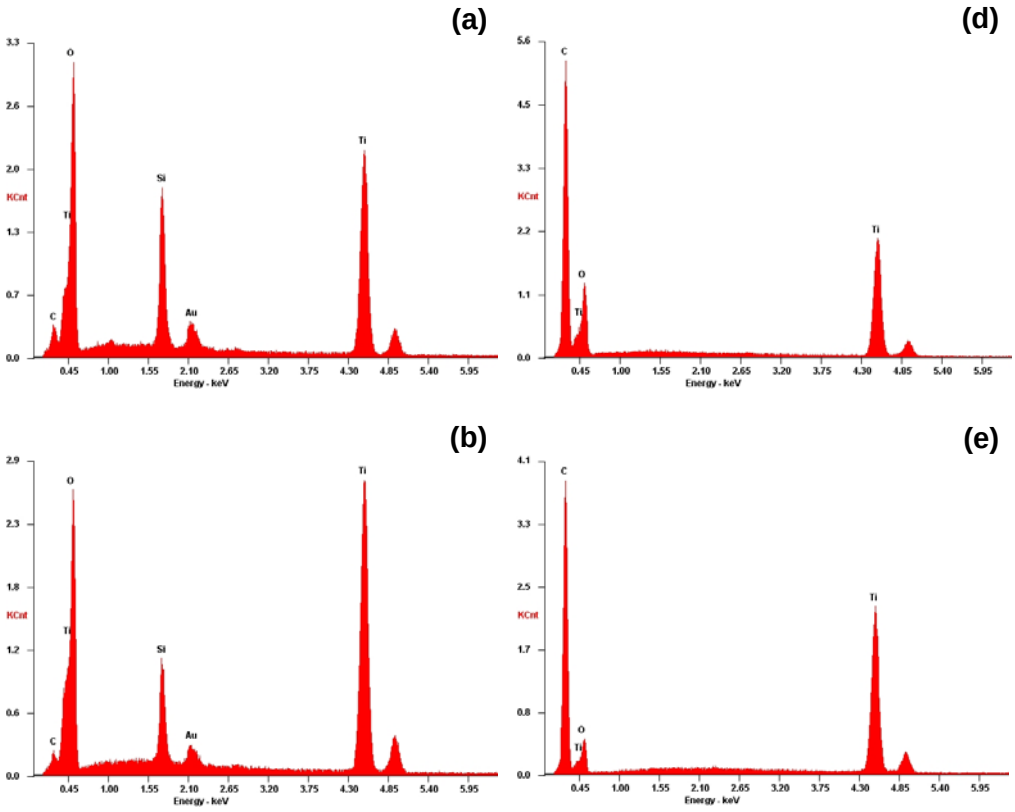

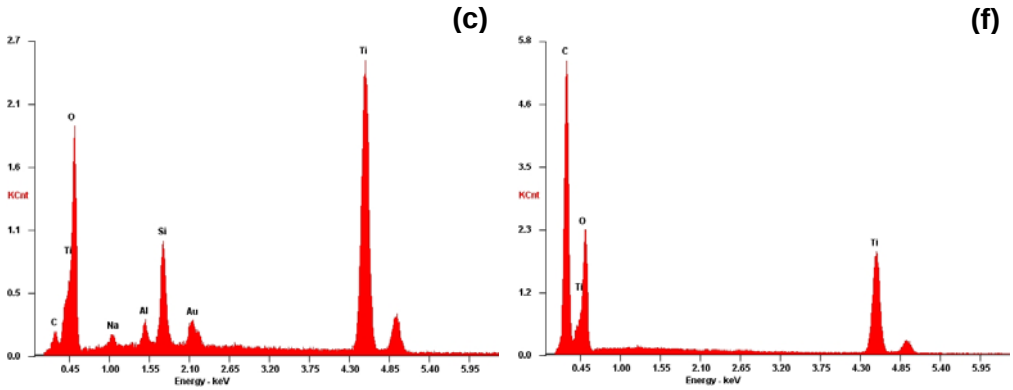

Figure 4.6 EDX spectra of the X-TiO_2 composite materials: (a) MCM41-TiO_2; (b) MCM48-TiO_2; (c) NaY-TiO_2; (d) ACF-TiO_2; (e) AC-TiO_2; (f) CNT-TiO_2.

The diffuse reflectance UV-Vis spectra of the different materials expressed in terms of Kulbelka-Munk equivalent absorption units are shown in Fig. 4.7.

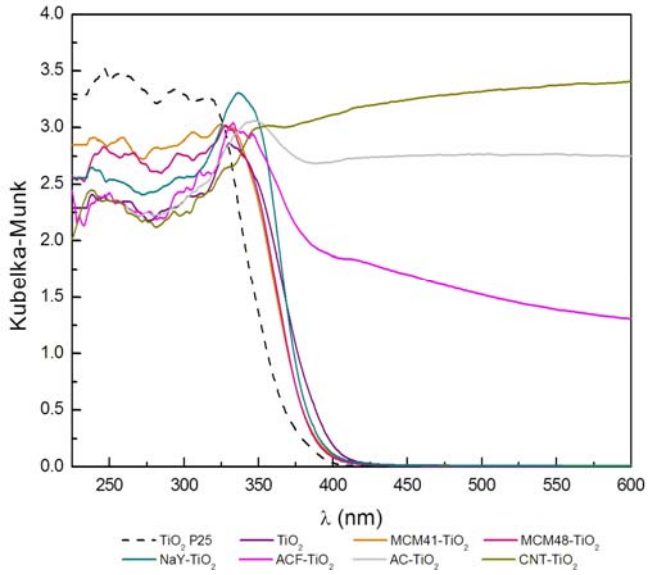

Figure 4.7 Diffuse reflectance UV-Vis spectra of commercial TiO_2 Degussa P25, TiO_2 prepared by sol-gel method and of the different composite catalyst.

As expected, TiO_2 P25 shows the characteristic spectrum with its fundamental absorption sharp edge rising at 400 nm, while the absorption spectrum of neat titania prepared by the sol-gel method shifts a bit into visible light region.

Similar absorption spectra were observed for MCM41-TiO_2, MCM48-TiO_2 and NaY-TiO_2 composite catalysts.

By the other hand, the introduction of a carbon phase into the TiO_2 matrix leads to a rise of light absorption in the visible spectral region. For the CNT-TiO_2 catalyst, the absorption spectrum changes dramatically with relation to neat TiO_2 and spawns over the whole range of the UV-Vis region, suggesting a strong interphase interaction.

4.3.2 Photocatalytic removal of phenol under visible irradiation

It was observed no appreciable photodegradation on the direct photolysis of phenol aqueous solutions. This is in-line with the fact that phenol has only a residual absorption in the visible range.

The photodegradation of phenol in aqueous suspensions containing TiO_2 and TiO_2-based catalysts under visible light follows pseudo-first-order kinetics. Kinetic rate constants were obtained from the plots of the linear transform of $\ln (A_0/A) = f(t)$, with A_0 and A being the absorbance of the solution for $t = 0$ and at the instant t, respectively (Table 4.2). The kinetic constants (k_{app}) correspond to the slope of the straight line obtained for $t < 60$ minutes.

Care should be taken, noticing that in this definition of k_{app} there is an uncertainty due to additive absorption of the different species at the used wavelength. This uncertainty was removed in the following chapters, by the determination of the concentration of both, reactant and intermediates, by HPLC.

A synergy factor (R), suggested in the previous literature [24-26], was used to quantify the effect caused by the introduction of each material into the TiO_2 matrix, being defined as:

$$R = \frac{k_{app}(X - TiO_2)}{k_{app}(TiO_2)}. \qquad (4.1)$$

All sol-gel synthesized catalysts revealed to have a better performance than commercial Degussa P25. Molecular sieves and zeolite NaY supported catalysts don't produce any appreciable effect on the photocatalytic degradation of phenol compared with neat sol-gel titania. In fact, as it's shown in the UV-Vis spectra,

these catalysts have quite similar absorption properties. On the other hand carbon materials do produce a visible effect on the kinetics of phenol removal. The increase in the synergy factor for these materials can be correlated to the UV-Vis absorption spectra of the catalysts.

Among carbon-based materials, carbon nanotubes appeared to be the most effective support. The introduction of CNT into titania matrix obviously creates a kinetic synergetic effect in phenol degradation with an increase in the rate constant by a factor of 2.7. To understand the role of the support in this composite catalyst, a suspended mechanical mixture of 20% CNT and TiO_2 was prepared by merely stirring both materials. As expected, the irradiated mixtures show less synergetic effect than the composite catalyst with the same CNT content. The calculated *R* value was of 2.3.

Table 4.2 Concentration of phenol after dark adsorption period ($C'_{0,PhOH}$), TOC removal after 9 hours of irradiation ($X_{TOC,9h}$), apparent rate constant (k_{app}) and synergy factor (R) for the different photochemical and photocatalytic systems.

Catalyst	$C'_{0,PhOH}$ (mg l^{-1})	$X_{TOC,9h}$ (%)	k_{app} ($\times 10^{-3}$ min^{-1})	R
TiO_2 P25	49.0	39	---	---
TiO_2	48.8	87	1.5 ± 0.1	---
MCM41-TiO_2	48.2	59	1.5 ± 0.1	1.0
MCM48-TiO_2	48.4	56	1.7 ± 0.1	1.2
NaY-TiO_2	48.6	60	1.7 ± 0.1	1.2
AC-TiO_2	33.8	72	3.1 ± 0.1	2.1
ACF-TiO_2	33.5	79	2.5 ± 0.1	1.7
CNT-TiO_2	48.2	90	3.9 ± 0.1	2.7
CNT+TiO_2	46.7	69	3.4 ± 0.1	2.3

Regarding the previous results on the characterization and photocatalytic activity of CNT-TiO_2, the synergetic effect of CNT on the activity of the composite catalyst can be explained in terms of its action as: a) dispersing agent; b) adsorbent; c) photosensitizer [27].

The effect induced by (a) is not likely to be dominant in accounting for the observed synergy, since neat TiO_2 shows relatively poor kinetic photo-efficiency under visible light irradiation. The introduction of CNT into the composite catalyst does not provide a major effect on its adsorption capacity. After the dark adsorption period, phenol concentration only decreases 4% for the CNT-TiO_2 catalyst. For titania composite catalysts on AC and ACF the concentration after the adsorption period decreases around 33%, but with these catalysts a synergetic factor of only 2.1 and 1.7 was observed respectively. Therefore, adsorption of phenol on the carbon material (effect (b)) doesn't seem to be the most important factor on the photocatalytic behavior of the prepared catalysts. Hence, it is reasonable to ascribe the observed synergy effect to CNT acting as photosensitizer (Scheme 4.1) rather than as adsorbent or dispersing agent in the composite catalyst.

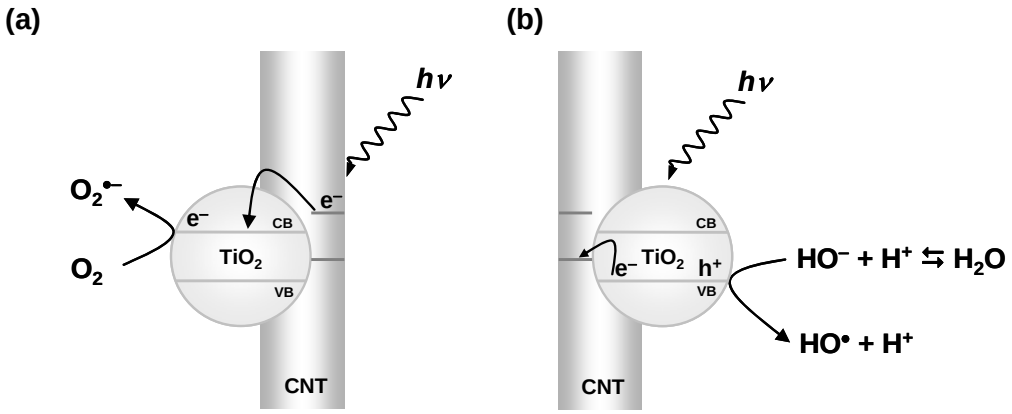

Scheme 4.1 CNT acting as photosensitizer in the composite catalyst: (a) electron injection into the conduction band of TiO_2 semiconductor; (b) electron back-transfer to CNT with the formation of a hole in the valence band of TiO_2 semiconductor and reduction of the so formed hole by adsorbed HO^- oxidation.

Considering the semiconductive properties of carbon nanotubes, CNT may absorb radiation and transfer the photo-induced electron (e^-) into the conduction band of the TiO_2 particles (Eq. 4.2). This electron transfer between carbon materials and TiO_2 semiconductor or the enhanced photocurrent of the composite materials was also experimentally observed in some other systems [28-30]. Simultaneously, a positive charged hole (h^+) might be formed by electron migrating from TiO_2

valence band to CNT (Eq. 4.3). With this understanding, the role played by CNT can be illustrated by injecting electrons into TiO_2 conduction band under visible light irradiation and triggering the formation of very reactive radicals superoxide radical ion $O_2^{\bullet -}$ (Eq. 4.4) and hydroxyl radical $HO^{\bullet}$ (Eq. 4.5), which are responsible for the degradation of the organic compound [27, 30-32].

$$CNT - TiO_2 \xrightarrow{h\nu} CNT^+ - TiO_2^- \quad (4.2)$$

$$CNT^+ - TiO_2^- + (O_2)_{ads} \longrightarrow CNT^+ - TiO_2 + O_2^{\bullet -} \quad (4.3)$$

$$CNT^+ - TiO_2 \longrightarrow CNT - TiO_2^+ \quad (4.4)$$

$$CNT - TiO_2^+ + (H_2O \leftrightarrow H^+ + HO^-)_{ads} \longrightarrow CNT - TiO_2 + H^+ + HO^{\bullet} \quad (4.5)$$

HPLC analysis was used to detect the main intermediates of the visible-light-driven photocatalytic degradation of phenol using CNT-TiO_2 catalyst. Similarly to UV light induced photo-reactions described in Chapter 3, hydroquinone and catechol were detected as main intermediates. This is in agreement with the probability of adduct formation by insertion of the hydroxyl radical. Compound like benzoquinone and 1,2,4-benzenetriol were detected at very low concentrations.

4.3.3 Catalyst separation and recovery

At the end of the photocatalytic runs, after illumination, gas feeding and stirring were turned off, the suspensions were allowed to sit for 30 minutes for gravity sedimentation of the suspended catalysts. Fig. 4.8 shows pictures of the photochemical reactor after that period when CNT-TiO_2 (Fig. 4.8a), TiO_2 sol-gel (Fig. 4.8b) and TiO_2 Degussa P25 (Fig. 4.8c) were used as catalysts, respectively.

Commercial TiO_2 Degussa P25 consists in an extremely fine powder being very difficult to separate by this procedure. In the case of the synthesized TiO_2, considerable particle sedimentation was observed and near to complete separation was achieved at approximately 1 hour after the end of the reaction. CNT-TiO_2 catalyst appears to be much easier to separate than neat TiO_2. In Fig.4.8a it is possible to identify two distinct and completely separated phases: the catalyst settled on the bottom of the reactor and the clean transparent solution above it.

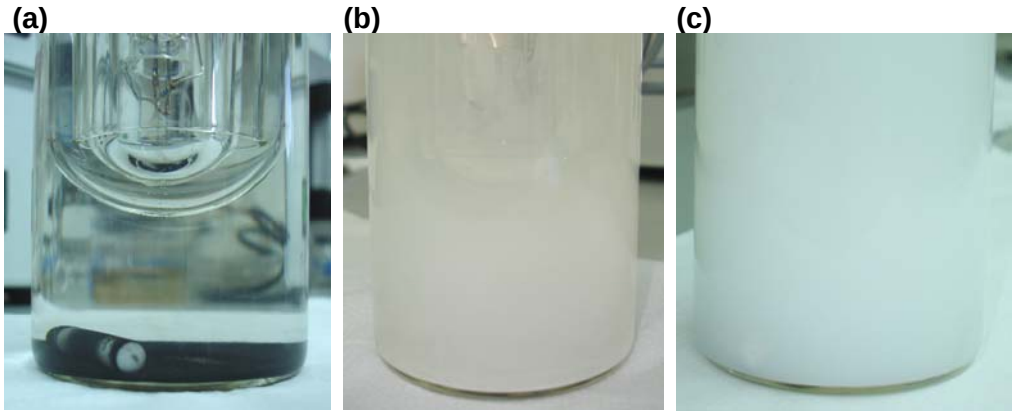

Figure 4.8 Overview of the bottom part of the photoreactor after a sedimentation period of 30 minutes for the different catalytic systems: (a) CNT-TiO_2; (b) TiO_2; (c) TiO_2-P25.

This feature appears to be a great advantage for the use of CNT-TiO_2 catalysts in batch treatment processes, in which separation and recovery of the catalyst is of extreme importance.

4.4 Conclusions

TiO_2-based composite catalysts prepared by a modified acid catalyzed sol-gel method were used in the photodegradation of phenol under visible irradiation.

The introduction of a porous substrate into the TiO_2 matrix produced a synergy effect in the photoefficiency of the semiconductor which is more pronounced for the carbon containing catalysts (ACF-TiO_2, AC-TiO_2 and CNT-TiO_2) than for the mesoporous molecular sieves and zeolite composites (MCM41-TiO_2, MCM48-TiO_2 and NaY-TiO_2). It was possible to correlate this synergy effect with the capacity of the composites to absorb radiation in the visible spectral range.

CNT-TiO_2 catalyst revealed to be very efficient in the photocatalytic oxidation of phenol. For this catalyst, the synergy was explained in terms of the support acting as photosensitizer rather than adsorbent or dispersing agent. Hydroquinone and catechol were found as the main reaction intermediates.

Supporting TiO_2 in different porous materials facilitates the separation and recovering of the photocatalysts in batch processes.

4.5 References

[1] M. Salaices, B. Serrano, H.I. de Lasa, *Photocatalytic conversion of phenolic compounds in slurry reactors*, Chem. Eng. Sci. 59 (2004) 3-15.

[2] R.L. Pozzo, M.A. Baltanás, A.E. Cassano, *Towards a precise assessment of the performance of supported photocatalysts for water detoxification processes*, Catal. Today. 54 (1999) 143-157.

[3] N.M. Mahmoodi, M. Arami, N.Y. Limaee, K. Gharanjig, F. Nourmohammadian, *Nanophotocatalysis using immobilized titanium dioxide nanoparticle - Degradation and mineralization of water containing organic pollutant: Case study of Butachlor*, Mater. Res. Bull. 42 (2007) 797-806.

[4] H.D. Mansilla, A. Mora, C. Pincheira, M.A. Mondaca, P.D. Marcato, N. Duran, J. Freer, *New photocatalytic reactor with TiO_2 coating on sintered glass cylinders*, Appl. Catal. B: Environ. 76 (2007) 57-63.

[5] B. Mounir, M.N. Pons, O. Zahraa, A. Yaacoubi, A. Benhammou, *Discoloration of a red cationic dye by supported TiO_2 photocatalysis*, J. Hazard. Mater. 148 (2007) 513-520.

[6] M.-J. López-Muñoz, R.v. Grieken, J. Aguado, J. Marugán, *Role of the support on the activity of silica-supported TiO_2 photocatalysts: Structure of the TiO_2/SBA-15 photocatalysts*, Catal. Today. 101 (2005) 307-314.

[7] P. Pucher, M. Benmami, R. Azouani, G. Krammer, K. Chhor, J.F. Bocquet, A.V. Kanaev, *Nano-TiO_2 sols immobilized on porous silica as new efficient photocatalyst*, Appl. Catal. A: Gen. 332 (2007) 297-303.

[8] M.S. Vohra, K. Tanaka, *Photocatalytic degradation of aqueous pollutants using silica-modified TiO_2*, Water Res. 37 (2003) 3992-3996.

[9] A.R. Torres, E.B. Azevedo, N.S. Resende, M. Dezotti, *A comparison between bulk and supported TiO_2 photocatalysts in the degradation of formic acid*, Braz. J. Chem. Eng. 24 (2007) 185-192.

[10] X. Zhang, M. Zhou, L. Lei, *Preparation of anatase TiO_2 supported on alumina by different metal organic chemical vapor deposition methods*, Appl. Catal. A: Gen. 282 (2005) 285-293.

[11] A.H. El-Sheikh, A.P. Newman, H. Al-Daffaee, S. Phull, N. Cresswell, S. York, *Deposition of anatase on the surface of activated carbon*, Surf. Coat. Technol. 187 (2004) 284-292.

[12] B. Tryba, A.W. Morawski, M. Inagaki, *Application of TiO_2-mounted activated carbon to the removal of phenol from water*, Appl. Catal. B: Environ. 41 (2003) 427-433.

[13] B. Tryba, A.W. Morawski, M. Inagaki, *A new route for preparation of TiO_2-mounted activated carbon*, Appl. Catal. B: Environ. 46 (2003) 203-208.

[14] W.D. Wang, C.G. Silva, J.L. Faria, *Photocatalytic degradation of Chromotrope 2R using nanocrystalline TiO_2/activated-carbon composite catalysts*, Appl. Catal. B: Environ. 70 (2007) 470-478.

[15] Z. Liuxue, L. Peng, S. Zhixing, *Photocatalysis anatase thin film coated PAN fibers prepared at low temperature*, Mater. Chem. Phys. 98 (2006) 111-115.

[16] R. Yuan, R. Guan, P. Liu, J. Zheng, *Photocatalytic treatment of wastewater from paper mill by TiO_2 loaded on activated carbon fibers*, Colloid Surf. A: Physicochem. Eng. Asp. 293 (2007) 80-86.

[17] A. Bhattacharyya, S. Kawi, M.B. Ray, *Photocatalytic degradation of orange II by TiO_2 catalysts supported on adsorbents*, Catal. Today. 98 (2004) 431-439.

[18] R. Chatti, S.S. Rayalu, N. Dubey, N. Labhsetwar, S. Devotta, *Solar-based photoreduction of methyl orange using zeolite supported photocatalytic materials*, Sol. Energy Mater. Sol. Cells. 91 (2007) 180-190.

[19] M. Huang, C. Xu, Z. Wu, Y. Huang, J. Lin, J. Wu, *Photocatalytic discolorization of methyl orange solution by Pt modified TiO_2 loaded on natural zeolite*, Dyes Pigment. 77 (2008) 327-334.

[20] E.P. Reddy, L. Davydov, P. Smirniotis, *TiO_2-loaded zeolites and mesoporous materials in the sonophotocatalytic decomposition of aqueous organic pollutants: the role of the support*, Appl. Catal. B: Environ. 42 (2003) 1-11.

[21] H.-M. Lin, S.-T. Kao, K.-M. Lin, J.-R. Chang, S.-G. Shyu, *Grafting TiO_2 on MCM-41 as a TiO_2 support for vanadia for catalytic oxidation of ethanol-EXAFS and XANES analyses of vanadium*, J. Catal. 224 (2004) 156-163.

[22] X. Wang, W. Lian, X. Fu, J.-M. Basset, F. Lefebvre, *Structure, preparation and photocatalytic activity of titanium oxides on MCM-41 surface*, J. Catal. 238 (2006) 13-20.

[23] S.E. Dapurkar, S.K. Badamali, P. Selvam, *Nanosized metal oxides in the mesopores of MCM-41 and MCM-48 silicates*, Catal. Today. 68 (2001) 63-68.

[24] J. Matos, J. Laine, J.-M. Herrmann, *Synergy effect in the photocatalytic degradation on a suspended mixture of titania and activated carbon*, Appl. Catal. B: Environ. 18 (1998) 281-291.

[25] J. Matos, J. Laine, J.-M. Herrmann, *Association of activated carbons of different origins with titania in the photocatalytic purification of water*, Carbon. 37 (1999) 1870-1872.

[26] J. Matos, J. Laine, J.-M. Herrmann, *Effect of the type of activated carbons on the photocatalytic degradation of aqueous organic pollutants by UV-irradiated titania*, J. Catal. 200 (2001) 10-20.

[27] W. Wang, P. Serp, P. Kalck, J.L. Faria, *Visible light photodegradation of phenol on MWNT-TiO_2 composite catalysts prepared by a modified sol-gel method*, J. Mol. Catal. A: Chem. 235 (2005) 194-199.

[28] K.H. Jung, J.S. Hong, R. Vittal, K.J. Kim, *Enhanced photocurrent of dye-sensitized solar cells by modification of TiO2 with carbon nanotubes*, Chem. Lett. (2002) 864-865.

[29] P.V. Kamat, I. Bedja, S. Hotchandani, *Photoinduced charge-transfer between carbon and semiconductor clusters - One-electron reduction of C-60 in colloidal TiO_2 semiconductor suspensions*, J. Phys. Chem. 98 (1994) 9137-9142.

[30] C. Lettmann, K. Hildenbrand, H. Kisch, W. Macyk, W.F. Maier, *Visible light photodegradation of 4-chlorophenol with a coke-containing titanium dioxide photocatalyst*, Appl. Catal. B: Environ. 32 (2001) 215-227.

[31] C.G. Silva, J.L. Faria, *Photochemical and photocatalytic degradation of an azo dye in aqueous solution by UV irradiation*, J. Photochem. Photobiol. A: Chem. 155 (2003) 133-143.

[32] W. Wang, P. Serp, P. Kalck, J.L. Faria, *Photocatalytic degradation of phenol on MWNT and titania composite catalysts prepared by a modified sol-gel method*, Appl. Catal. B: Environ. 56 (2005) 305-312.

Part IV

Carbon nanotube-TiO_2 catalysts

Chapter 5

Carbon Nanotube-TiO_2 catalysts for the photocatalytic oxidation of benzene derivatives in aqueous suspensions

The role played by carbon nanotubes (CNT) in CNT-TiO_2 composite catalysts is discussed in this chapter. Multi-walled carbon nanotube-TiO_2 composite catalysts produced by a modified acid catalyzed sol-gel method are extensively characterized by thermogravimetry, N_2 adsorption-desorption isotherms at 77K, X-ray diffraction, transmission electron microscopy and diffuse reflectance UV-Vis spectroscopy. Nanostructured composite catalysts with different CNT contents are tested in the photo-oxidation of phenol under UV (253.7 nm), UV-visible (254, 313, 366, 405 and 436 nm) and visible (313, 366, 405 and 436 nm) irradiation. Additionally, CNT with different surface chemical properties are used to produce CNT-TiO_2 composites. A correlation between CNT the presence and nature of surface groups and the photocatalytic activity of the resulting catalysts is discussed. Carbon nanotube surface groups are determined by temperature programmed desorption technique. Besides phenol, the photocatalytic oxidation of other monosubstituted benzene derivatives such as aniline, nitrobenzene and benzoic acid, are investigated using visible irradiation.

5.1 Introduction

Since they were discovered [1], carbon nanotubes (CNT) have been the focus of various studies due to their unique structural, electronic and mechanical properties. In a recent review, attention has been drawn to the fact that CNT can compete with activated carbon as catalyst support [2]. Some recent works have emphasized the preparation of carbon nanotube-TiO_2 nanocomposite catalysts aiming at a synergetic combination of their intrinsic properties and thus enhanced performance to meet new requirements imposed by advanced applications in distinct fields such as optoelectronics, solar energy utilization and heterogeneous photocatalysis [3-8].

A sol–gel method has been used to prepare the inclusion of CNT into an inorganic film of TiO_2 matrix [9]. Multi-walled carbon nanotube-based titania composite material has been prepared by an impregnation method, which provides a homogeneous inorganic cover layer on the surface of CNT [10]. Rutile TiO_2 has been immobilized on the sidewall of CNT by a simple one-step scheme, which produces three distinct morphologies of hybrid CNT at different reaction temperatures [11]. Coating CNT surface with TiO_2 has also been performed by a sol–gel method using different alkoxides and by hydrothermal hydrolysis of $TiOSO_4$, which can lead to different morphologies [12]. However, the reported study with a low CNT content (1.5 wt%) failed to confirm the predicted synergetic effect in phenol degradation under UV illumination [13].

In the present study, TiO_2 was combined with multi-walled carbon nanotubes by means of an acid-catalyzed sol-gel method to produce composite catalysts to be used in water treatment processes. Composite catalysts with different CNT contents were tested in the photocatalytic degradation of phenol under distinct irradiation wavelengths. The role of CNT chemical surface groups in the photo-efficiency of the composite catalysts under visible irradiation is discussed. Besides phenol, other monosubstituted aromatic pollutants namely aniline, nitrobenzene and benzoic acid were chosen as model molecules in order to evaluate the photocatalytic activities of the synthesized catalysts under visible irradiation. A study about the influence of the substituent groups on the formation of main intermediates is also presented.

5.2 Experimental

5.2.1 Catalysts preparation

CNT-TiO_2 composite catalysts were prepared following the procedure described in Chapter 4, section 4.2.1, by introducing a certain amount of carbon nanotubes in the $Ti(OC_3H_7)_4$ ethanol solution. Catalysts are named as (1:X)CNT-TiO_2, where X (2.5, 5, 10, and 20) corresponds to the weight ratio of pure TiO_2 per unity of CNT.

In order to modify the surface chemical properties of the carbon nanotubes, the material was submitted to two distinct treatments: sample CNT_{red} was obtained by thermal treatment under a flow of hydrogen at 973K during one hour and then stabilized under an air flow at room temperature for one hour; sample CNT_{ox} was obtained by oxidation of the original material with nitric acid 6M at the boiling temperature during 3 hours. Composite catalysts using these modified materials were prepared as described for original CNT with a 1:5 CNT to TiO_2 mass ratio.

5.2.2 Catalysts characterization

Characterization of CNT-TiO_2 catalysts was performed by thermogravimetric analysis, N_2 adsorption-desorption isotherm measurements at 77K, powdered X-ray diffraction, transmission electron microscopy and diffuse reflectance UV-Vis and infrared spectroscopy, following the procedures described in Chapter 2, section 2.2.2.

Carbon nanotubes surface oxygen groups were characterized by temperature programmed desorption (TPD). The analyses were performed in an AMI-200 (Altamira Instruments) apparatus. In a typical experiment, 100 mg of sample was subjected to a 5 K min^{-1} linear temperature rise up to 1373K under helium flow of 25 cm^3 min^{-1}. A mass spectrometer (Dymaxion 200 amu, Ametek) was used to monitor CO (m/z = 28) and CO_2 (m/z = 44).

5.2.3 Photodegradation experiments

Photocatalytic activities of the prepared catalysts were evaluated by phenol (PhOH, Aldrich redistilled 99+%) removal in aqueous media under UV UV-Visible and Visible light irradiation. The UV radiation source, located axially in a quartz immersion tube, was a Heraeus TNN 15/32 low pressure mercury vapor lamp (λ_{exc} = 253.7 nm). The UV-Visible irradiation source consisted in a Heraeus TQ 150 medium pressure mercury vapor lamp (λ_{exc} = 254, 313, 366, 436 and 546 nm), which was located axially and held in a quartz immersion tube. A quartz jacket with water recirculation was employed to cool the irradiation source and cancel the infrared radiation, thus preventing any heating of the suspension. A DURAN® glass cooling jacket was used as UV filter when barely visible radiation (λ_{exc} = 366, 436 and 546 nm) was required.

The experiments were carried out in a glass immersion photochemical reactor charged with 800 ml of solution/suspension. The initial phenol concentration was set at 50 mg l^{-1}. The amount of suspended photocatalyst was kept at 1 g l^{-1} of TiO_2, with the corresponding amount of carbon being calculated accordingly for the composite catalysts. Before turning on illumination, the suspension containing phenol and photocatalyst was magnetically stirred in the dark for 30 minutes, to establish an adsorption-desorption equilibrium. Then, the suspension was irradiated with UV, UV-Visible or Visible light at constant stirring speed. The first sample was taken out at the end of the dark adsorption period, just before the light was turned on, in order to determine the phenol concentration in solution, which was hereafter considered as the initial concentration (C_0) after dark adsorption. Samples were then withdrawn regularly from the reactor and centrifuged immediately to separate any suspended solid.

The photocatalytic degradation of other single substituted benzene derivatives such as aniline (AN, Aldrich, 99%), nitrobenzene (NB, Aldrich, 99%) and benzoic acid (BA, Fluka, p.a.) by visible light irradiation was also performed. Initial concentration of the organic compounds was set at 50 mg l^{-1}. Reactions in the absence of catalyst were performed in order to characterize de pure photochemical regime.

Initial compounds and reaction intermediates were detected by HPLC analysis using a Hitachi Elite Lachrom HPLC equipped with a L-2450 diode array detector. For phenol, aniline and nitrobenzene, the stationary phase was a Purospher Star RP-18 column (250 mm × 4.6 mm), while for benzoic acid, nitrites and nitrates

determination an YMC Hydrosphere C18 column (250 mm × 4.6 mm) was used. In both cases, stationary phases worked at room temperature and mobile phases were used at a flow rate of 1 ml min^{-1}. Phenol and its oxidation intermediates were analyzed by using a mixture of water and methanol in a gradient concentration as mobile phase. For aniline and the oxidation products formed during reaction, the mobile phase was a mixture of water and acetonitrile with a gradient concentration. Nitrobenzene and respective degradation compounds were analyzed under isocratic elution with a mixture of water and methanol. In the case of benzoic acid, HPLC measurements were performed under isocratic elution with a mixture of water, NaH_2PO_4 and *o*-phosphoric acid at pH 2.8. Nitrites and nitrates were also detected using this later method.

The degree of mineralization was followed by TOC analysis in a Shimadzu TOC-5000A Analyzer.

5.3 Results and discussion

5.3.1 Catalysts characterization

5.3.1.1 Effect of CNT loading

XRD patterns of neat CNT, TiO_2 and CNT-TiO_2 composites prepared with different CNT to TiO_2 proportions are shown in Fig. 5.1. CNT characteristic peaks corresponding to the (0 0 2) and (1 0 0) reflection planes are identified (Fig 5.1a). Only anatase phase can be identified in neat TiO_2 and composite catalysts. The XRD patterns of the CNT-TiO_2 composite catalysts are very similar to the one of TiO_2 with the CNT contribution hardly been identified. The dimensions of the anatase crystallites (d_A), listed in Table 5.1, were determined by the diffraction broadening of the (2 0 0) reflection plane from anatase ($2\theta = 48.1º$), where there is no interference from CNT, using Scherrer's equation. The crystallite sizes of composite catalysts decrease gradually from 11.2 nm to 7.2 nm, from sample (1:20)CNT-TiO_2 to (1:2.5)CNT-TiO_2, respectively.

The anatase crystallites present in (1:20)CNT-TiO_2 and (1:10)CNT-TiO_2 composites showed bigger dimensions than pure TiO_2 crystallites. The introduction of increasing percentage of CNT seems to avoid particle agglomeration, and therefore, crystallites tend to get smaller.

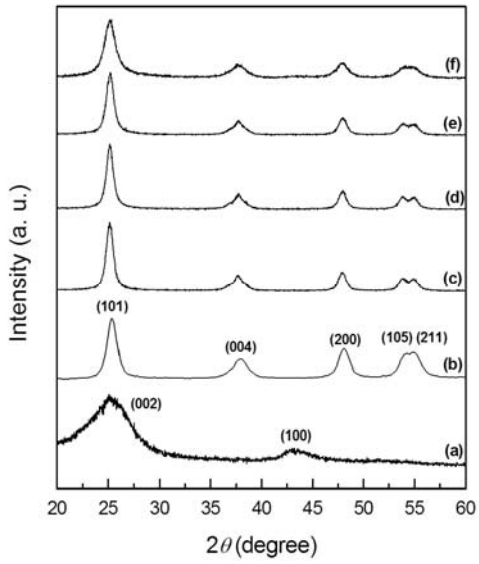

Figure 5.1 X-ray diffraction patterns of: (a) CNT; (b) TiO_2; (c) (1:20)CNT-TiO_2; (d) (1:10)CNT-TiO_2; (e) (1:5)CNT-TiO_2; (f) (1:2.5)CNT-TiO_2.

The carbon content of the CNT-TiO_2 composite catalysts determined by TG analysis (C_{TG}) agrees very well with the calculated (C_{calc}) from CNT:TiO_2 ratio, meaning there is no appreciable degradation of the carbon phase during the calcination step.

The N_2 adsorption-desorption isotherms of CNT and CNT-TiO_2 composite catalysts (not shown) can be ascribed to Type IV [14, 15], indicating a mesoporous pore structure. Figure 5.2 shows the example of (1:5)CNT-TiO_2 catalyst.

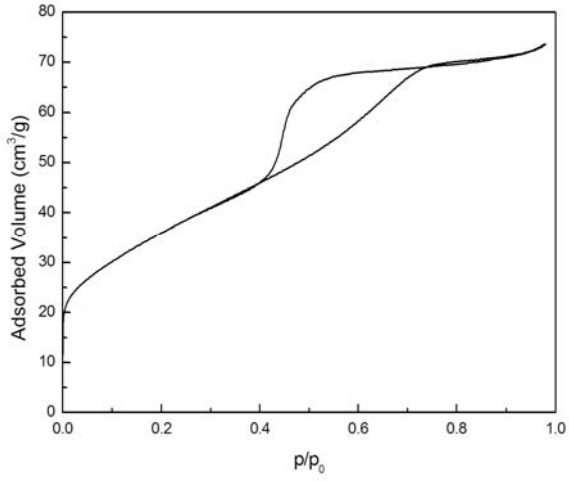

Figure 5.2 N_2 adsorption-desorption isotherm of (1:5)CNT-TiO_2 catalyst.

The BET surface areas (S) of the prepared catalysts are listed in Table 5.1. Catalysts with lower carbon content, namely (1:20)CNT-TiO_2 and (1:10)CNT-TiO_2 composites, showed surface areas lower than the ones estimated by the mass ratio between the two solid phases (S_{calc}). In fact in these cases, surface areas are even lower than for neat TiO_2.

Table 5.1 Surface area (S), carbon content determined by thermogravimetry (C_{TG}) and dimension of the anatase crystallites (d_A) for TiO_2 and the different CNT-TiO_2 composites.

Catalyst	S ($m^2\ g^{-1}$)	S_{calc} ($m^2\ g^{-1}$)	C_{TG} (%)	C_{calc} (%)	d_A (nm)
TiO_2	107	---	---	---	8.5
CNT	185	---	---	---	---
(1:20)CNT-TiO_2	70	111	3.53	4.76	11.2
(1:10)CNT-TiO_2	94	114	7.58	9.09	9.4
(1:5)CNT-TiO_2	131	120	15.1	16.7	8.3
(1:2.5)CNT-TiO_2	192	129	27.7	28.6	7.2

When small amounts of CNT are used, TiO_2 crystallites grow around the substrate leading to the agglomeration of anatase crystallites of sizes bigger than in pure TiO_2 and therefore reducing the surface area of the composite catalyst. TEM image of (1:5)CNT-TiO_2 composite (Fig. 5.3) shows CNT, with external diameters less than 10 nm, embedding in the TiO_2 matrix. TiO_2 nanoparticles, constituted by few anatase crystallites can be observed on CNT surface.

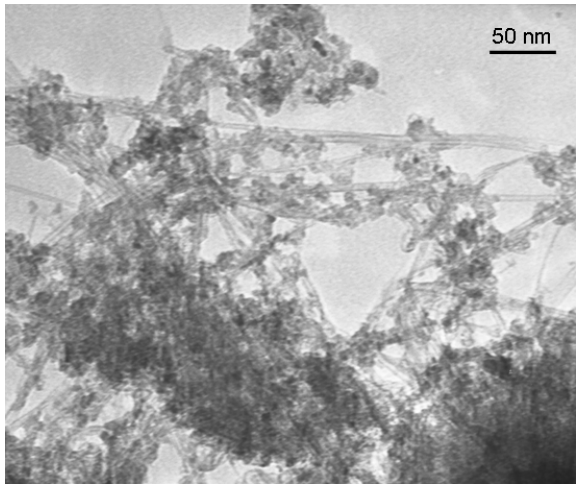

Figure 5.3 Transmission electron microscopy image of (1:5)CNT-TiO_2 composite catalyst.

Diffuse reflectance UV-Vis spectra of pure anatase TiO_2 powder and CNT-TiO_2 composite catalysts are shown in Fig. 5.4. As expected, TiO_2 shows the characteristic absorption sharp edge rising at 400 nm. The introduction of the carbon phase into the TiO_2 matrix leaded to a rise of light absorption in the visible spectral region. This effect revealed to be proportional to the CNT content on the composite catalysts, supporting the creation of an interphase interaction.

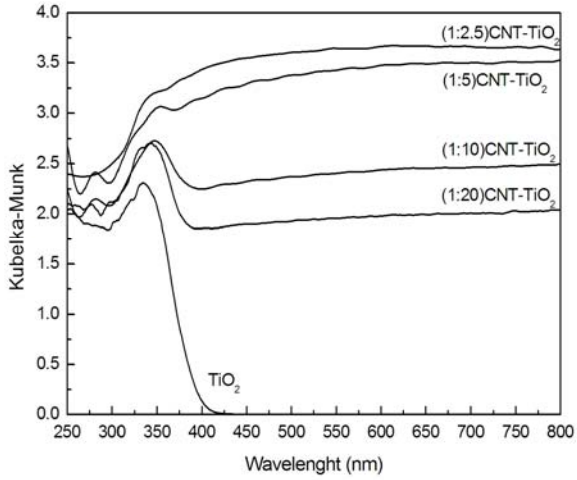

Figure 5.4 Diffuse reflectance UV-Vis spectra of TiO_2 and CNT-TiO_2 composite catalysts with different CNT to TiO_2 weight ratio.

It can be noticed that (1:2.5)CNT-TiO_2 absorption is even totally over the whole range of the UV-Vis spectrum. These observations may indicate an increment of surface electric charge of the metal oxide in the composite catalysts due to the introduction of CNT.

5.3.1.2 Effect of CNT surface groups

Carbon materials surface groups are believed to take an important role in the electronic transfer process to titania phase [16] as well as in the way that TiO_2 and CNT are interconnected. Li *et al.* [17] developed a method for labeling surface defects on single-walled carbon nanotubes using TiO_2 particles as markers. Chemical adsorption occurred between carboxylic acid groups present at the surface

of carbon nanotubes and hydroxyl groups on the TiO_2 nanoparticles via the formation of ester-like bonds.

Temperature programmed desorption technique was used for the determination and quantification of chemical oxygen species present at the surface of the carbon nanotube materials. CO and CO_2 TPD profiles, presented in Fig. 5.5 show that, even without any further treatment, original CNT sample presents a considerable amount of oxygen containing surface groups. After the liquid phase oxidation treatment, an increase in the amount of surface oxygen groups of CNT is evidenced by the increase of the CO and CO_2 peaks.

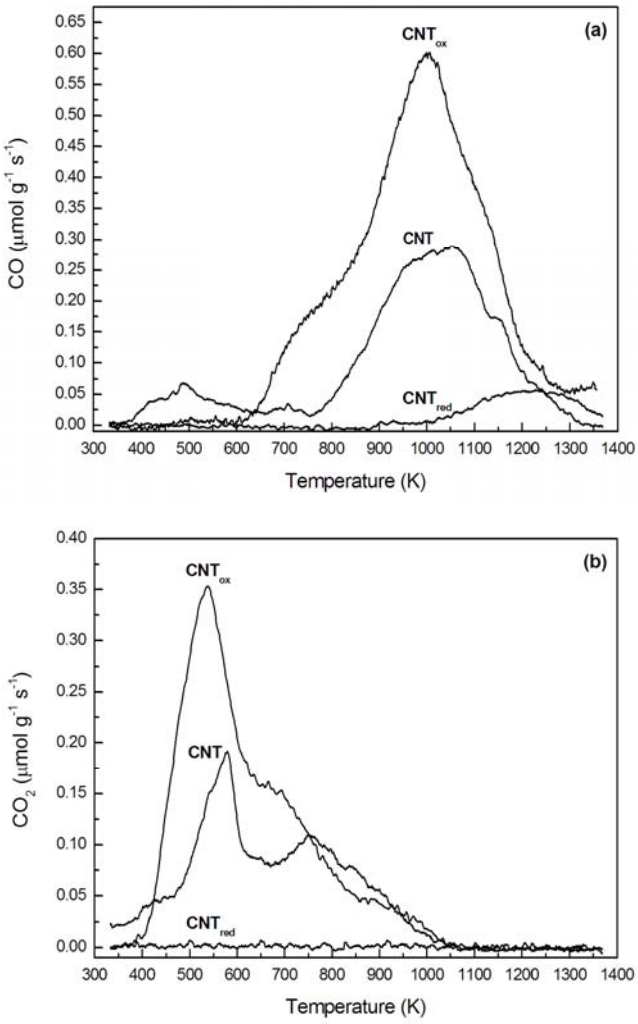

Figure 5.5 TPD profiles for original CNT, CNT_{ox} and CNT_{red}: (a) CO evolution; (b) CO_2 evolution.

For the CNT sample thermally treated under hydrogen at 973K, the CO_2 releasing groups (carboxylic acids, anhydrides and lactones) have been practically removed and only a small amount of CO releasing groups at higher temperatures remains in the CNT surface, which can be assigned to carbonyl, pyrone and chromene groups [18, 19]. Thus, CNT_{red} shows higher CO/CO_2 ratio, when compared to CNT and CNT_{ox}.

The total amount of released CO and CO_2, obtained by the integration of the CO and CO_2 peaks, respectively, are presented on Table 5.2. When comparing CNT_{ox} with original CNT, an increase on the amount of released CO and CO_2 of 87% and a 61% was observed, respectively.

Table 5.2 Concentration of CO and CO_2 releasing groups.

Material	CO (μmol g^{-1})	CO_2 (μmol g^{-1})	CO/CO_2
CNT	1293	606	2.1
CNT_{ox}	2414	973	2.5
CNT_{red}	215	13	16.5

In order to determine the amount of each surface group, the deconvolution of the CO and CO_2 TPD spectra of CNT and CNT_{ox} was carried out, using a non-linear least-square procedure based in the Levenberg-Marquardt (LM) algorithm assuming a multi-Gaussian peak shape, described by Figueiredo *et al.* [18, 19] (Fig. 5.6).

(a)

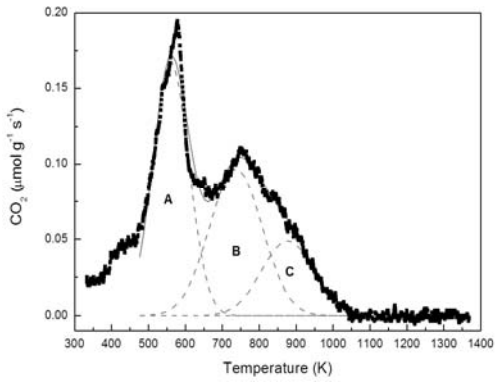

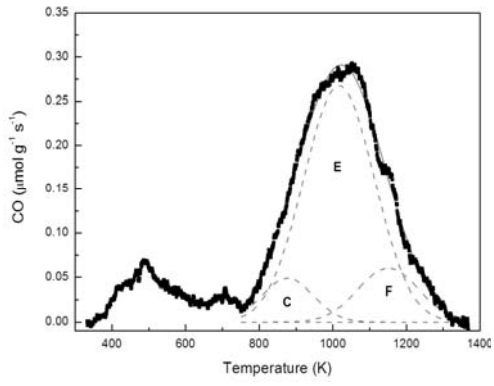

(b)

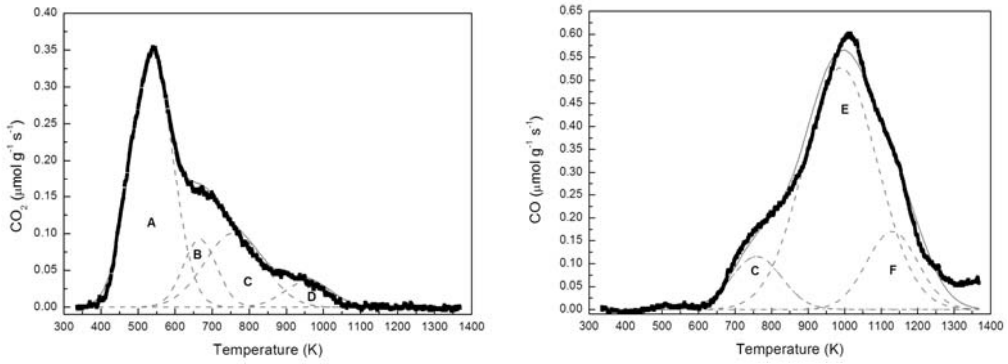

Figure 5.6 Deconvolution of TPD spectra using a multiple Gaussian function: (a) original CNT sample; (b) CNT_{ox} sample. (■ experimental data; --- individual peaks; – sum of the individual peaks)

The release of CO_2 is attributed to carboxylic acids, carboxylic anhydrides and lactones. Low temperature (strongly acidic) and high temperature (less acidic) decomposing carboxylic acids were considered in order to better represent the groups released between 373 and 673K. The CO releasing is mainly attributed to carboxylic anhydrides, phenols and high temperature decomposed carbonyl/quinone groups.

Table 5.3 summarizes the concentration of the different oxygen functional groups present at the CNT materials surface. The small differences between the CO and CO_2 values given in Table 5.3 and the sum of the individual CO and CO_2 values in Table 5.2 arises from small amounts of unidentified oxygen functional groups present at the materials surface.

Table 5.3 Concentration (μmol g^{-1}) of surface groups in CNT and CNT_{ox} obtained by deconvolution of the CO and CO_2 TPD spectra using a multiple Gaussian function.

	CO_2		$CO+CO_2$	CO	
Material	Carboxylic acid	Lactone	Carboxylic anhydride	Phenol	Quinone
	(A+B)	(D)	(C)	(E)	(F)
CNT	452	---	103	773	150
CNT_{ox}	714	67	240	1600	360

XRD analysis of the composites produced with modified carbon nanotubes revealed the presence of very small anatase crystallites of about 7.2 nm when CNT_{red} material was used (Table 5.4) and therefore, an increase in the surface area for this catalyst is observed.

Table 5.4 Surface area (S), anatase content (x_A) and dimension of the anatase crystallites (d_A) for the different materials.

Catalyst	S (m^2 g^{-1})	x_A (%)	d_A (nm)
TiO_2	107	100	8.5
CNT	185	---	---
CNT_{red}	181	---	---
CNT_{ox}	196	---	---
CNT-TiO_2	131	100	8.3
CNT_{red}-TiO_2	150	100	7.2
CNT_{ox}-TiO_2	78	98	9.2

In opposition, anatase crystallites in CNT_{ox}-TiO_2 catalyst were of sizes even bigger than in pure TiO_2. Additionally, for this catalyst, a small percentage of rutile phase was detected, with crystal dimensions of 12 nm. This increase in crystallite size and phase transformation is believed to be related to an excess of surface groups in oxidized CNT sample. In the condensation step of sol-gel TiO_2 formation, the polymeric chains ≡Ti-OH will compete to the carboxylic acid and phenol groups at the surface of CNT_{ox} and undergo etherification and/or oxolation reactions, respectively [20] (Scheme 5.1). Due to the high abundance of surface defects the polymeric chains tend to agglomerate leading to the formation of big crystallite clusters after calcination. The formation of rutile may result from an increase of the temperature inside the composite catalyst due to the presence of crystallite agglomerates. Moreover, a very significant decrease in the surface area was observed for CNT_{ox}-TiO_2 catalyst as a result of TiO_2 crystal agglomeration.

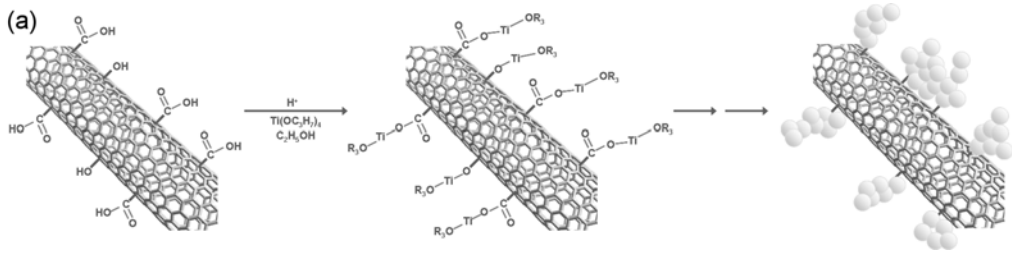

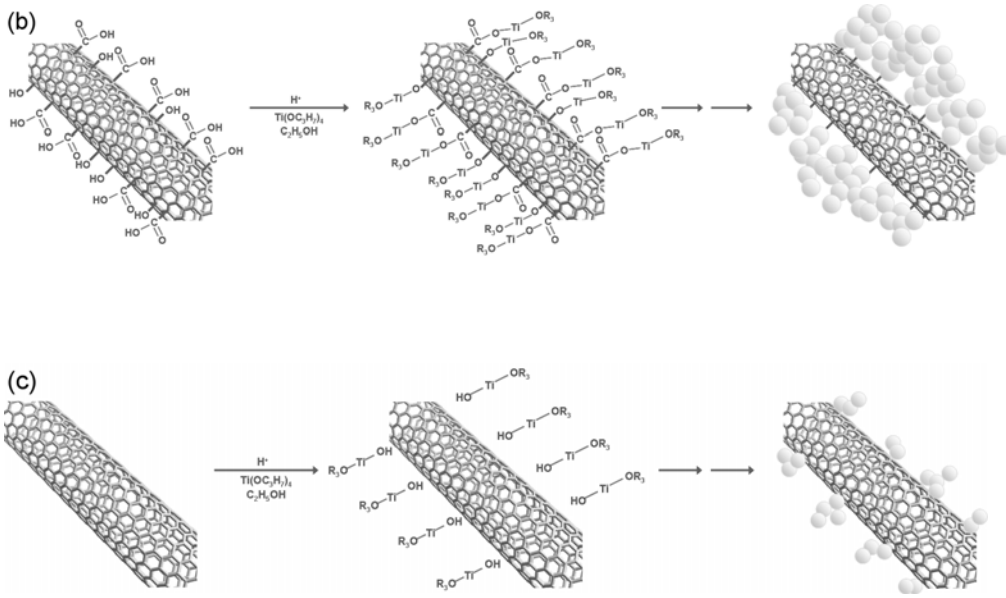

Scheme 5.1 Formation of the different composite catalysts produced with original and modified carbon nanotubes: (a) CNT-TiO_2; (b) CNT_{ox}-TiO_2; (c) CNT_{red}-TiO_2.

The diffuse reflectance UV-Vis absorption spectra of the composite catalysts (Fig. 5.7) reveal a decline in absorption mainly in the visible range of the spectrum, indicating a decrease in the electronic interaction between TiO_2 and carbon phases when modified CNT are used.

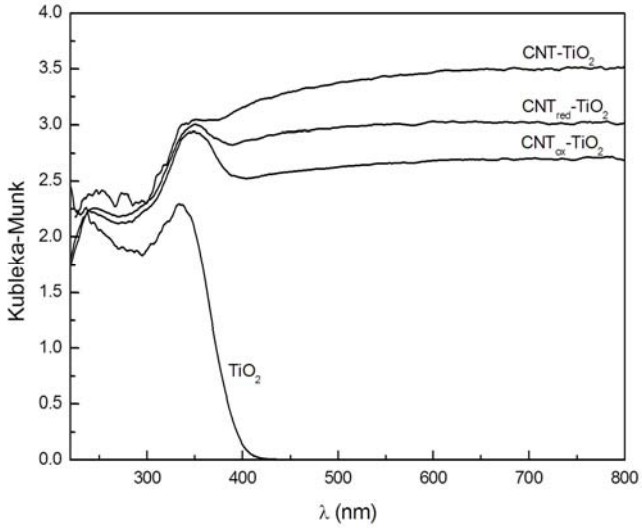

Figure 5.7 Diffuse reflectance UV-Vis spectra of the composite catalysts prepared with original and treated CNT materials.

The thermal treatment under hydrogen lead to the complete removal of the surface groups which are believed to be responsible to the linkage between the two phases. In CNT_{red}-TiO_2 catalyst, TiO_2 particles are probably mixed with CNT_{red}, consequently generating a fairly loose contact between semiconductor and carbon phase and a decrease in the electronic interaction between the two phases. For CNT_{ox}-TiO_2 catalyst a even more expressive decline of the absorption in the visible range was observed, attributed to an increase in TiO_2 particle dimensions due to the agglomeration of TiO_2 crystallites.

5.3.2 Photocatalytic oxidation of organic pollutants with CNT-TiO_2 catalysts

5.3.2.1 Photocatalytic removal of phenol using different irradiation systems

Pure sol-gel TiO_2 and CNT-TiO_2 composite catalysts were tested in the photocatalytic oxidation of phenol in aqueous suspensions. In order to understand the photo-induced degradation reaction and the role played by carbon nanotubes in the photocatalytic process, composites with different CNT contents were used under different radiation sources: i. monochromatic ultraviolet light with an emission line at 253.7 nm (UV); ii. a medium pressure mercury vapor lamp emitting in the range 200-600 nm (UV-Vis); iii. the same light source as described in (ii) equipped with a cut-off filter for wavelength below 300 nm (Vis).

Despite the irradiation system in use, the photochemical and photocatalytic degradation of phenol appeared to follow a pseudo-first order rate law. As phenol absorbs at $\lambda<300$ nm, with its maximum at 270 nm under natural pH, the pure photochemical regime cannot be excluded when using UV and UV-Vis systems. UV radiation by itself is capable to oxidize phenol with a conversion of around 80% at the end of 2 hours of irradiation with an apparent kinetic constant of 1.40×10^{-2} min^{-1}. However at the end of the reaction, a TOC removal of merely 19% was achieved, meaning low mineralization of the organic compounds in solution (Fig. 5.8). The fraction of non-mineralized organics probably corresponds to aliphatic acids, not detected by HPLC in these experimental conditions, such as lactic, acetic, formic, maleic, oxalic and others resulting from the aromatic ring opening [21, 22].

The photocatalytic reaction using pure anatase TiO_2 appeared to be much more efficient than photolysis with an increase of about 33% in k_{app} and a TOC

removal of 83% at the end of 4 hours of irradiation. The utilization of CNT-TiO_2 composite catalysts did not introduce any major effect on the photodegradation of phenol under UV irradiation. Although phenol abatement ($X_{PhOH,2h}$) and TOC removal ($X_{TOC,4h}$) show a little increase with increasing CNT content in the composite catalysts, no synergic kinetic effect was observed. In this case, as photolysis and photocatalysis are competing processes, carbon nanotubes may act as light filter dispersing the radiation. Additionally, as can be observed in Fig. 5.4, TiO_2 and CNT-TiO_2 catalysts show quite similar absorption at 254 nm an therefore, the role of CNT as photosensitizer is reduced.

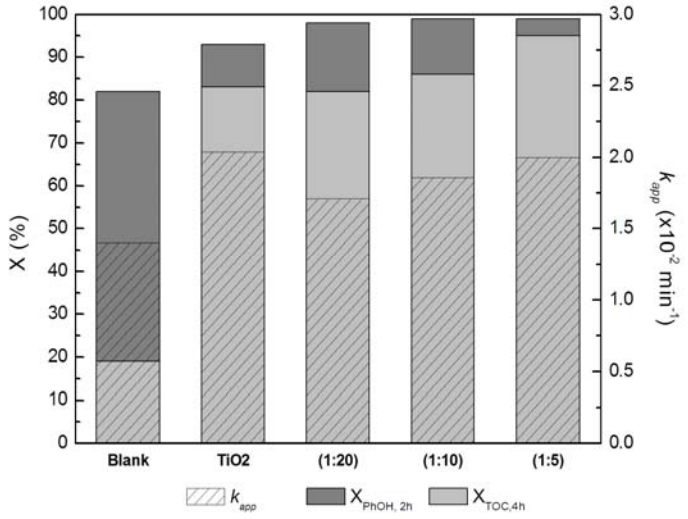

Figure 5.8 First-order apparent rate constant (k_{app}), phenol conversion at 2 hours of irradiation ($X_{PhOH,2h}$) and TOC conversion at 4 hours of irradiation ($X_{TOC,4h}$) for experiments under UV irradiation.

The photo-oxidation of phenol using UV-Vis light revealed to be a very efficient process, with total degradation of the molecule at the end of two hours of irradiation (Fig. 5.9). As happened when sole UV light was used, in the absence of catalyst TOC removal in much inferior than phenol conversion, which indicates that there is a fraction of organic matter that was not totally mineralized and remains in solution. The efficiency of CNT-TiO_2 catalysts revealed to be slightly better than TiO_2. Even when the composite catalyst with the lower amount of carbon nanotube was used, a kinetic synergy effect was observed, with k_{app} of 5.02×10^{-2} min^{-1} and 5.62×10^{-2} min^{-1} for TiO_2 and (1:20)CNT-TiO_2, respectively.

With CNT content increasing in the composites, a decrease in k_{app} was observed. As the 254 nm line is one of the most intense in this radiation source, photolysis cannot be excluded when using this system. Once again, the introduction of increasing amounts of carbon nanotubes may cause light scattering, leading to a decrease in the photo-efficiency of the process.

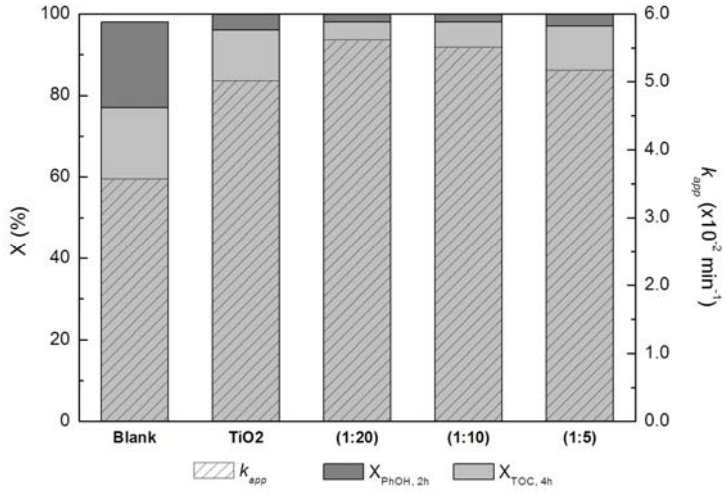

Figure 5.9 First-order apparent rate constant (k_{app}), phenol conversion at 2 hours of irradiation ($X_{PhOH,2h}$) and TOC conversion at 4 hours of irradiation ($X_{TOC,4h}$) for experiments under UV-Vis irradiation.

Visible irradiation of phenol solution in the absence of catalyst did not produce any degradation of the organic compound, since phenol has no absorption in the visible range (Fig. 5.10). Hence, in the presence of a catalyst it can be assumed that the reaction takes place under total photocatalytic regime. A synergy effect was observed for CNT-TiO_2 composite catalysts proportionally to the carbon content up to a 1:5 mass ratio. An optimal synergy effect was found for (1:5)CNT-TiO_2 catalyst. This synergy behavior can be correlated with the UV-Vis spectrum of the composite materials. However, when (1:2.5)CNT-TiO_2 was used, a very pronounced decrease in activity was observed ascribed to exceedingly absorbing and scattering of photons by surplus carbon in the photoreaction system [7].

By these results it can be noticed that the effect of the addition of carbon nanotubes into the titania matrix is of much more significance when visible light is used and therefore some conjectures can be made in order to explain the role played by CNT in the composite catalysts. In Chapter 4, was already suggested that carbon

nanotubes may act as a dispersing agent for TiO_2 nanoparticles as well as a co-adsorbent and/or as a photosensitizer [6-8].

The first explanation was used for mechanical mixtures of activated carbon and TiO_2 with the synergy effect ascribed to an extended adsorption of the pollutant on activated carbon following by a transfer to titania where it was photocatalytically degraded [23-26]. However, this seems not to be the major contribution for the synergy effect observed for CNT-TiO_2 catalysts, since adsorption capacities of TiO_2 and CNT-TiO_2 composites were quite similar with a decrease in phenol concentration after dark adsorption period of less than 10% for all cases. Furthermore, when compared to a mixture of CNT and TiO_2 with the same proportions, (1:5)CNT-TiO_2 composite reveal to be much more efficient (Fig. 5.11).

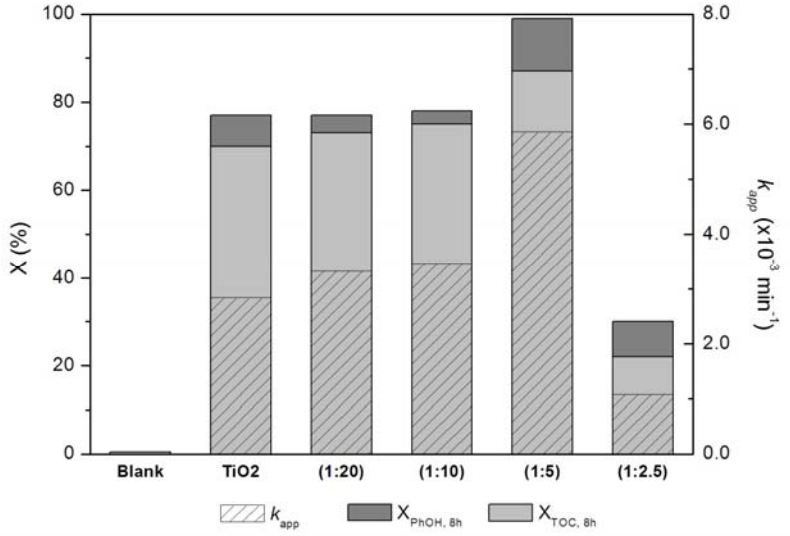

Figure 5.10 First-order apparent rate constant (k_{app}), phenol conversion at 8 hours of irradiation ($X_{PhOH,2h}$) and TOC conversion at 8 hours of irradiation ($X_{TOC,4h}$) for experiments under visible irradiation.

It was observed that the increase in CNT loading in the composite materials leaded to a progressive decrease in TiO_2 crystallite dimensions. The photoefficiency of the composite catalysts increased with increasing CNT content up to a 1:5 CNT to TiO_2 ratio. Although the smallest crystallites of 7.2 nm were obtained for (1:2.5)CNT-TiO_2 catalyst, its photoefficiency for the degradation of phenol was very low. Being so, the action of CNT as a dispersing media for titania

nanoparticles is not likely to be the most important factor accounting for the observed synergy effect.

It is then more reasonable to ascribe the synergy effect to the action of CNT as a photosensitizer rather than a co-adsorbent or a dispersing agent. After being irradiated, excited carbon nanotubes may inject electrons to the TiO_2 conduction band triggering the photocatalytic generation of very reactive radical species such as hydroxyl ($HO^{\bullet}$) and superoxide ($O_2^{\bullet-}$) radicals, which are responsible to the degradation of phenol [6-8, 27-29].

5.3.2.2 Effect of CNT's surface chemistry in the photo-efficiency of CNT-TiO_2 catalysts

The photocatalytic degradation of phenol using CNT-TiO_2 produced with CNT samples with different surface chemical groups was performed under visible irradiation. Figure 5.11 shows the concentration profiles for phenol removal obtained during the photocatalytic reactions using the different catalysts.

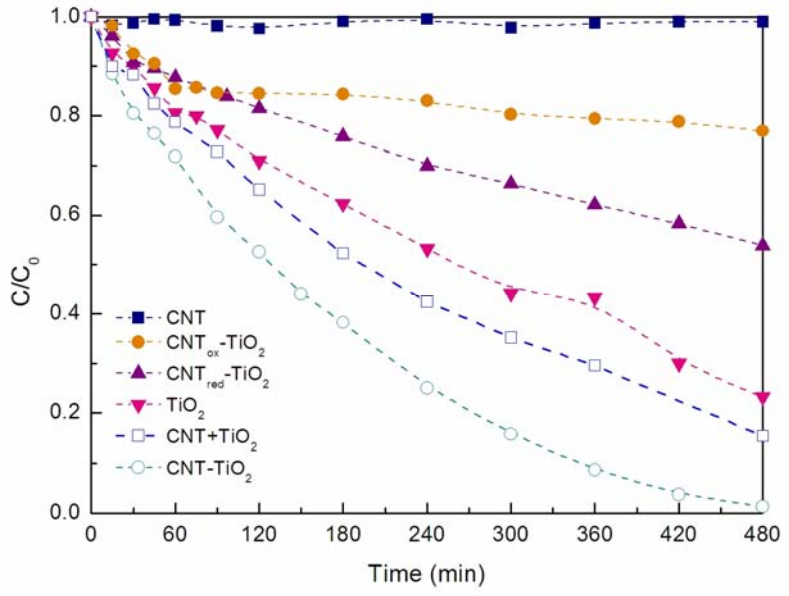

Figure 5.11 Evolution of the dimensionless concentration of phenol during photocatalytic oxidation reactions using different catalytic systems.

It can be noticed that no appreciable degradation was observed in the presence of neat CNT. Carbon nanotube surface groups are believed to play an important role not only in the way that TiO_2 and the carbon phase are linked together but also in the possibility of electronic interaction between carbon and metal oxide phases. The presence of oxygen containing groups confers electron availability to the CNT surface leading to an increment of surface electric charge of the metal oxide in the composite materials. Therefore, a modification of the fundamental process of the electron/hole pair formation is expected.

In the case of CNT_{red}, the almost total inexistence of oxygen containing surface groups resulted in a poor electronic interaction with TiO_2. Composite catalyst CNT_{red}-TiO_2 showed very low photocatalytic efficiency with no synergetic effect observed between the carbon phase and TiO_2. On the other hand, an excess in surface groups leads not only to the agglomeration of TiO_2 nanoparticles, with a consequent decrease in the surface area and formation of rutile, but also to an ineffective electronic transfer process due to a surplus surface electric charge in CNT_{ox}. In fact, composite catalyst CNT_{ox}-TiO_2 showed even worse photoefficiency than CNT_{red}-TiO_2. Composite catalyst produced with the original carbon nanotubes, containing a mild surface chemistry, appeared to be the most photoactive catalyst. In this case, the observed synergy effect is attributed to the moderate electron availability. CNT may absorb radiation and transfer the photo-induced electrons into the conduction band of TiO_2 leading to a decrease in the bandgap energy of the semiconductor and to an enhancement of the quantum yield of the process.

5.3.2.3 Photocatalytic removal of benzene derivatives under visible irradiation

The photocatalytic degradation of various mono-substituted benzene derivatives, namely aniline, nitrobenzene and benzoic acid was performed under visible irradiation using TiO_2 and (1:5)CNT-TiO_2 catalyst. Photochemical degradation of the organic compounds was performed for comparison purposes. Since we are irradiating in the visible spectral region (λ>300 nm), very little contribution of the photochemical process is expected. As can be seen in Fig. 5.12, for these wavelengths, light is absorbed predominantly by the catalysts rather by the organic molecules.

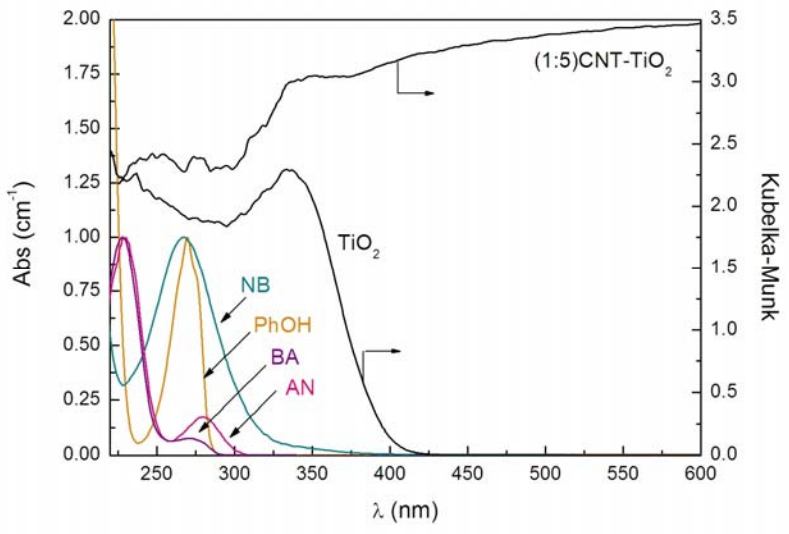

Figure 5.12 Diffuse reflectance and absorption UV-Vis spectra of the catalysts and of the organic compounds, respectively.

HPLC analysis of the samples collected during the photo-oxidation reactions revealed that the primary reaction intermediates are single substituted hydroxy derivatives, which indicates that $HO^{\bullet}$ radicals are the key species involved in the oxidation process. In the case of phenol, the main intermediates found were catechol (2-hydroxyphenol) and hydroquinone (4-hydroxyphenol). Traces of benzoquinone (in equilibrium with hydroquinone) were also identified. 2-Nitrophenol and 4-nitrophenol were detected as main reaction intermediates in the photocatalytic oxidation of aniline. Also a small amount of nitrobenzene was identified during the irradiation experiments, resulting from the oxidation of the amino group. During the direct photodegradation of aniline, the solution passed from colorless to brown, pointing to a polymerization process, probably by formation of azobenzene [30]. The main intermediates resulting from photocatalytic oxidation of nitrobenzene were 3-nitrophenol and 4-nitrophenol. 2-nitrophenol was present at very low concentrations. Nitrates were also formed and analyzed by HPLC. From the photocatalytic oxidation of benzoic acid, 3-hydroxybenzoic and 4-hydroxybenzoic acids resulted as main intermediates. Trace concentrations of 2-hydroxybenzoic acid were detected.

The results are in agreement with the orientating properties of benzene substituent groups (Scheme 5.2). Photocatalytic oxidation of substrates containing electron donor groups such as phenol and aniline generate *ortho* and *para* mono-hydroxy derivatives as primary intermediates. By the other hand, electron

withdrawing groups such as $–NO_2$ from nitrobenzene and –COOH from benzoic acid are mostly *meta* orientating substituents in photocatalytic oxidation [31].

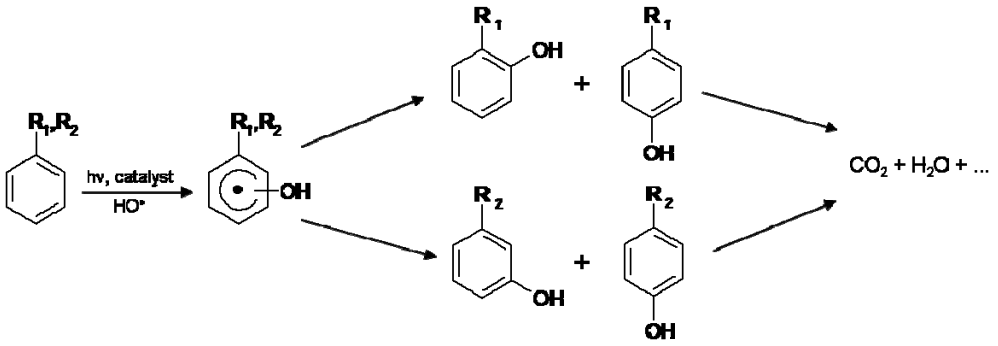

Scheme 5.2 Simplified photocatalytic reaction pathway (R_1: electron donor group; R_2: electron withdrawing group).

The pure photochemical reaction, in the absence of any catalyst, resulted in very minute degradation of the organic molecules. In this case, conversion and total organic carbon removal at the end of the irradiation runs time were less than 10% for all compounds (Fig. 5.13). The photochemical conversion occurs due to residual absorption of light by the substrate molecule, leading to the formation of reactive radical species.

The photocatalytic process involving TiO_2 revealed to be much more efficient than the pure photochemical one. For phenol, aniline and nitrobenzene a further increase on the efficiency of the photocatalytic process was observed in the presence of (1:5)CNT-TiO_2 composite. For example, photocatalytic oxidation of phenol using (1:5)CNT-TiO_2 composite catalyst resulted in practically total (99%) conversion of the molecule after 8 hours of irradiation, while using neat TiO_2 a conversion of only 77% was obtained. In the case of aniline and nitrobenzene, similar behavior was observed. Nitrobenzene revealed to be the most refractory compound with only 31% and 47% of conversion at the end of the photocatalytic runs using TiO_2 and (1:5)CNT-TiO_2 catalysts, respectively. On the other hand, benzoic acid was the most easily degraded compound. After 8 hours of irradiation, total conversion of the parent compound was achieved for both TiO_2 and CNT-TiO_2 mediated photocatalytic processes. A TOC removal of more than 80% was achieved using both photocatalytic systems.

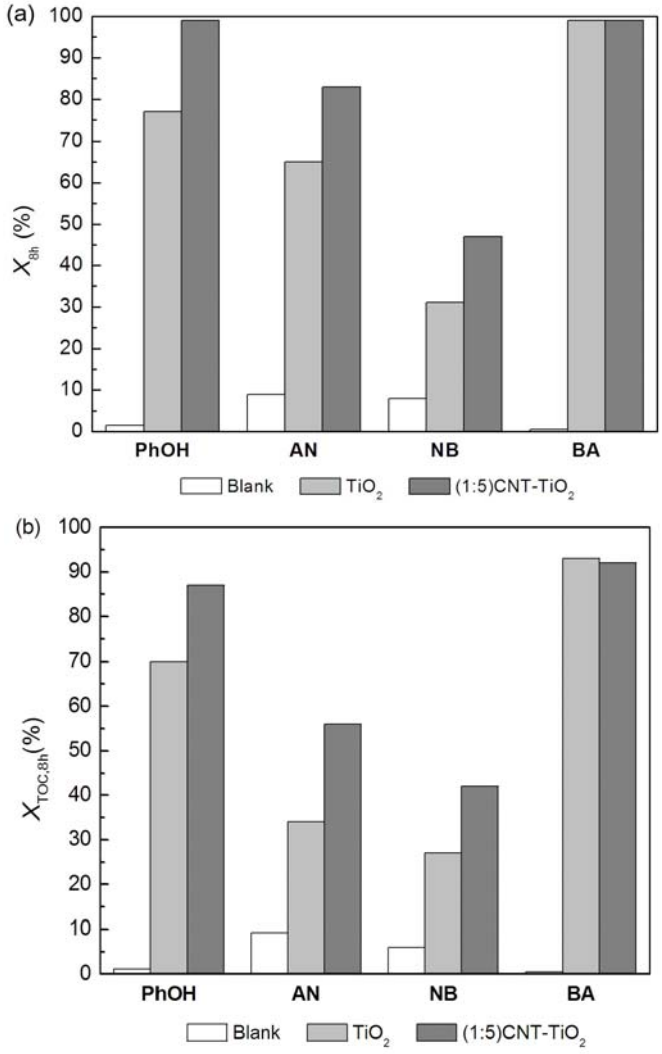

Figure 5.13 Conversion (a) and total organic carbon removal (b) obtained for phenol (PhOH), aniline (AN), nitrobenzene (NB) and benzoic acid (BA) and after 8 hours of irradiation.

Kinetics of photocatalytic degradation of the aromatic compounds followed a pseudo-first order rate law. Apparent kinetic rate constants (k_{app}) were obtained by non-linear regression of the experimental data. In order to quantify the effect of the introduction of the CNT in the composite catalyst, a synergy factor (R), defined as $R=k_{app,(1:5)CNT\text{-}TiO2}/k_{app,TiO2}$ [23] was calculated (Table 5.5).

Table 5.5 First order apparent rate constants and synergy factor obtained for the aromatic compounds using TiO_2 and CNT-TiO_2 catalysts.

Compound	$k_{app,TiO2}$ ($\times 10^{-3}$ min^{-1})	$k_{app,(1:5)CNT\text{-}TiO2}$ ($\times 10^{-3}$ min^{-1})	R
Phenol	2.84 ± 0.04	5.86 ± 0.03	2.06
Aniline	2.31 ± 0.06	3.93 ± 0.04	1.70
Nitrobenzene	1.40 ± 0.09	1.60 ± 0.08	1.07
Benzoic acid	6.63 ± 0.01	6.26 ± 0.04	0.94

In the case of phenol and aniline it is obvious that the introduction of CNT into TiO_2 matrix induces to a beneficial effect on its photoactivity. The highest value of synergy factor R of 2.06 was obtained for phenol, which means a double k_{app} value when composite catalyst was used. Benzoic acid is successfully degraded by neat TiO_2 catalyst up to it almost complete mineralization. In this case the use of (1:5)CNT-TiO_2 catalyst didn't show any relevant effect. In fact, a slight decrease in the kinetic constant for (1:5)CNT-TiO_2 mediated reaction was observed. In the case of nitrobenzene and benzoic acid, in which $–NO_2$ and –COOH are deactivating groups in what concerns to ring reactivity, there is no significant synergy effect, probably due to a weak interaction with the catalyst surface.

5.4 Conclusions

Multi walled carbon nanotube-TiO_2 composite catalysts produced by a modified acid catalyzed sol-gel procedure can be used as catalysts in photocatalytic processes for water treatment.

The introduction of increasing amounts of CNT into the TiO_2 matrix prevents particles from agglomerating, thus increasing surface area of the composite materials.

A synergy effect on the photocatalytic degradation of phenol was noticed mostly for the reaction activated by visible (λ>300 nm) irradiation. This improvement on the efficiency of the photocatalytic process appeared to be proportional to the shift of the UV-Vis spectra of the CNT-TiO_2 composites for longer wavelengths, indicating a strong interphase interaction between carbon and

semiconductor phases. This effect was explained in terms of CNT acting as a photosensitizer agent rather than an adsorbent or a dispersing agent.

Surface defects at the surface of carbon nanotubes revealed to be essential not only in the anchoring of the titania particles but also in the electron transfer to the semiconductor. Original carbon nanotubes, containing mild amount of oxygen surface groups, produced the highest synergetic effect on the degradation of phenol under visible irradiation.

The efficiency of CNT-TiO_2 catalysts in the photocatalytic oxidation of mono-substituted organic compounds under visible irradiation was dependent from the ring activating/deactivating properties of the aromatic molecules. Higher synergy factor was observed for compounds presenting electron donor groups such as phenol and aniline. For nitrobenzene and benzoic acid an R value near to 1 was obtained, indicating the inexistence of any synergy effect between CNT and TiO_2 in the photocatalytic degradation of these pollutants.

5.5 References

[1] S. Iijima, *Helical microtubules of graphitic carbon*, Nature. 354 (1991) 56-58.

[2] P. Serp, M. Corrias, P. Kalck, *Carbon nanotubes and nanofibers in catalysis*, Appl. Catal. A: Gen. 253 (2003) 337-358.

[3] W. Feng, Y.Y. Feng, Z.G. Wu, A. Fujii, M. Ozaki, K. Yoshino, *Optical and electrical characterizations of nanocomposite film of titania adsorbed onto oxidized multiwalled carbon nanotubes*, J. Phys.-Condes. Matter. 17 (2005) 4361-4368.

[4] S.L. Kim, S.R. Jang, R. Vittal, J. Lee, K.J. Kim, *Rutile TiO_2-modified multi-wall carbon nanotubes in TiO_2 film electrodes for dye-sensitized solar cells*, J. Appl. Electrochem. 36 (2006) 1433-1439.

[5] Y. Ou, J. Lin, S. Fang, D. Liao, *MWNT-TiO_2:Ni composite catalyst: A new class of catalyst for photocatalytic H_2 evolution from water under visible light illumination*, Chemical Physics Letters. 429 (2006) 199-203.

[6] W. Wang, P. Serp, P. Kalck, J.L. Faria, *Photocatalytic degradation of phenol on MWNT and titania composite catalysts prepared by a modified sol-gel method*, Appl. Catal. B: Environ. 56 (2005) 305-312.

[7] W. Wang, P. Serp, P. Kalck, J.L. Faria, *Visible light photodegradation of phenol on MWNT-TiO_2 composite catalysts prepared by a modified sol-gel method*, J. Mol. Catal. A: Chem. 235 (2005) 194-199.

[8] W. Wang, P. Serp, P. Kalck, C.G. Silva, J.L. Faria, *Preparation and characterization of nanostructured MWCNT-TiO_2 composite materials for photocatalytic water treatment applications*, Mater. Res. Bull. 43 (2008) 958-967.

[9] P. Vincent, A. Brioude, C. Journet, S. Rabaste, S.T. Purcell, J. Le Brusq, J.C. Plenet, *Inclusion of carbon nanotubes in a TiO_2 sol-gel matrix*, J. Non-Cryst. Solids. 311 (2002) 130-137.

[10] K. Hernadi, E. Ljubovic, J.W. Seo, L. Forró, *Synthesis of MWNT-based composite materials with inorganic coating*, Acta Mater. 51 (2003) 1447-1452.

[11] Q. Huang, L. Gao, *Immobilization of rutile TiO_2 on multiwalled carbon nanotubes*, J. Mater. Chem. 13 (2003) 1517-1519.

[12] A. Jitianu, T. Cacciaguerra, R. Benoit, S. Delpeux, F. Béguin, S. Bonnamy, *Synthesis and characterization of carbon nanotubes-TiO_2 nanocomposites*, Carbon. 42 (2004) 1147-1151.

[13] J. Sun, L. Gao, *Development of a dispersion process for carbon nanotubes in ceramic matrix by heterocoagulation*, Carbon. 41 (2003) 1063-1068.

[14] G. Leofanti, M. Padovan, G. Tozzola, B. Venturelli, *Surface area and pore structure of catalysts*, Catal. Today. 41 (1998) 207-219.

[15] K.S.W. Sing, D.H. Everett, R.A.W. Haul, L. Moscou, R.A. Pierotti, J. Rouquérol, T. Siemieniewska, *Reporting physisorption data for gas/solid systems with special reference to the determination of surface area and porosity*, Pure Appl. Chem. 57 (1985) 603-619.

[16] C.G. Silva, J.L. Faria, *Photochemical and photocatalytic degradation of an azo dye in aqueous solution by UV irradiation*, J. Photochem. Photobiol. A: Chem. 155 (2003) 133-143.

[17] X.H. Li, J.L. Niu, J. Zhang, H.L. Li, Z.F. Liu, *Labeling the defects of single-walled carbon nanotubes using titanium dioxide nanoparticles*, J. Phys. Chem. B. 107 (2003) 2453-2458.

[18] J.L. Figueiredo, M.F.R. Pereira, M.M.A. Freitas, J.J.M. Orfao, *Characterization of active sites on carbon catalysts*, Ind. Eng. Chem. Res. 46 (2007) 4110-4115.

[19] J.L. Figueiredo, M.F.R. Pereira, M.M.A. Freitas, J.J.M. Órfão, *Modification of the surface chemistry of activated carbons*, Carbon. 37 (1999) 1379-1389.

[20] L. Chen, B.L. Zhang, M.Z. Qu, Z.L. Yu, *Preparation and characterization of CNTs-TiO_2 composites*, Powder Technol. 154 (2005) 70-72.

[21] B. Tryba, A.W. Morawski, M. Inagaki, M. Toyoda, *The kinetics of phenol decomposition under UV irradiation with and without H_2O_2 on TiO_2, Fe-TiO_2 and Fe-C-TiO_2 photocatalysts*, Appl. Catal. B: Environ. 63 (2006) 215-221.

[22] Z. Wang, W. Cai, X. Hong, X. Zhao, F. Xu, C. Cai, *Photocatalytic degradation of phenol in aqueous nitrogen-doped TiO_2 suspensions with various light sources*, Appl. Catal. B: Environ. 57 (2005) 223-231.

[23] J. Matos, J. Laine, J.-M. Herrmann, *Synergy effect in the photocatalytic degradation on a suspended mixture of titania and activated carbon*, Appl. Catal. B: Environ. 18 (1998) 281-291.

[24] J. Matos, J. Laine, J.-M. Herrmann, *Association of activated carbons of different origins with titania in the photocatalytic purification of water*, Carbon. 37 (1999) 1870-1872.

[25] J. Matos, J. Laine, J.-M. Herrmann, *Effect of the type of activated carbons on the photocatalytic degradation of aqueous organic pollutants by UV-irradiated titania*, J. Catal. 200 (2001) 10-20.

[26] J. Matos, J. Laine, J.M. Herrmann, D. Uzcategui, J.L. Brito, *Influence of activated carbon upon titania on aqueous photocatalytic consecutive runs of phenol photodegradation*, Appl. Catal. B: Environ. 70 (2007) 461-469.

[27] G. An, W. Ma, Z. Sun, Z. Liu, B. Han, S. Miao, Z. Miao, K. Ding, *Preparation of titania/carbon nanotube composites using supercritical ethanol and their photocatalytic activity for phenol degradation under visible light irradiation*, Carbon. 45 (2007) 1795-1801.

[28] C.G. da Silva, J.L. Faria, *Photochemical and photocatalytic degradation of an azo dye in aqueous solution by UV irradiation*, J. Photochem. Photobiol. A: Chem. 155 (2003) 133-143.

[29] C. Lettmann, K. Hildenbrand, H. Kisch, W. Macyk, W.F. Maier, *Visible light photodegradation of 4-chlorophenol with a coke-containing titanium dioxide photocatalyst*, Appl. Catal. B: Environ. 32 (2001) 215-227.

[30] M. Canle L, J.A. Santaballa, E. Vulliet, *On the mechanism of TiO_2-photocatalyzed degradation of aniline derivatives*, J. Photochem. Photobiol. A: Chem. 175 (2005) 192-200.

[31] G. Palmisano, M. Addamo, V. Augugliaro, T. Caronna, A.D. Paola, E.G. López, V. Loddo, G. Marcì, L. Palmisano, M. Schiavello, *Selectivity of hydroxyl radical in partial oxidation of aromatic compounds in heterogeneous photocatalysis*, Catal. Today. 122 (2007) 118-127.

Chapter 6

Photocatalytic oxidation of phenolic compounds using carbon nanotube-TiO_2 composite catalyst

Pure anatase TiO_2 and CNT-TiO_2 composite are tested in the photocatalytic degradation of four para-substituted phenols: 4-chlorophenol, 4-aminophenol, 4-hydroxybenzoic acid and 4-nitrophenol. The effect of several operational parameters on the photoefficiency of the CNT-TiO_2 catalyst are studied using 4-chlorophenol as model compound, namely catalyst loading, pH of the medium, concentration of hydrogen peroxide and concentration of substrate. Recovery and reuse of CNT-TiO_2 on three consecutive degradation reactions is performed. A progressive lost of efficiency of the catalyst is observed. A relationship between the Hammet constant of each para-substituted phenolic compound and its degradability by TiO_2 and CNT-TiO_2 photocatalysts is found. For both catalysts, the faster initial degradation rate occurred for 4-aminophenol and the slowest for 4-nitrophenol. These results are in line with the activating/deactivating nature of the substituent groups in the phenol molecule. The effect of CNT in the CNT-TiO_2 catalyst is described in terms of its action as a photosensitizer, by changing the electronic properties of the semiconductor in the composite catalyst. A clear beneficial effect is observed by introducing CNT in the CNT-TiO_2 composite catalyst when used for the degradation of 4-aminophenol and 4-chlorophenol. For the molecules with stronger electron withdrawing (deactivating) groups such as 4-hydroxybenzoic acid and 4-nitrophenol no synergy effect is observed.

6.1 Introduction

Multi-walled carbon nanotube/TiO_2 catalysts revealed to show better efficiency than pure TiO_2 when irradiated with visible light. Furthermore, in the previous chapter, CNT-TiO_2 catalyst with a mass ratio of CNT to TiO_2 of 1:5 induced to a 100% increase in the apparent degradation rate constant of phenol, as well as a beneficial effect in the mineralization of the organic content, when comparing to neat TiO_2. The study on the photocatalytic degradation of other mono-substituted benzene derivatives using (1:5)CNT-TiO_2 catalyst, showed that the efficiency of the catalyst depended on the compound to be degraded, the difference being attributed to the electronic properties of the substituent groups of the aromatic ring. Among the four mono-substituted benzene derivatives in study (phenol, aniline, benzoic acid and nitrobenzene), phenol appeared to be the most easily degraded by CNT-TiO_2 catalyst, which was attributed to the electron-donating properties of hydroxyl group.

In the present chapter (1:5)CNT-TiO_2 catalyst, hereafter designated by CNT-TiO_2, is used for the photocatalytic degradation of four *para*-substituted phenols (4-chlorophenol, 4-aminophenol, 4-hydroxybenzoic acid and 4-nitrophenol) under visible irradiation. Phenolic derivatives are common compounds in industrial wastewaters. For example, olive mill wastewater contains polyphenols up to several grams per liter, which are phytotoxic and toxic to bacteria used in biological wastewater treatment plants [1, 2]. Cellulose bleaching effluents contain phenolic lignin-like material and high molecular mass compounds, which are responsible for the heavy color of the effluent [3].

The heterogeneous photocatalytic process using the hybrid CNT-TiO_2 catalyst was characterized by studying the effect of several operational parameters, such as catalyst concentration, pH of the medium, addition of hydrogen peroxide and substrate concentration, in the photoefficiency of the degradation of 4-chlorophenol under visible irradiation. The effect of the electronic nature of the substituent group in the photoreactivity of the *para*-substituted phenols using both TiO_2 and CNT-TiO_2 catalysts was studied.

6.2 Experimental

6.2.1 Catalysts preparation and characterization

CNT-TiO_2 composite catalyst was produced by means of an acid catalyzed sol-gel method using a CNT to titania weight ratio of 1:5. The procedure was similar to the described in Chapter 4, section 4.2.1, with CNT being introduced into the $Ti(OC_3H_7)_4$ ethanol solution.

Detailed characterization of the materials used in this study is described in the previous chapters.

6.2.2 Photodegradation experiments

The photocatalytic degradation of four phenolic compounds namely 4-chlorophenol (CP, Aldrich 99+%), 4-aminophenol (AP, Aldrich 98+%), 4-nitrophenol (NP, Aldrich 98%) and 4-hydroxybenzoic acid (HBA, Fluka ≥99%) were performed in aqueous solution under visible irradiation. The experiments were carried out in a 300 ml glass immersion photochemical reactor charged with 250 ml of solution/suspension. The reactor was equipped with a Heraeus TQ 150 medium-pressure mercury vapor lamp (more intense lines at λ_{exc} of 366, 436 and 546 nm, the UV line at 254 nm being filtered by a DURAN 50® glass jacket) which was located axially and held in a quartz immersion tube. The initial concentration (C'_0) of the substrates was set at 50 mg l^{-1}. A 200 ml min^{-1} oxygen/argon (20% vol. of oxygen) stream was continuously supplied to the reactor. Reactions took place under natural pH (pH_{nat}) conditions ($pH_{nat,CP}$ = 5.6; $pH_{nat,AP}$ = 6.6; $pH_{nat,NP}$ = 5.4; $pH_{nat,HBA}$ = 4.0).

Before turning on the illumination, the suspensions were saturated with the gas mixture and magnetically stirred for 30 minutes to establish an adsorption-desorption equilibrium. The first sample was taken at the end of the dark adsorption period, just before the light was turned on, in order to determine the concentration of the compound in solution, which was hereafter considered as the initial concentration (C_0) after dark adsorption. Then, the suspensions were irradiated with visible light at constant stirring speed. Reactions were stopped at the end of 2 hours of irradiation. Samples were withdrawn regularly from the reactor and centrifuged for separation of any suspended solid, prior to analysis.

The clean transparent solution was then analyzed by HPLC using a Hitachi Elite LaChrom liquid chromatograph equipped with an L-2450 diode array detector.

The stationary phase consisted in a YMC-Pack ODS-AQ endcapped column (250 mm × 4.6 mm, 5μm particles) working at room temperature. The mobile phase was a mixture of a 20 mM NaH_2PO_4/H_3PO_4 (pH=2.8) buffer solution and acetonitrile with a gradient concentration at a flow rate of 1 ml min^{-1}. For known compounds, the relationship between area and concentration was determined by using standards. The concentration of ammonium ions (NH_4^+) in samples was determined by the 4500-NH_3 ammonia-selective electrode method [4]. Total organic carbon (TOC) measurements were performed in a Shimadzu TOC-5000 analyzer.

6.3 Results and discussion

6.3.1 Photocatalytic degradation of CP

6.3.1.1 Effect of operational parameters

As already been mentioned, heterogeneous photocatalytic reactions are influenced by several parameters such as catalyst loading, nature and concentration of the substrate to be degraded, pH of the medium and presence of oxidant species [5]. 4-Chlorophenol was chosen as model compound in order to study the effect of key operational parameters in the visible-light-driven photodegradation reaction using CNT-TiO_2 composite catalyst. Preliminary experiments revealed that photocatalytic oxidation of 4-chlorophenol follow a pseudo-first order kinetic rate model, as described by the following equation:

$$C_{CP} = C_{0,CP} e^{-k_{app} t} \tag{6.1}$$

where C_{CP} corresponds to phenol concentration, k_{app} is the apparent first order kinetic constant, t is the reaction time and $C_{0,CP}$ is the phenol concentration for $t = 0$ (at the instant that illumination is turned on). Operational parameters were therefore evaluated comparing the values of k_{app}, obtained by non-linear regression of the experimental data, conversion of substrate and total organic carbon removal measurements.

6.3.1.1.1 Catalyst concentration

The rate of photocatalytic reaction is strongly influenced by the concentration of the catalyst in the reaction media. In heterogeneous photocatalysis reaction rate is known to increase proportionally to the concentration of the catalyst. The optimal loading is generally determined to avoid the use of excess catalyst and ensure total absorption of efficient photons. A catalyst overload can cause unfavorable light scattering and reduction of light penetration into the solution. In the present study the concentration of CNT-TiO_2 catalyst was varied from 250 mg l^{-1} to 1.5 g l^{-1}.

As shown in Fig. 6.1, k_{app} increased with the mass of catalyst up to a concentration of 1.2 g l^{-1}, confirming the heterogeneous nature of the photocatalytic process. This behavior can be associated to an increment of the active sites available for CP adsorption and degradation. However, an increase on the catalyst loading to 1.5 g l^{-1} resulted in a decrease in the apparent rate constant, which can be attributed to a screening effect due to the redundant dispersion of radiation caused by the substantial amount of suspended photocatalyst. Furthermore, catalyst particle agglomeration can occur causing a decrease in active sites available for adsorption and for the catalytic reaction.

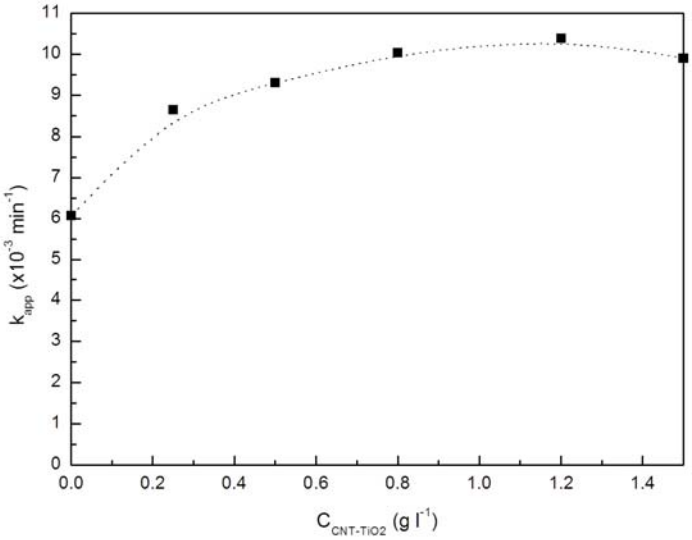

Figure 6.1 Effect of CNT-TiO_2 loading on the kinetics of the photocatalytic degradation of 4-chlorophenol.

The results obtained in terms of conversion of CP and total organic carbon removal at the end of the photocatalytic reactions are consistent with evaluation based on the kinetic parameter (Table 6.1). A maximum conversion at 2 hours of irradiation of 72.3% was obtained when a 1.2 g l^{-1} loading of catalyst was used, resulting in the mineralization of 47.5% of the organic matter present in solution at the beginning of the reaction.

It has to be noticed that even without catalyst (pure photochemical reaction), considerable degradation of CP occurs. However, at these conditions, TOC removal is very low with only 2% of the organic content being removed. Although CP can be oxidized by visible light, at the end of the reaction most of the reaction intermediates are still present in the solution.

Table 6.1 First-order apparent rate constant (k_{app}), conversion ($X_{CP,2h}$) and TOC removal ($X_{TOC,2h}$) after two hours of irradiation for the photocatalytic degradation of 4-chlorophenol.

$C_{CNT\text{-}TiO2}$ (g l^{-1})	k_{app} ($\times 10^{-2}$ min^{-1})	$X_{CP,2h}$ (%)	$X_{TOC,2h}$ (%)
0	0.61 ± 0.04	54	2
0.25	0.86 ± 0.02	64	14
0.5	0.93 ± 0.03	69	35
0.8	1.00 ± 0.02	71	46
1.2	1.04 ± 0.01	72	48
1.5	0.99 ± 0.03	70	46

Following these observations, it was decided to keep the amount of CNT-TiO_2 at the optimum value of 1.2 g l^{-1} in subsequent photocatalytic degradation experiments.

6.3.1.1.2 pH of the medium

The effect of pH on the photocatalytic reaction is generally attributed to changes in the surface charge of the photocatalyst. The point of zero charge (pzc) of sol-gel TiO_2 was found to be of 6.4. At pH higher than pH_{pzc}, TiO_2 surface is negatively charged (TiO^-) and for lower pH values, titania surface is in the

protonated form ($TiOH_2^+$). During sol-gel production of CNT-TiO_2 composite, the linkage between carbon nanotubes and titania is believed to occur between hydroxyl groups in the titania polymeric chain and carboxylic acid groups present at the surface of CNT [6]. The removal of some of the hydroxyl groups from titania and the presence of a carbon phase with acidic groups at its surface are expected to produce some decrease in the pH_{pzc} of the resulting composite material.

Electric charge properties of both, catalyst and substrate, are found to play an important role on adsorption process. Under aqueous media, 4-chlorophenol shows a pKa of 9.4 (at 25 ºC), which means that for pH < pKa, it is in the molecular form and at pH > pKa the molecule undergoes deprotonation becoming negatively charged.

The effect of pH on the photocatalytic degradation of CP was investigated for three pH values: 3.0, 5.6 (natural pH) and 11.0. The pH of the solution was adjusted before irradiation and was not controlled during the course of the reaction. As can be seen in Fig. 6.2, an increase in pH resulted in an enhancement in the photocatalytic degradation of CP. At pH 11.0, CP is almost totally removed after two hours of irradiation. However, at these conditions, very low mineralization of the organic compounds in solution was achieved (Table 6.2).

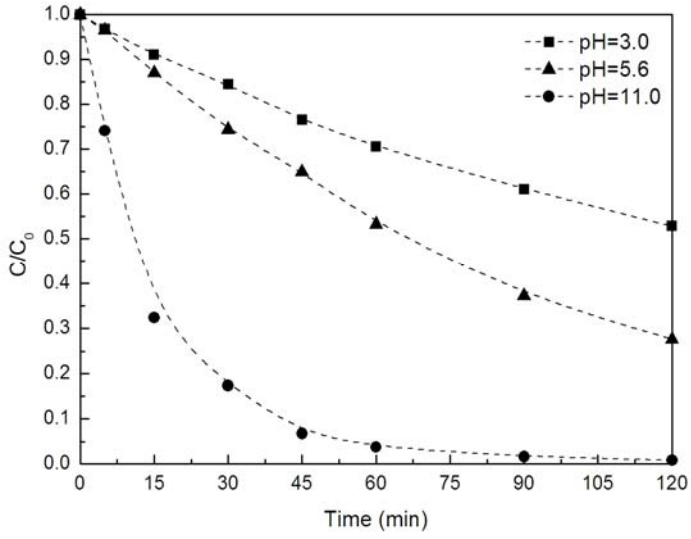

Figure 6.2 Evolution of the dimensionless concentration of CP during the photocatalytic degradation under different initial pH.

At pH 11.0, the catalyst surface is negatively charged and 4-chlorophenol molecule is in the anionic form. Therefore, repulsive forces exist between the catalyst surface and the substrate, which is proved by the small amount of CP adsorbed during the dark adsorption period (C_0). In this case, the fast removal of CP is attributed to a high amount of HO^- ions in the reaction medium favoring the formation of $HO^\bullet$ radicals which attack CP molecule.

Table 6.2 Effect of initial pH in the apparent rate constant (k_{app}), CP conversion ($X_{CP,2h}$) and TOC removal ($X_{TOC,2h}$) after 2 hours of irradiation for the photocatalytic degradation of CP.

pH	C_0 (mg l^{-1})	k_{app} ($\times 10^{-2}$ min^{-1})	$X_{CP,2h}$ (%)	$X_{TOC,2h}$ (%)
3.0	39.1	0.55 ± 0.04	47	26
5.6	44.0	1.04 ± 0.01	72	48
11.0	46.7	5.51 ± 0.09	99	8.9

On the other hand, at pH 3.0 there is a significant amount of CP that is adsorbed by the catalyst during the dark adsorption period, producing a near to 20% decrease in the concentration of the organic molecule. At these conditions CP is present in the molecular form and catalyst is positively charged. Simultaneously, as there is predominance of H^+ species in solution rather than hydroxyl anions low amounts of hydroxyl radicals are generated decreasing the rate of degradation of CP.

For an initial pH of 5.6, although k_{app} and CP conversion were not as favorable as the obtained for basic conditions, a higher TOC removal was achieved. In this case, CP is moderately adsorbed by CNT-TiO_2 catalyst. Hence, in order to establish a compromise between kinetic and mineralization photo-efficiency it was decided to proceed with further CP degradation studies at natural pH conditions.

6.3.1.1.3 Addition of hydrogen peroxide

The effect of the addition of hydrogen peroxide in the efficiency of the photocatalytic degradation of 4-chlorophenol was studied by varying the concentration of H_2O_2 from 0 to 30 mM. It was observed that the addition of a small

amount of H_2O_2 into de reaction system produced a decrease in the apparent rate constant (Table 6.3). This may not be an expected result since hydrogen peroxide is generally established as an electron acceptor agent, preventing TiO_2 electron-hole recombination and therefore increasing the efficiency of the photocatalyst [7].

Table 6.3 Effect of H_2O_2 concentration in the photocatalytic degradation of CP.

$[H_2O_2]$ (mM)	k_{app} ($\times 10^{-2}$ min^{-1})	$X_{CP,2h}$ (%)	$X_{TOC,2h}$ (%)
0	1.04 ± 0.01	72	48
3	0.58 ± 0.04	50	20
10	0.96 ± 0.05	68	26
30	1.08 ± 0.08	73	30

The observed decrease in k_{app} may indicate the existence of competing mechanisms [8, 9], with hydrogen peroxide acting as: i) electron acceptor (Eq. 6.2); ii) hydroxyl radical producer (Eqs. 6.3 and 6.4); iii) positive hole scavenger (Eq. 6.5 and 6.6); iv) hydroxyl radical scavenger (Eq. 6.7).

$$H_2O_2 + e^- \longrightarrow HO^- + HO^\bullet \tag{6.2}$$

$$H_2O_2 + O_2^{\bullet -} \longrightarrow HO^\bullet + HO^- + O_2 \tag{6.3}$$

$$H_2O_2 \xrightarrow{h\nu} 2HO^\bullet \tag{6.4}$$

$$H_2O_2 + 2h^+ \longrightarrow 2H^+ + O_2 \tag{6.5}$$

$$H_2O_2 + h^+ \longrightarrow HO_2^\bullet + H^+ \tag{6.6}$$

$$H_2O_2 + HO^\bullet \longrightarrow H_2O + HO_2^\bullet \tag{6.7}$$

In the presence of low amounts of hydrogen peroxide, reaction described in Eq. 6.4 is not expected to the most important since H_2O_2 shows fair absorption of light in the visible range. At low concentrations, hydrogen peroxide may adsorb on the catalyst surface and react with positive holes (Eqs. 6.5 and 6.6) inhibiting the formation of hydroxyl radicals. Moreover, H_2O_2 can react with hydroxyl radicals in both adsorbed and bulk phases (Eq. 6.7). The above two processes may negatively affect the concentration of hydroxyl radicals and the rate of 4-chlorophenol

degradation. As H_2O_2 concentration increases mechanisms i and ii start to take progressive importance and hydroxyl radical formation by the processes described by Eqs. 6.2 to 6.3 can in part compensate for the reduction in hydroxyl radical concentration. Therefore, the kinetic rate constant tends to increase with further addition of hydrogen peroxide to the CNT-TiO_2 slurry.

6.3.1.1.4 Substrate concentration

The influence of the CP loading in the photocatalytic reaction is an important parameter from both mechanistic and application point of view. For comparison purposes, CP concentration before dark adsorption period was varied from 10 to 50 mg l^{-1} for photocatalytic reactions using TiO_2 and CNT-TiO_2 catalysts. Results showed that for this range of concentrations the reaction rate gets slower as the initial amount of phenol in solution increases (Fig. 6.3). CNT-TiO_2 catalyst showed better photocatalytic efficiency in the whole range of CP concentrations.

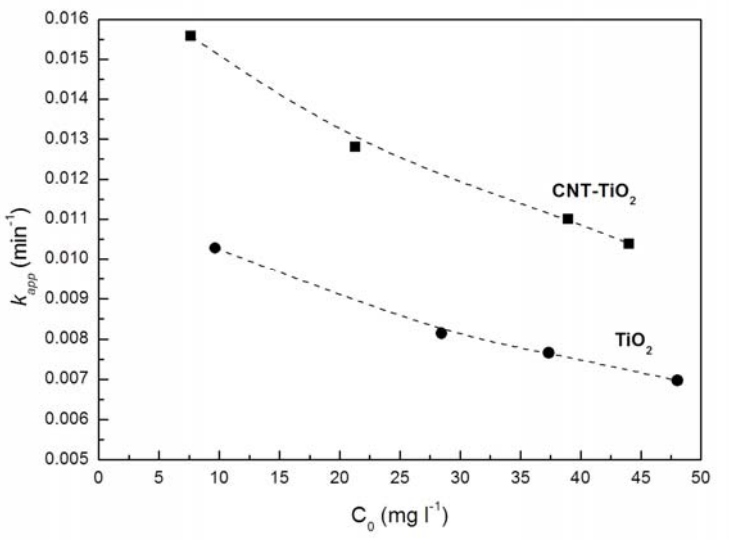

Figure 6.3 Apparent first order kinetic rate constant as a function of the initial CP concentration for TiO_2 and CNT-TiO_2 catalytic systems.

As 4-chlorophenol concentration increases, adsorption of the reactant and of the intermediate compounds increases, and therefore the generation of hydroxyl

radicals will be reduced since are only a fewer active sites for adsorption of hydroxyl anions and formation of hydroxyl radicals.

The dependency of the photocatalytic reaction rate on the concentration of the organic substrate was described by a Langmuir-Hinshelwood kinetic model, taking in consideration the pseudo-steady state approach [10-13], has already been discussed in Chapter 3, section 3.3.1.8. The values of Langmuir-Hinshelwood adsorption equilibrium constant, and the rate constant, were $K_{LH} = 1.38\times10^{-2}$ l mg^{-1} and $k_{LH} = 8.37\times10^{-1}$ mg l^{-1} min^{-1} for photocatalytic reactions using TiO_2 as catalyst and $K_{LH} = 1.47\times10^{-2}$ l mg^{-1} and $k_{LH} = 1.17$ mg l^{-1} min^{-1} for CNT-TiO_2. It is to be noticed that while the kinetic rate constant increased (relative to the TiO_2 alone situation), the values of K_{LH} are comparable in the cases of TiO_2 and CNT-TiO_2 suggesting that the thermodynamics of adsorption are similar, the difference being in the kinetics of the process. The conclusion that follows is that the CNT does not dramatically change the adsorption properties of the resulting catalyst with relation to the initial pollutant molecule, but it plays an important role in the kinetics of the photocatalytic process.

6.3.1.2 Catalyst reuse

The possibility of catalyst recovery and reuse in further catalytic cycles is of great importance since it can substantially contribute to the decrease of operational costs and at the same time reduce the possible negative environmental impact resulting from disposal and/or elimination of the used material.

Fresh CNT-TiO_2 catalyst was used in a first photodegradation experiment (1st run). At the end of two hours of irradiation, catalyst was separated by centrifugation and reused in a second reaction using a new solution of CP (2nd run). The process was repeated in a consecutive experiment using again a fresh 50 mg l^{-1} CP solution (3rd run). As can be seen in Fig. 6.4 catalyst efficiency declined as it was used for successive reactions.

Apparent rate constant decreased 30% from the 1st to the 2nd photodegradation runs and a not so expressive decrease of about 12% from 2nd to 3rd reutilization was observed. This tendency was also observed for CP conversion and TOC removal at the end of each reaction.

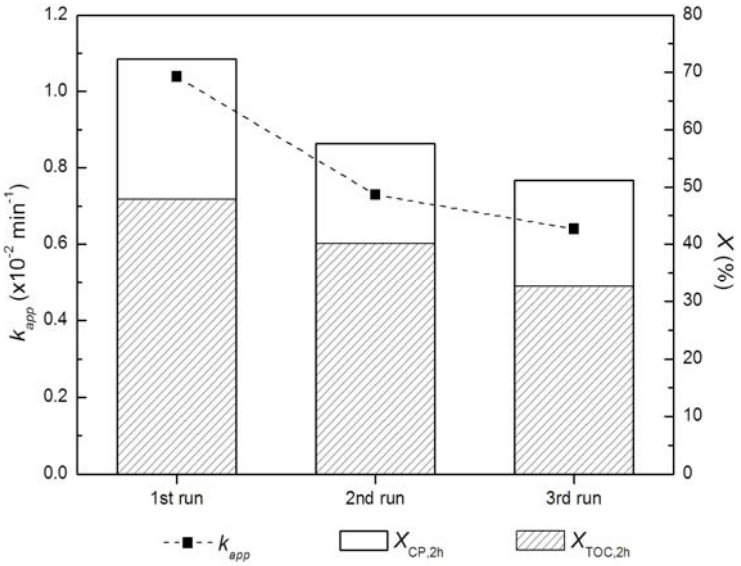

Figure 6.4 Apparent first-order rate constant (k_{app}), CP conversion ($X_{CP,2h}$) and TOC removal ($X_{TOC,2h}$) during photocatalytic degradation over fresh (1st run) and recovered (2nd and 3rd runs) CNT-TiO_2 suspensions.

The observed deterioration of catalyst photoefficiency can be attributed to the presence of reaction intermediates adsorbed on the active sites of the catalyst. Concurrently, as suspensions are magnetically stirred, mechanical stress of the catalyst particles can occur. Both factors account for the reduction of the number of available photoactive sites and therefore to a decease in the catalyst ability to photodecompose 4-chlorophenol.

6.3.2 Photocatalytic degradation of para-substituted phenolic compounds

The photocatalytic degradation of four *para*-substituted phenol derivatives, namely 4-aminophenol, 4-chlorophenol, 4-hydroxybenzoic acid and 4-nitrophenol was performed under visible irradiation using TiO_2 and CNT-TiO_2 catalysts. Photochemical degradation of the organic compounds was performed for comparison purposes. Figure 6.5 shows the UV-Vis absorption spectra of the organic compounds and catalysts.

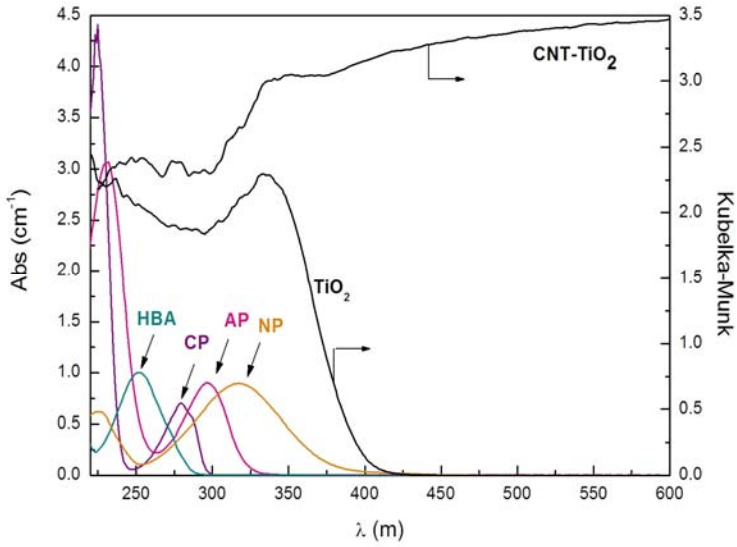

Figure 6.5 Diffuse reflectance and absorption UV-Vis spectra of the catalysts and of the organic compounds, respectively.

The photocatalytic reactivity of aromatic compounds can be affected by the number of substituents, their electronic nature and their position in the aromatic ring [14]. Some studies have shown that organic molecules containing electron-donor substituents are easily degraded by photocatalytic oxidation processes [15, 16]. The effect that a substituent has on the electronic character of a given aromatic system is represented by the Hammet constant (σ). By definition, hydrogen *para*-substituted phenol is taken as reference with σ_p=0. A modified Hammet constant (σ_p^-) is normally used for situations in which the substituent enter in some resonance with the reaction center in an electron-rich transition state, which is the case of reactions involving phenols [17]. Electron donating groups such as $-NH_2$, $-OH$, $-OCH_3$ show negative Hammet constants while for electron withdrawing groups as $-NO_2$, $-COOH$, $-Cl$, $-CN$, $\sigma_p^- > 0$. Hammet constants for AP, CP, HBA and NP are presented on Table 6.4 [17].

Among the studied compounds 4-aminophenol presents the lowest Hammet constant (σ_p^-=–0.66) which means that it is the least electrophilic molecule while 4-nitrophenol shows a σ_p^- value of 1.25, confirming the deactivating nature of the $-NO_2$ group.

Table 6.4 Hammet constant (σ_p^-), concentration after dark adsorption period (C_0), apparent first order kinetic rate constant (k_{app}), synergy factor (R), conversion (X_{2h}) and TOC removal ($X_{TOC,2h}$) after 2 hours of irradiation obtained for the photochemical and photocatalytic degradation of AP, CP, HBA and NP.

Compound	σ_p^-	System	C_0 (mg l^{-1})	k_{app} ($\times 10^{-2}$ min^{-1})	R	X_{2h} (%)	$X_{TOC,2h}$ (%)
		Blank	50.0	n.a.*		n.a.*	n.a.*
AP	-0.66	TiO_2	46.3	0.83± 0.02	2.21	47	5.1
		CNT-TiO_2	45.4	1.83± 0.05		60	7.7
		Blank	50.0	0.59± 0.04		54	2.2
CP	0.23	TiO_2	48.0	0.69± 0.05	1.51	55	42
		CNT-TiO_2	44.0	1.04± 0.01		72	48
		Blank	50.0	n.a.**		n.a.**	n.a.**
HBA	0.73	TiO_2	47.3	0.61± 0.03	1.07	49	38
		CNT-TiO_2	40.7	0.66± 0.01		54	48
		Blank	50.0	0.17± 0.04		4.9	1.0
NP	1.25	TiO_2	49.5	0.46± 0.07	0.70	23	21
		CNT-TiO_2	43.2	0.32± 0.03		16	13

n.a.*: formation of a precipitate; n.a.**: no HBA degradation

Photochemical and photocatalytic degradation reactions were performed in the absence of catalyst and using TiO_2 or CNT-TiO_2 catalysts, respectively. For all compounds, photodegradation reactions fit well a pseudo-first order kinetic rate model. Apparent rate constants (k_{app}) obtained for the different compounds and degradation systems are listed in Table 6.4. During the direct photodegradation of AP, the solution passed from colorless to brown, pointing to a polymerization process, probably by formation of dihydroxyazobenzene species. Direct photolysis of HBA didn't produce any degradation of the initial compound, since it doesn't absorb in the range that the aqueous solution is being irradiated. Despite showing residual absorption in the visible range of the spectrum, photodegradation of CP in the absence of catalyst was observed and a 54% of conversion of the organic molecule at the end of 2 hours of irradiation was observed. However only 2% of TOC reduction was achieved which indicates that most of the initial organic content is still present in the treated solution. In the case of NP, although it shows absorption at λ>300 nm, with a maximum at λ=317 nm, very little degradation was

observed with only 4.9% of NP being converted at the end of the reaction. This result is associated to the strong deactivating nature of $-NO_2$ group.

Although with distinct extension for the four *para*-substituted phenols, the photocatalytic process revealed to be much more efficient than the pure photochemical reaction. Since each *para*-substituted phenolic compound show different adsorption behavior in both TiO_2 and CNT-TiO_2 catalysts, concentration after the dark adsorption period (C_0) was determined and initial reaction rate (r_0) was calculated. Hammet constants were used to establish a correlation with initial degradation rates for the different organic compounds. A plot of r_0 as a function of σ_p^- is shown in Fig. 6.6 for photocatalytic reactions using both TiO_2 and CNT-TiO_2 catalysts.

The good correlation observed between σ_p^- and r_0 for the different compounds indicate the electrophilic nature of the photocatalytic reaction. The photocatalytic degradation rates are in a good degree depending on the effect of the substituents on the aromatic ring being accelerated by electron donating groups, which is the case of $-NH_2$ in AP, and retarded by electron-withdrawing substituents such as –Cl, –COOH and $-NO_2$ in CP, HBA and NP, respectively. For each category of substituents, the effect on the photodegradation depends on the activating or deactivating ability of each substituent, which is directly related with the value of σ_p^- as shown in Fig. 6.6.

The effect of the introduction of the CNT in the composite catalyst was quantified by means of a synergy factor, R (Table 6.4). The highest value for synergy factor R of 2.21 was obtained for AP, which means a double k_{app} value when composite catalyst was used. CNT-TiO_2 catalyst also showed higher efficiency than TiO_2 alone for the degradation of CP, with a 50% increase in k_{app}.

For HBA and NP quite different results were obtained. Apparent first order kinetic rate constant obtained for the photocatalytic degradation of HBA with CNT-TiO_2 and TiO_2 catalysts were similar, and therefore no kinetic synergy effect was observed for this compound. Nevertheless, in terms of mineralization a higher TOC removal was achieved when composite catalyst was used. In the case of NP, a lower k_{app} was obtained for photocatalytic reaction with CNT-TiO_2 catalyst. This result can be explained by the high deactivating nature of NP molecule. Although adsorption of NP is greater in CNT-TiO_2 catalyst than in TiO_2, the organic molecule resist to the attack of hydroxyl radicals at the catalyst surface leading to a decrease in the efficiency of the photodegradation process.

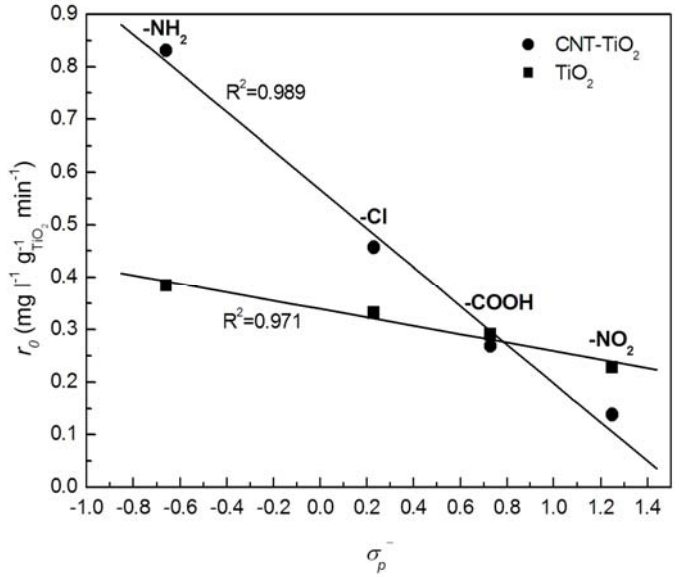

Figure 6.6 Relationship between initial degradation rate (r_0) and Hammet constant (σ_p^-) for the different *para*-substituted phenols.

Graphically, it can be considered that no benefit on the use of CNT-TiO_2 composite catalyst is observed for *p*-substituted phenols with Hammet constants higher than the correspondent to the crossing point of the two straight lines represented in Fig. 6.6, *i.e.*, for molecules with $\sigma_p^- > 0.79$.

6.3.3 Reaction mechanism and intermediates

HPLC analysis of the samples collected during the photocatalytic degradation of AP, NP and CP revealed that the main reaction intermediates are hydroquinone and benzoquinone. Trace concentrations of 4-nitrocatechol and 4-chlorocatechol were detected as degradation intermediates for NP and CP, respectively (Figs. 6.7a and 6.7b).

The main HBA degradation intermediate was found to be 3,4-hydroxybenzoic acid. Also, very low concentrations of hydroquinone and benzoquinone were detected. Nitrates were also detected as by-products of NP photocatalytic degradation. No nitrites were found in the samples, probably because the expected NO_2^- ions are converted to NO_3^- under the strong oxidizing conditions.

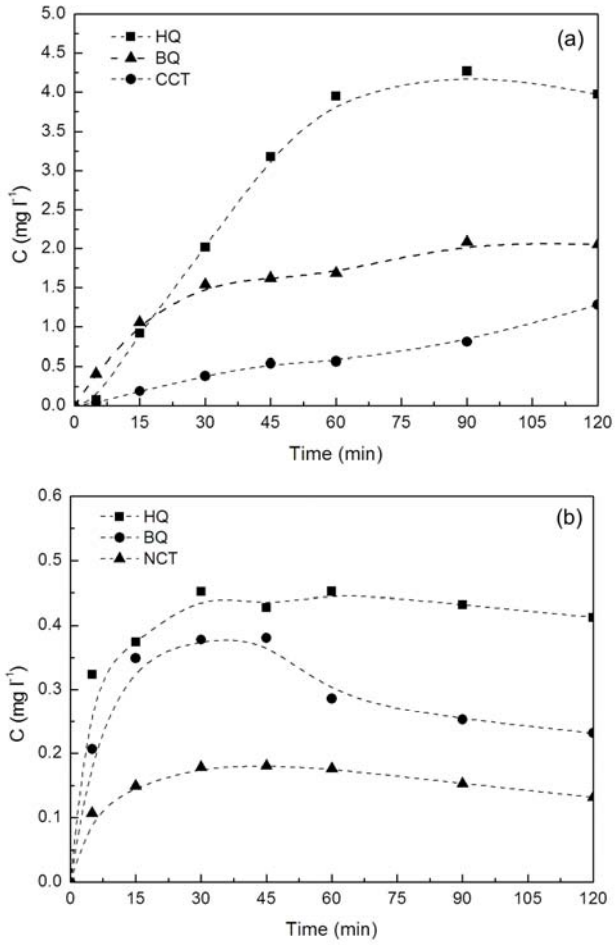

Figure 6.7 Concentration of main intermediates during the photocatalytic degradation of CP (a) and NP (b) using CNT-TiO_2 catalyst: hydroquinone (HQ); benzoquinone (BQ); 4-chlorocatechol (CCT); 4-nitocatechol (NCT).

In the case of AP, ammonium ion should be expected as a by-product of the deamination of the starter molecule. Since the reaction takes place at pH lower than pK_a of NH_4^+ (pK_a = 9.27) ammonia occurs mostly as the ammonium ion (NH_4^+) instead of NH_3. However, negligible amounts of NH_4^+ were measured and NO_3^- was detected as main by-product, meaning that ammonium is oxidized to nitrate under the reaction conditions. Despite not being quantified in this work, taking into account the detected intermediates chloride anion (Cl^-) is also expected to be a by-product of the photocatalytic degradation of the organic molecule [18]. A simplified photocatalytic degradation mechanism of the studied *para*-substituted phenols is shown in Scheme 6.1.

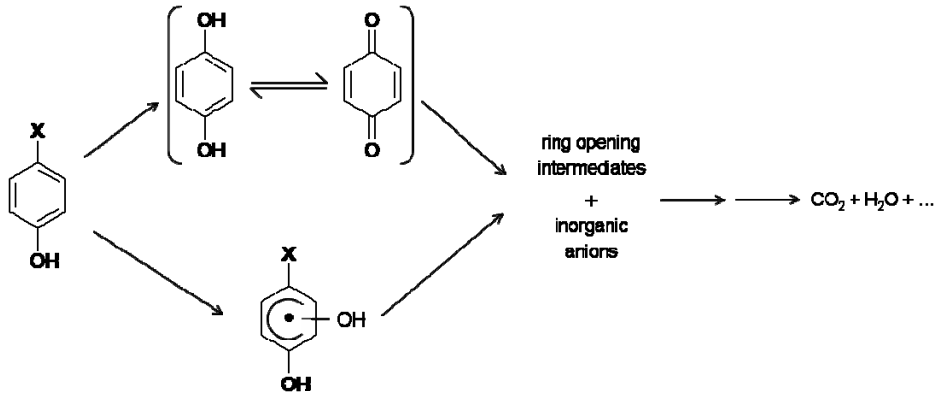

Scheme 6.1 Simplified photocatalytic degradation mechanism of *para*-substituted phenols.

By these results it can be stated that hydroxyl radicals are the key species responsible for the degradation of the studied compounds. Hydroquinone is formed when the attack of the $HO^{\bullet}$ radical takes place in the *para* position by abstraction of the substituent group. Benzoquinone is one of the intermediate products of hydroquinone degradation, which can be reduced to hydroquinone by reaction with the electrons from the conduction band of the semiconductor, establishing a keto–enolic tautomery oxidoreductive equilibrium [19]. On the other hand, hydroxyl radical can attack the aromatic ring by addition of a hydroxyl group followed by the elimination of a hydrogen atom. The position of the insertion of the hydroxyl group follows the orientating properties of benzene substituent groups. Therefore, 4-chlorocatechol, 4-nitrocatechol and 3,4-dihydroxybenzoic acid were found as reaction intermediates from CP, NP and HBA degradation, respectively.

6.4 Conclusions

Multi walled carbon nanotube-TiO_2 composite catalyst produced by a modified acid catalyzed sol-gel procedure was used in the photocatalytic degradation of para-substituted phenols under visible (λ>300 nm) irradiation.

4-Chlorophenol was used as model compound to study the effect of operational parameters on the photo-efficiency of the degradation reaction using CNT-TiO_2 catalyst namely catalyst loading, pH of the medium, hydrogen peroxide concentration and substrate concentration. An optimal concentration of catalyst of

1.2 g l^{-1} was found. At natural pH conditions (pH = 5.6) an optimal compromise between kinetic and mineralization photoefficiency of CNT-TiO_2 catalyst was achieved. The introduction of low concentrations of hydrogen peroxide in the reactional media leaded to a decrease in the efficiency of the degradation process, which was attributed to the action of H_2O_2 as hydroxyl radical scavenger. With increasing concentration of H_2O_2 apparent first order constant tend to gradually increase as a result of the raise of the relative importance of its role as electron acceptor and hydroxyl radical generator. The reutilization of the recovered CNT-TiO_2 catalyst resulted in a gradual decrease in the efficiency of the catalyst. A Langmuir-Hinshelwood model, based on a pseudo-steady state approach, was successfully used to represent the dependency of the photocatalytic reaction rate on the concentration of CP for both TiO_2 and CNT-TiO_2 catalysts.

Beside 4-chlorophenol, CNT-TiO_2 was used as catalyst for the photocatalytic degradation of other *para*-substituted phenols namely 4-aminophenol, 4-hydroxybenzoic acid and 4-nitrophenol. The photoreactivity of the substituted phenols showed to be affected by the electronic nature of the substituents. Initial degradation rate tend to increase with increasing electronic density on the aromatic ring in the following order: 4-nitrophenol < 4-hydroxybenzoic acid < 4-chlorophenol < 4-aminophenol. The Hammet constant, which represents the effect that different substituents have on the electronic character of a given aromatic system, appears to be an adequate descriptor of the photocatalytic degradability of the studied *para*-substituted phenols using both TiO_2 and CNT-TiO_2 catalysts.

The effect of the introduction of CNT into the TiO_2 matrix was quantified in terms of a synergy factor. This synergy factor was inversely proportional to the Hammet constant of the studied molecules. For AP and CP the use of a CNT-TiO_2 composite catalyst caused a beneficial effect in the photoefficiency of the degradation process. Conversely, for HBA practically no synergy effect was observed while for NP the use of CNT-TiO_2 resulted on a negative synergy effect. By these results it can be concluded that the photoefficiency of the catalysts is not only related to its intrinsic properties but also to the activating/deactivating nature of the substrate to be degraded.

Hydroquinone and benzoquinone were detected as reaction intermediates for all compounds. Also 4-chlorocatechol, 4-nitrocatechol and 3,4-dihydroxybenzoic acid were detected as CP, NP and HBA degradation intermediates, respectively.

6.5 References

[1] W. Gernjak, M.I. Maldonado, S. Malato, J. Caceres, T. Krutzler, A. Glaser, R. Bauer, *Pilot-plant treatment of olive mill wastewater (OMW) by solar TiO_2 photocatalysis and solar photo-Fenton*, Sol. Energy. 77 (2004) 567-572.

[2] H.T. Gomes, J.L. Figueiredo, J.L. Faria, *Catalytic wet air oxidation of olive mill wastewater*, Catal. Today. 124 (2007) 254-259.

[3] M.C. Yeber, J. Rodriguez, J. Freer, N. Duran, H.D. Mansilla, *Photocatalytic degradation of cellulose bleaching effluent by supported TiO_2 and ZnO*, Chemosphere. 41 (2000) 1193-1197.

[4] M.H. Franson, A.D. Eaton, L.S. Clesceri, A.E. Greenberg, *Standard Methods for the Examination of Water and Wastewater*. 21st Edition ed. American Public Health Association, American Water Works Association and Water Environment Federation (2005), Washington D.C.

[5] J.M. Herrmann, *Heterogeneous photocatalysis: State of the art and present applications*, Top. Catal. 34 (2005) 49-65.

[6] X.H. Li, J.L. Niu, J. Zhang, H.L. Li, Z.F. Liu, *Labeling the defects of single-walled carbon nanotubes using titanium dioxide nanoparticles*, J. Phys. Chem. B. 107 (2003) 2453-2458.

[7] E. Evgenidou, E. Bizani, C. Christophoridis, K. Fytianos, *Heterogeneous photocatalytic degradation of prometryn in aqueous solutions under UV-Vis irradiation*, Chemosphere. 68 (2007) 1877-1882.

[8] W. Chu, C.C. Wong, *The photocatalytic degradation of dicamba in TiO_2 suspensions with the help of hydrogen peroxide by different near UV irradiations*, Water Res. 38 (2004) 1037-1043.

[9] Y.J. Zang, R. Farnood, *Effect of hydrogen peroxide on the photocatalytic degradation of methyl tert-butyl ether*, Top. Catal. 37 (2006) 91-96.

[10] A.V. Emeline, V. Ryabchuk, N. Serpone, *Factors affecting the efficiency of a photocatalyzed process in aqueous metal-oxide dispersions: Prospect of distinguishing between two kinetic models*, J. Photochem. Photobiol. A: Chem. 133 (2000) 89-97.

[11] A. Mills, J. Wang, D.F. Ollis, *Kinetics of liquid phase semiconductor photoassisted reactions: Supporting observations for a pseudo-steady-state model*, J. Phys. Chem. B. 110 (2006) 14386-14390.

[12] D.F. Ollis, *Kinetics of liquid phase photocatalyzed reactions: An illuminating approach*, J. Phys. Chem. B. 109 (2005) 2439-2444.

[13] D.F. Ollis, *Kinetic disguises in heterogeneous photocatalysis*, Top. Catal. 35 (2005) 217-223.

[14] M.H. Priya, G. Madras, *Kinetics of photocatalytic degradation of phenols with multiple substituent groups*, J. Photochem. Photobiol. A: Chem. 179 (2006) 256-262.

[15] G. Palmisano, M. Addamo, V. Augugliaro, T. Caronna, A.D. Paola, E.G. López, V. Loddo, G. Marcì, L. Palmisano, M. Schiavello, *Selectivity of hydroxyl radical in partial oxidation of aromatic compounds in heterogeneous photocatalysis*, Catal. Today. 122 (2007) 118-127.

[16] S. Parra, J. Olivero, L. Pacheco, C. Pulgarin, *Structural properties and photoreactivity relationships of substituted phenols in TiO_2 suspensions*, Appl. Catal. B: Environ. 43 (2003) 293-301.

[17] G.W. Gokel, *Dean's Handbook of Organic Chemistry (2nd Edition)*. 2004, McGraw-Hill.

[18] B. Malinowska, J. Walendziewski, D. Robert, J.V. Weber, M. Stolarski, *The study of photocatalytic activities of titania and titania-silica aerogels*, Appl. Catal. B: Environ. 46 (2003) 441-451.

[19] A.G. Rincón, C. Pulgarin, N. Adler, P. Peringer, *Interaction between E. coli inactivation and DBP-precursors -- dihydroxybenzene isomers -- in the photocatalytic process of drinking-water disinfection with TiO_2*, J. Photochem. Photobiol. A: Chem. 139 (2001) 233-241.

Part V

Future work and conclusions

Chapter 7

Photocatalytic oxidation of clofibric acid under visible irradiation using nanocrystalline sol-gel TiO_2 catalysts

TiO_2 catalysts produced by an acid catalyzed sol-gel method using different calcination temperatures are used in the visible-light-driven photocatalytic degradation of clofibric acid, a lipid regulator drug. The photoefficiency of TiO_2 catalysts, quantified in terms of kinetic rate constant, total organic carbon removal and initial quantum yield, increases with calcination temperature up to 673K. A lower photo-efficiency was observed for the catalyst obtained at 573K due to the presence of amorphous titania. As calcination temperature increases, a decline in the photo-efficiency of the catalysts is observed which is attributed to the phase transformation from anatase to rutile and simultaneously, to the increase in the crystallite dimensions. The photochemical and photocatalytic oxidation of clofibric acid follows a pseudo-first order kinetic rate law. 4-Chlorophenol, isobutyric acid, hydroquinone, benzoquinone and 4-chlorocatechol are detected as main intermediates.

7.1 Introduction

In the present work TiO_2 nanocrystalline powders produced from Ti(IV) isopropoxide by an acid catalyzed sol-gel method and extensively characterized in Chapter 2 were tested in the photocatalytic oxidation of clofibric acid (2-(p-chlorophenoxy)-2-methylpropionic acid) under visible irradiation.

Clofibric acid is the active metabolite of several fibrate drugs prescribed to reduce blood cholesterol levels. These drugs act to lower elevated serum lipids by reducing the very low density lipoprotein fraction that is rich in triglycerides. It is also classified as a plant growth regulator (antiauxin) pesticide [1]. Pharmaceuticals are a class of emerging environmental contaminants that are extensively and increasingly being used in human and veterinary medicine [2]. A considerable percentage of these compounds are excreted unchanged through urine and feces or as metabolites entering the waste water streams. If they are not biodegraded or eliminated in sewage treatment plants they may enter the aquatic environment and eventually reach drinking water [3-5]. These type of chemicals are designed to be very stable in the organism and when present in the environment they show refractory behavior which may lead to its bio-accumulation. Clofibric acid is resistant to degradation, having an estimated persistence in the environment of 21 years [6].

Kinetics of clofibric acid photocatalytic degradation was studied and reaction intermediates were determined. A correlation between morphological, crystalline and spectroscopic properties of the synthesized TiO_2 materials and its ability for the degradation of this organic pollutant was attempted.

7.2 Experimental

TiO_2 preparation and characterization is described in Chapter 2. Photocatalytic activity of the prepared materials was evaluated following clofibric acid (Aldrich 97%) degradation in aqueous solution under visible irradiation. The experiments were carried out in a glass immersion photochemical reactor charged with 250 ml of suspension. The reactor was equipped with a Heraeus TQ 150 medium-pressure mercury vapor lamp (more intense lines at λ_{exc} of 366, 436 and 546 nm, the UV line at 254 nm being filtered by a DURAN 50® glass jacket) which was located axially and held in a quartz immersion tube. In a typical experiment,

the initial clofibric acid concentration and the amount of suspended TiO_2 were set at 8.33×10^{-5} M (~18 mg l^{-1}) and 1 g l^{-1}, respectively. A 200 ml min^{-1} oxygen/argon (20% vol. of oxygen) stream was continuously supplied to the reactor. Reactions took place under natural pH conditions (pH~4.2). Before turning on the illumination, the suspensions were saturated with the gas mixture and magnetically stirred for 30 minutes to establish an adsorption-desorption equilibrium. Then, the suspensions were irradiated with visible light at constant stirring speed. Samples were withdrawn regularly from the reactor and centrifuged for separation of any suspended solid, prior to analysis. The clean transparent solution was then analyzed by HPLC using a Hitachi Elite LaChrom liquid chromatograph equipped with an L-2450 diode array detector. The stationary phase consisted in a YMC-Pack ODS-AQ endcapped column (250 mm × 4.6 mm, 5μm particles) working at room temperature. The mobile phase was a mixture of a 20 mM NaH_2PO_4/H_3PO_4 (pH=2.8) buffer solution and acetonitrile with a gradient concentration at a flow rate of 1 ml min^{-1}. For known compounds, the relationship between area and concentration was determined by using standards. Total organic carbon (TOC) measurements were performed in a Shimadzu TOC-5000 analyzer.

7.3 Results and discussion

In order to explore the photo-efficiency of the prepared materials, TiO_2 nanocrystalline catalysts were tested in the photocatalytic oxidation of clofibric acid aqueous solutions under visible irradiation. A pure photochemical reaction, without any catalyst, was carried out for comparison purposes. Photochemical and photocatalytic degradation of clofibric acid followed a pseudo-first order kinetic model:

$$C_{CA} = C_{CA,0} e^{-k_{app} t} \tag{7.1}$$

where C_{CA} is the concentration of clofibric acid at different reaction times (t), $C_{CA,0}$ is the initial clofibric acid concentration for t=0 (the instant when illumination is turned on) and k_{app} is the apparent pseudo-first order kinetic rate constant. Kinetic rate constants were determined by non-linear fit of Eq. 5 to the experimental data and are listed on Table 7.1. From pure photochemical reaction resulted an apparent rate constant of 3.62×10^{-3} min^{-1}, while the higher k_{app} of 1.11×10^{-1} min^{-1} was obtained for TiO_2-673. For this catalyst, close to complete clofibric acid removal

was achieved after only 30 minutes of irradiation. Catalysts obtained at higher temperatures resulted on progressively lower kinetic rate constants. Catalyst TiO_2-973, constituted by pure rutile crystals, showed a k_{app} of 1.02×10^{-2} min^{-1}, close to ten times less than the pure anatase catalyst produced at 673K.

Table 7.1 Pseudo-first order apparent kinetic rate constant (k_{app}), clofibric acid conversion after 30 minutes of irradiation ($X_{30\ min}$) and total organic carbon removal at the end of 4 hours of irradiation ($X_{TOC,}$) for the photocatalytic tests using the different TiO_2 catalysts and pure photochemical reaction.

Catalyst	k_{app} (min^{-1})	$X_{30\ min}$ (%)	$X_{TOC,\ 4h}$ (%)
TiO_2-573	8.03×10^{-2}	91	76
TiO_2-673	1.11×10^{-1}	97	79
TiO_2-723	7.50×10^{-2}	88	73
TiO_2-773	4.76×10^{-2}	74	64
TiO_2-823	2.76×10^{-2}	59	51
TiO_2-873	2.14×10^{-2}	50	40
TiO_2-973	1.02×10^{-2}	28	20
Blank*	3.62×10^{-3}	15	2.6

* no catalyst

The main reaction intermediates detected by HPLC analysis were found to be 4-chlorophenol, isobutyric acid, hydroquinone, benzoquinone and 4-chlorocatechol. Figure 7.1 shows the concentration profiles of clofibric acid and reaction intermediates for photocatalytic experiments using TiO_2-673 and TiO_2-973. The main reaction intermediate was found to be 4-chlorophenol, the others being detected at lower concentrations. As can be observed in Fig. 7.1a, reaction using TiO_2-673 produced an abrupt abatement on clofibric acid concentration. Its complete removal was achieved at very early reaction times. The concentration of the main intermediates initially rises and then decreases until complete disappearance at the end of four hours of irradiation. Clofibric acid removal appeared to be much slower when TiO_2-973 catalyst was used. At the end of the irradiation run there was still a considerable amount of the initial compound and reaction intermediates in solution (Fig. 7.1b).

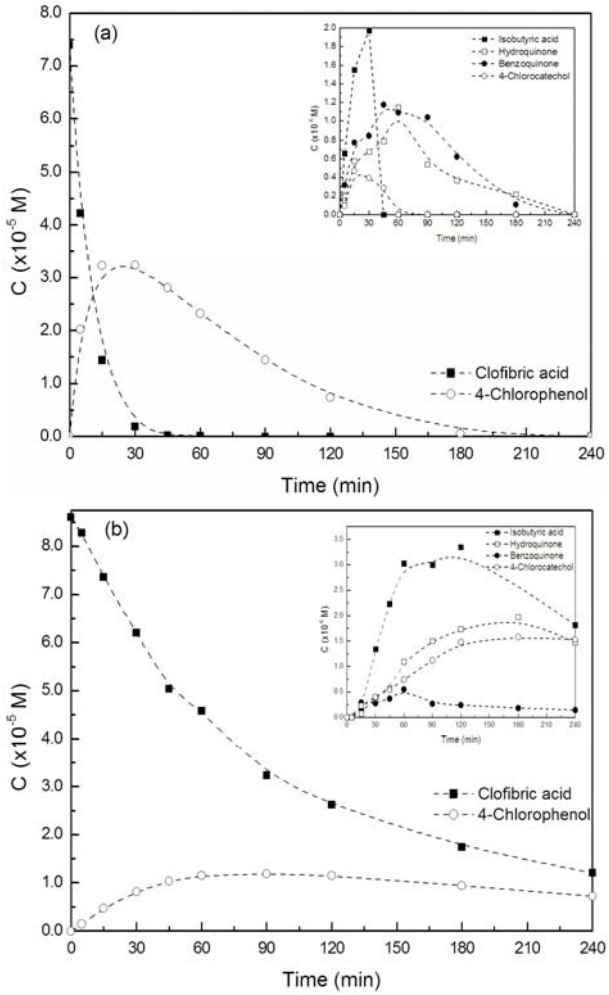

Figure 7.1 Concentration profiles of clofibric acid and 4-chlorophenol during the photocatalytic reaction using TiO_2-673 (a) and TiO_2-973 (b) catalysts (inset: concentration profiles of isobutyric acid, hydroquinone, benzoquinone and 4-chlorocatechol).

Total organic carbon analysis provided valuable information about the efficiency of the photo-assisted processes. It is obvious that the presence of a catalyst improves the removal of organic compounds from the solutions. At the end of the photodegradation runs (4 hours of irradiation) it was observed a merely 2.6% decrease in organic content for reaction without catalyst and 79.4% of TOC removal for reaction in the presence of TiO_2-673. The fraction of non-mineralized organics probably corresponds to aliphatic acids, not detected by HPLC in these experimental conditions, such as lactic, acetic, formic, maleic, oxalic and others

resulting from the aromatic ring opening. Based on the previous results, a possible degradation pathway is presented on Scheme 7.1.

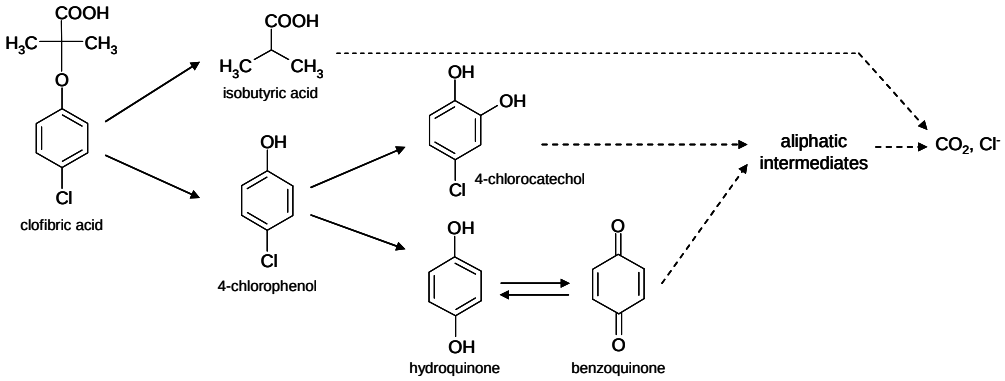

Scheme 7.1 Simplified degradation pathway for the photocatalytic degradation of clofibric acid.

From an energetic point of view, the photonic efficiency of the photo-induced process was quantified in terms of its quantum yield (Φ), *i.e.,* the number of molecules which react according to this process divided by the number of photons absorbed by the system during the same time [7]. The determination of the quantum yield was performed by using Eq. 3.2 (Chapter 3) [8].

The photonic flux (φ) is related to the radiant power of the lamp used in the degradation experiments as well as the wavelength of radiation emission. In the present work, a medium-pressure mercury lamp was used with the most important emission line at 366 nm. The photon flux for this wavelength, determined by potassium ferrioxalate actinometry [9], was of 2.38×10^{-6} Einstein s^{-1}. The initial quantum yields for the photochemical and photocatalytic reactions with the different catalysts are compared in Fig. 7.2.

Results are consistent with the previous observations based on first-order kinetics rate constants and TOC removal. TiO_2-673 appear to be the most photo-efficient catalyst, with a quantum yield of 1.55%, while for the pure rutile TiO_2 material a much lower quantum yield of 0.15% was obtained. The pure photochemical process revealed the worst photo-efficiency with a quantum yield of merely 0.06%.

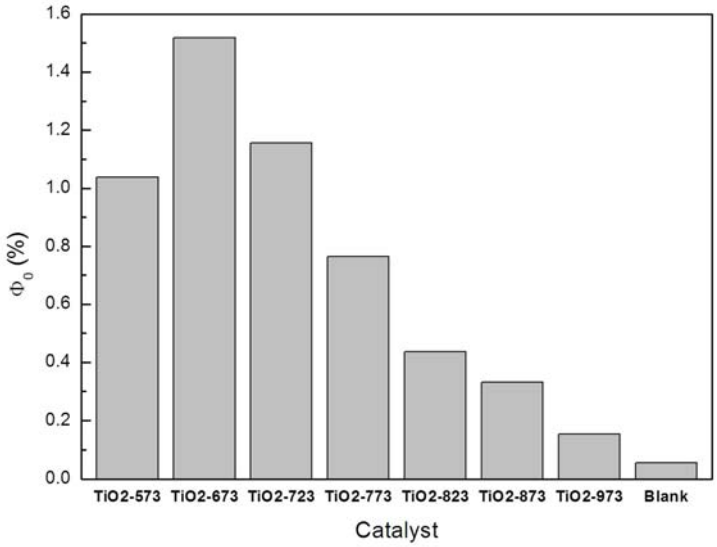

Figure 7.2 Initial quantum yields (Φ_0) for the different photochemical and photocatalytic systems.

From these results it is obvious that the physical-chemical properties of the sol-gel TiO_2 materials play a crucial role on its photocatalytic performance. Titanium dioxide obtained at 573K has the highest surface area and is mainly composed of anatase. Nevertheless, XRD measurements revealed broad peaks which indicate that the crystallization process is not complete. Amorphous titania is known to have low photocatalytic activity due to a high electron-hole recombination rate [10]. It was found that TiO_2 photocatalytic efficiency increases with calcination temperature up to 673K. The catalysts obtained at this temperature revealed to be the most active for photocatalytic degradation of clofibric acid. For higher calcination temperature a progressive loss in photocatalytic efficiency was observed. The sample TiO_2-973 showed only little photocatalytic efficiency to decompose clofibric acid. The decline in photoefficiency for higher calcination temperatures is attributed to the phase transformation from anatase to rutile. Simultaneously, the larger-sized titanium dioxide crystals resulted from higher temperatures also gives raise to a decrease in the photocatalytic performance of the semiconductor.

7.4 Conclusions

Morphological and spectroscopic properties appeared to be determining factors affecting TiO_2 performance on the photocatalytic removal of clofibric acid under visible irradiation. The best photo-efficiency, quantified in terms of kinetic rate constant, TOC removal and initial quantum yield, was achieved for the catalyst produced at 673K (pure anatase) resulting in the total removal of clofibric acid and main reaction intermediates (4-chlorophenol, isobutyric acid, hydroquinone, benzoquinone and 4-chlorocatechol) after four hours of irradiation.

At 573K there is a fraction of titania that is still not crystallized reducing its photo-efficiency. Higher calcination temperature promotes phase transition from anatase to rutile and simultaneously the increase in crystallite and particle dimensions with the resultant decrease in surface area conducing to a loss on the activity of the photocatalysts.

This study opens the possibility of use of nanocrystalline TiO_2 based catalysts for the effective mineralization of this type of pharmaceutical compounds in wastewaters.

7.5 References

[1] J.P. Emblidge, M.E. DeLorenzo, *Preliminary risk assessment of the lipid-regulating pharmaceutical clofibric acid, for three estuarine species*, Environ. Res. 100 (2006) 216-226.

[2] M.D. Hernando, M. Mezcua, A.R. Fernandez-Alba, D. Barcelo, *Environmental risk assessment of pharmaceutical residues in wastewater effluents, surface waters and sediments*, Talanta. 69 (2006) 334-342.

[3] D. Bendz, N.A. Paxeus, T.R. Ginn, F.J. Loge, *Occurrence and fate of pharmaceutically active compounds in the environment, a case study: Hoje River in Sweden*, J. Hazard. Mater. 122 (2005) 195-204.

[4] N. Lindqvist, T. Tuhkanen, L. Kronberg, *Occurrence of acidic pharmaceuticals in raw and treated sewages and in receiving waters*, Water Res. 39 (2005) 2219-2228.

[5] E. Zuccato, S. Castiglioni, R. Fanelli, *Identification of the pharmaceuticals for human use contaminating the Italian aquatic environment*, J. Hazard. Mater. 122 (2005) 205-209.

[6] H.R. Buser, M.D. Muller, N. Theobald, *Occurrence of the pharmaceutical drug clofibric acid and the herbicide mecoprop in various Swiss lakes and in the North Sea*, Environ. Sci. Technol. 32 (1998) 188-192.

[7] A.M. Braun, M.T. Maurette, E. Oliveros, *Photochemical Technology*, ed. J.W. Sons (1991), Chichester, England.

[8] J.M. Herrmann, *Heterogeneous photocatalysis: State of the art and present applications*, Top. Catal. 34 (2005) 49-65.

[9] H.J. Kuhn, S.E. Braslavsky, R. Schmidt, *Chemical actinometry*, Pure Appl. Chem. 76 (2004) 2105-2146.

[10] B. Ohtani, Y. Ogawa, S. Nishimoto, *Photocatalytic activity of amorphous-anatase mixture of titanium(IV) oxide particles suspended in aqueous solutions*, J. Phys. Chem. B. 101 (1997) 3746-3752.

Chapter 8

Concluding remarks and suggestions for future work

During the course of this research work, a number of conclusions have been reached, regarding the preparation, characterization and utilization of TiO_2 based photocatalysts in the degradation of organic pollutants in water.

The acid catalyzed sol-gel method, lead to the formation of crystalline TiO_2 materials. By controlling the calcination temperature it is possible to tailor the crystalline and spectroscopic properties of titania materials.

Increasing temperatures lead to an increase in crystallite dimensions and promote phase transformation from anatase to rutile. Pure anatase TiO_2 was found to be more active than anatase/rutile mixtures or pure rutile, in the photocatalytic degradation of phenol, under UV (253.7 nm) light. As anatase to rutile transformation occurs, crystallites tend to agglomerate from quantum to bulk-size particles with the progressive loss of activity of the catalyst.

Operational parameters such as pH, catalyst concentration, phenol initial concentration, presence of oxidant species, oxygen partial pressure and photon flux, have shown to play an important role in the photo-efficiency of TiO_2 as catalyst. Optimal conditions were found at natural pH (pH=5.6) using 1 g l^{-1} of pure anatase catalyst and an oxygen partial pressure of 0.2 atm. Oxidants like H_2O_2 and $Na_2S_2O_8$ produce a beneficial effect in the efficiency of the photodegradation process, since they act as electron acceptors, thus avoiding electron/hole recombination.

A modified Langmuir-Hinshelwood kinetic rate model, considering a pseudo-steady state approach, was used to describe the kinetics of the photocatalytic process dependency on the initial concentration of the substrate and on illumination intensity. An increase in the photon flux results in an increase in the kinetic rate constant and in a decrease in the adsorption constant, which is attributed to an increasing concentration of $HO^{\bullet}$ radicals accelerating the oxidation of the organic molecule and, at the same time, to a decrease in the available sites for adsorption and therefore a decrease in K_{LH}.

Main reaction intermediates were found to be phenol hydroxy-derivatives, namely hydroquinone and catechol, meaning that the key species involved in the photodegradation of the organic pollutant are hydroxyl radicals.

Kinetics of both, phenol consumption and intermediates formation and consumption, fit well pseudo-first order rate laws, which means that effective water detoxification, can be achieved in a convenient time scale.

Reutilization of TiO_2 catalyst resulted in a loss of the efficiency of the photo-oxidation process, attributed to the presence of adsorbed compounds and/or to the change in the catalyst surface and morphological properties.

A modified acid catalyzed sol-gel technique revealed to be a good method for the preparation of TiO_2 based composite catalysts.

Composite photocatalysts produced using mesoporous molecular sieves, MCM41 and MCM48, and zeolite NaY didn't provide any effect in the activity of TiO_2. Conversely, composites prepared with carbon based materials such as activated carbon, carbon fibers and multi-walled carbon nanotubes originate a beneficial effect in the photodegradation of phenol under visible light. This synergy effect is correlated to the capacity of the resultant materials to absorb light in the visible spectral range.

Among composite materials, carbon nanotube-TiO_2 photocatalysts showed the highest efficiency in the photocatalytic degradation of phenol. The synergy effect caused by the introduction of CNT into the titania matrix is attributed to its action as photosensitizer rather than adsorbent or dispersing agent. Supporting TiO_2 on multi-walled carbon nanotubes facilitates the separation and recovering of the photocatalyst from the slurry.

A more detailed study on the CNT-TiO_2 catalyst showed that the introduction of increasing amounts of CNT into the TiO_2 matrix prevents particles from agglomerating, thus increasing surface area of the composite materials. Also, oxygenated groups at the surface of CNT, mainly carboxylic acid and phenol groups, play an important role in the structure of the composite materials since they act as anchoring points to titania particles. Original carbon nanotubes, containing mild amount of oxygen surface groups, produced the highest synergetic effect on the degradation of phenol under visible irradiation.

The effect of the introduction of CNT on the photocatalytic degradation of phenol was noticed mostly under visible light irradiation, rather than in UV and UV-Vis illuminated reactions. This improvement on the efficiency of the photocatalytic process appeared to be proportional to the shift of the UV-Vis spectra of the CNT-TiO_2 composites for longer wavelengths, indicating a strong interphase interaction between carbon and semiconductor phases.

The efficiency of CNT-TiO_2 catalysts in the photocatalytic oxidation of mono-substituted organic compounds under visible irradiation revealed to be

dependent from the ring activating/deactivating properties of the aromatic molecules. Higher synergy factor was observed for compounds presenting electron donor groups such as phenol and aniline.

CNT-TiO_2 catalyst was also used in the photocatalytic degradation of *para*-substituted phenols under visible irradiation. The photocatalytic process was characterized using 4-chlorophenol as model compound. An optimal concentration of catalyst of 1.2 g l^{-1} was found. At natural pH conditions (pH = 5.6) an optimal compromise between kinetic and mineralization photoefficiency of CNT-TiO_2 catalyst was achieved.

The introduction of low concentrations of hydrogen peroxide in the reaction media produced a decline in the efficiency of the degradation process, which was attributed to the action of H_2O_2 as hydroxyl radical scavenger. Increasing concentrations of hydrogen peroxide leaded to a gradually increase in apparent first order rate constant, as a result of the raise of the relative importance of its role as electron acceptor and hydroxyl radical generator.

CNT-TiO_2 reutilization in three consecutive photodegradation reactions resulted in a gradual decrease of the efficiency of the catalyst. Apparent rate constant decreased 30% from the first to the second photodegradation runs and about 12% from second to the third reutilization. The observed deterioration of catalyst photoefficiency is attributed to the presence of reaction intermediates adsorbed on the active sites of the catalyst and to the modification of the catalyst by mechanical stress caused by the magnetic stirring.

A Langmuir-Hinshelwood model, based on a pseudo-steady state approach, was successfully used to represent the dependency of the photocatalytic reaction rate on the concentration of 4-chlorophenol for both TiO_2 and CNT-TiO_2 catalysts. It was found that while the kinetic rate constant increased (relative to the TiO_2 alone situation), the values of K_{LH} are comparable for reactions using either TiO_2 or CNT-TiO_2 catalysts, suggesting that the thermodynamics of adsorption are similar, the difference being in the kinetics of the process.

Photocatalytic degradation of other phenolic compounds, namely 4-aminophenol, 4-hydroxybenzoic acid and 4-nitrophenol were studied in the presence of TiO_2 and CNT-TiO_2 catalysts irradiated with visible light.

Hydroquinone and benzoquinone were detected as reaction intermediates for all compounds. Also 4-chlorocatechol, 4-nitrocatechol and

3,4-dihydroxybenzoic acid were detected as CP, NP and HBA degradation intermediates, respectively.

The photoreactiviy of the substituted phenols was affected by the electronic nature of the substituents. Initial degradation rate tend to increase with increasing electronic density on the aromatic ring in the following order: 4-nitrophenol < 4-hydroxybenzoic acid < 4-chlorophenol < 4-aminophenol. The Hammet constant, which represents the effect that different substituents have on the electronic character of a given aromatic system, appears to be an adequate descriptor of the photocatalytic degradability of the studied para-substituted phenols using both TiO_2 and CNT-TiO_2 catalysts.

The effect of the introduction of CNT into the TiO_2 matrix was quantified in terms of a synergy factor. This synergy factor was inversely proportional to the Hammet constant of the studied molecules. For AP and CP the use of a CNT-TiO_2 composite catalyst caused a beneficial effect in the photoefficiency of the degradation process. Conversely, for HBA practically no synergy effect was observed while for NP the use of CNT-TiO_2 resulted on a negative synergy effect. By these results it can be concluded that the photoefficiency of the catalysts is not only related to its intrinsic properties but also to the activating/deactivating nature of the substrate to be degraded.

Finally, visble-ligth-driven photocatalytic degradation of clofibric acid, a lipid regulator drug, using nanocrystalline TiO_2 was described as a possible initiator for future work. The best photo-efficiency, quantified in terms of kinetic rate constant, TOC removal and initial quantum yield, was achieved for TiO_2 produced at 673K resulting in the total removal of clofibric acid and main reaction intermediates (4-chlorophenol, isobutyric acid, hydroquinone, benzoquinone and 4-chlorocatechol). TiO_2 assisted photocatalysis revealed to be an efficient technique for the mineralization of this type of pharmaceutical compounds in water.

In summary, the obtained results show that the efficiency of a photocatalytic degradation process largely depends from the physical-chemical characteristics of both catalyst and molecule to be degraded. Photocatalytic reactions are very complex with several operational parameters to be taken into account. CNT-TiO_2 catalysts appear to be very promising materials for the photocatalytic degradation of several aromatic compounds under visible light.

From an applied point of view, and due to the great complexity of real effluents, the integration of several treatment methods has to be considered.

Photocatalytic oxidation processes using TiO_2 based catalysts appear to be a very useful technique for the detoxification of water containing moderate organic content, leading to the mineralization of the pollutants or to their conversion to more biodegradable compounds.

As suggestions for future work, it would be interesting to work on the immobilization of CNT-TiO_2 catalysts in order to minimize mechanical stress of the catalyst particles and to avoid a step of catalyst recovery. Catalyst immobilization facilitates its reutilization and also opens the possibility of working in a continuous regime.

Additionally, CNT-TiO_2 catalysts could be used in the photocatalytic degradation of other priority pollutants such as dyes, pesticides and pharmaceuticals.

Finally, as CNT-TiO_2 catalysts showed to be very active in the visible spectral range, the possibility of using natural solar light as irradiation source can result on both environmental and economical advantages.